



UNIVERSITY OF LEEDS

This is a repository copy of *Shelf-derived mass-transport deposits: origin and significance in the stratigraphic development of trench-slope basins*.

White Rose Research Online URL for this paper:
<https://eprints.whiterose.ac.uk/176887/>

Version: Accepted Version

Article:

Claussmann, B, Bailleul, J, Chanier, F et al. (6 more authors) (2022) Shelf-derived mass-transport deposits: origin and significance in the stratigraphic development of trench-slope basins. *New Zealand Journal of Geology and Geophysics*, 65 (1). pp. 17-52. ISSN 0028-8306

<https://doi.org/10.1080/00288306.2021.1918729>

Reuse

Items deposited in White Rose Research Online are protected by copyright, with all rights reserved unless indicated otherwise. They may be downloaded and/or printed for private study, or other acts as permitted by national copyright laws. The publisher or other rights holders may allow further reproduction and re-use of the full text version. This is indicated by the licence information on the White Rose Research Online record for the item.

Takedown

If you consider content in White Rose Research Online to be in breach of UK law, please notify us by emailing eprints@whiterose.ac.uk including the URL of the record and the reason for the withdrawal request.



eprints@whiterose.ac.uk
<https://eprints.whiterose.ac.uk/>

Shelf-derived mass-transport deposits: origin and significance in the stratigraphic development of trench-slope basins

Claussmann B.^{1,2,*}, Bailleul J.¹, Chanier F.³, Mahieux G.⁴, Caron V.⁴, McArthur A. D.⁵, Chaptal C.¹,
Morgans H. E. G.⁶, Vendeville B. C.³

1. U2R 7511, Basins-Reservoirs-Resources (B2R), Geosciences department, UniLaSalle - University of Picardie Jules Verne, 60026, Beauvais, France

2. Schlumberger, Software Integrated Solutions, London, SW1E 6AJ, United Kingdom

3. University of Lille, CNRS, ULCO, UMR 8187, Laboratory of Oceanology and Geosciences (LOG), Lille, France

4. U2R 7511, Basins-Reservoirs-Resources (B2R), University of Picardie Jules Verne - UniLaSalle, 80039 Amiens, France

5. School of Earth and Environment, University of Leeds, Leeds, LS2 9JT, United Kingdom

6. GNS Science, Lower Hutt, New Zealand

Accepted Manuscript version (unedited PDF accepted for publication).

Published Journal Article version available online, 27 May 2021:

<https://www.tandfonline.com/doi/abs/10.1080/00288306.2021.1918729?journalCode=tnzg20>

Published by Taylor & Francis in the New Zealand Journal of Geology and Geophysics:

*Correspondence: bclaussmann@slb.com

21 1. ABSTRACT

22 Continental shelves generally supply large-scale mass-wasting events. Yet, the origin and significance
23 of shelf-derived mass-transport deposits (MTDs) for the tectonostratigraphic evolution of subduction
24 complexes and their trench-slope basins have not been extensively studied. Here, we present high-
25 resolution, outcrop-scale insights on both the nature of the reworked sediments, and their mechanisms
26 of development and emplacement along tectonically active margins, by examining the Middle Miocene
27 shelf-derived MTDs outcropping in the exhumed southern portion of the Hikurangi subduction margin.
28 Results show that periods of repeated tectonic activity (thrust propagation, uplift) in such compressional
29 settings not only affect and control the development of shelfal environments but also drive the recurrent
30 generation and destruction of oversteepened slopes, which in turn, favour the destabilisation and
31 collapses of the shelves and their substratum. Here, these events produced both large-scale, shelf-
32 derived sediment mass-failures and local debris flows, which eventually broke down into a series of
33 coalescing, erosive, genetically-linked surging flows downslope. The associated MTDs have a regional
34 footprint, being deposited across several trench-slope basins. Recognition of tectonic activity as another
35 causal mechanism for large-scale shelf failure (in addition to sea-level changes, high-sedimentation
36 fluxes) has implications for both stratigraphic predictions and understanding the tectonostratigraphic
37 evolution of deep-marine fold-and-thrust belts.

38 **Keywords:** active margin, shelf failure, intra-slope basins, mass-wasting deposits, outcrop study,
39 tectonics

40 2. INTRODUCTION

41 Along active margins, tectonics predominate and exert a crucial control on the stratigraphic development
42 of the related sedimentary basins (e.g., trench-slope basins) and their basin-bounding structures (Moore
43 and Karig 1976; Karig et al. 1980; Underwood and Bachman 1982; Chanier and Ferrière 1991;
44 Underwood and Moore 1995; Bailleul et al. 2013; McArthur et al. 2019). Recurrent mass-wasting occurs
45 and thus, associated mass-wasting products, known as mass-transport deposits (MTDs) form throughout
46 the margin's history, flanking the sedimentary basins, such as trench-slope basins (Moore and Karig
47 1976; Underwood and Bachman 1982; Bailleul et al. 2007; Vinnels et al. 2010; Festa et al. 2015; Ortiz-
48 Karpf et al. 2018; McArthur et al. 2019).

49 A diverse range of MTDs has been described along tectonically active margins (Moscardelli and Wood
50 2015; Festa et al. 2016 and references therein) and numerous studies have investigated the potential
51 causal mechanisms for the related mass-wasting events (e.g., Pickering & Corregidor 2005; Moscardelli
52 et al. 2006; Lamarche et al. 2008; Romero-Otero et al. 2010; Vinnels et al. 2010; Gamberi et al. 2011;
53 Nelson et al. 2011; Strasser et al. 2011; Urgeles & Camerlenghi 2013; Ogata et al. 2014; Alves 2015;
54 Lehu et al. 2015; Festa et al. 2016; Ortiz-Karpf et al. 2018; Festa et al. 2019; Moore et al. 2019; Ogata
55 et al. 2019; Raymond 2019; Carey et al. 2019).

56 Based on the relationships that exist between their source region, sizes, and potential causal
57 mechanisms, Moscardelli and Wood (2008) and Moscardelli and Wood (2015) proposed to refine the
58 classification of mass-wasting products by grouping them into *attached* and *detached* systems,
59 respectively (1) sourced from regional (e.g., shelf) or local slopes; (2) regionally extensive (potentially
60 reaching hundreds to thousands of square kilometres in area, tens of kilometres in width and length, and
61 hundreds of metres in thickness) or smaller, local (occupying less than tens of square kilometres in area
62 and a few kilometres in width and length); and (3) essentially controlled by extrabasinal regional
63 processes (e.g., climate) or localised gravitational instabilities (Figure 1).

64 Continental shelves unequivocally supply some of the greatest mass-wasting events and deposits
65 recorded worldwide (i.e., *attached* systems) (Posamentier and Walker 2006). Yet, the origin and
66 significance of shelf-derived mass-wasting products for the tectonostratigraphic evolution of subduction
67 complexes and their related trench-slope basins have not been extensively scrutinised.

68 In this study, we propose to address this knowledge gap by presenting new occurrences of mass-wasting
69 systems, sourced from the shelf, cropping out in the emerged southern portion of the Hikurangi

70 subduction wedge (Coastal Ranges, North Island of New Zealand) (Figure 2). The related products are
71 Middle Miocene in age and include several episodes of mass-wasting that reworked shelf-derived
72 material (macrofaunas and sediments), can reach over 100 metres (minimum thickness, not
73 decompacted) at outcrop and were deposited across several trench-slope basins along a 70 kilometre-
74 long transect (Whareama, Te Wharau and Akitio trench-slope basins) (Figure 3).

75 Most studies on the shelf-derived mass-wasting events and deposits are based on seismic-reflection
76 data. Therefore, this work aims at bringing new high-resolution, outcrop-scale insights on both the nature
77 of the reworked sediments, and the mechanisms of development and emplacement of these MTDs along
78 tectonically active margins. Sea-level changes and high sedimentation rates are commonly inferred to be
79 the main causal mechanisms triggering the large-scale destabilisation, downslope mass-transport and
80 resulting deposition of shelf-derived sediments into deep-water (Posamentier and Kolla 2003; Moscardelli
81 and Wood 2008; Moscardelli and Wood 2015; Bull et al. 2020). Yet, the role of tectonics is undoubtedly
82 important, particularly along active margins (e.g., Lewis et al. 2004; Lamarche et al. 2008; Watson et al.
83 2020; Couvin et al. 2020).

84 Here, we specifically explore how continued period of tectonic activity (shortening, uplift and related
85 seismicity) can lead to the recurrent generation and destruction of oversteepened slopes at the shelf-
86 margins and in turn favour the repeated destabilisation and collapses of the shelf(ves).

87 Specific objectives are to:

- 88 • Describe the nature, geometries and internal characteristics of the reworked sediments (e.g.,
89 lithofacies) and assess the implication for subsurface assessment of similar, seismic-scale
90 MTDs,
- 91 • Gain a better understanding on the mechanism of development and emplacement of shelf-
92 derived MTDs in subduction complexes,
- 93 • Use the lithofacies and their associations to reconstruct the depositional environments and
94 palaeogeography of the Coastal Ranges of the Hikurangi Margin during the Middle Miocene,
- 95 • Highlight the role of shelf-derived MTDs as markers of the tectonic activity in mature trench-
96 slope basins.

97 3. GEOLOGICAL SETTING

98 3.1. Geological history

99 The Hikurangi subduction wedge started to form about 25 Ma ago as a result of the westward subduction
100 of the oceanic Pacific Plate beneath the Australian Plate along the eastern margin of the North Island of
101 New Zealand (Figure 2) (Ballance 1976; Spörl 1980; Pettinga 1982; Chanier and Ferrière 1991; Field et
102 al. 1997; Nicol et al. 2007).

103 Bounded by the Hikurangi Trench to the south-east and the Forearc Basin *sensu stricto* to the west, the
104 Hikurangi subduction wedge is made of a series of elongate, trench-parallel intra-slope basins (*i.e.*,
105 trench-slope basins (*sensu* Underwood and Moore 1995)) separated and confined by tectonically active,
106 sublinear bathymetric highs that are controlled by underlying landward-dipping thrust faults and
107 asymmetrical seaward-verging folds (Lewis and Pettinga 1993; Barnes et al. 2010; Bailleul et al. 2013;
108 Bland et al. 2015; McArthur et al. 2019).

109 Since the onset of subduction, the Hikurangi subduction wedge has undergone a complex and
110 polyphased tectonic history (Figure 4).

111 As the Pacific Plate began to subduct beneath the Australian Plate, the related compressional stresses
112 resulted in the seaward emplacement of ESE thrust nappes (25 – 18 Ma), on the back of which thrust-
113 bounded depocenters provided the necessary space for the development of trench-slope basins (17.5 –
114 15 Ma) (Pettinga 1982; Chanier and Ferrière 1989; Chanier and Ferrière 1991; Rait et al. 1991; Nicol et
115 al. 2007; Bailleul et al. 2013; Malie et al. 2017).

116 Then, from Middle to Late Miocene times (15 – 6.5 Ma), the entire margin experienced a period of mixed
117 N-S to NE-SW extension and compression, leading to general subsidence, gravitational collapses and
118 normal faulting in the inner portion of the wedge, as well as continued outward migration of the
119 deformation front in the middle and outer portions (Chanier 1991; Chanier et al. 1999; Barnes et al. 2002;
120 Bailleul et al. 2013).

121 Finally, from the Late Miocene to present-day (6.5 – 0 Ma), renewed E-W to NW-SE compressional
122 deformation and tectonic inversion dominated the margin and resulted in regional folding and reverse
123 faulting. Shortening has accelerated within the last million year and has led to the uplift and emergence
124 of part of the inner portion of the subduction wedge (*i.e.*, trench-slope break), which now forms the Coastal
125 Ranges of the eastern North Island of New Zealand (Figure 2) (Lamb and Vella 1987; Cape et al. 1990;

126 Chanier 1991; Chanier et al. 1999; Nicol et al. 2002; Nicol et al. 2007; Bailleul et al. 2013) and outboard
127 frontal accretion (Barnes et al. 2018).

128 The close interplay between the evolution of the margin and the development of the associated
129 sedimentary basins resulted in intricate trench-slope basin fills that are disrupted by a series of
130 discontinuities (Neef 1992; Neef 1999; Bailleul et al. 2007; Bailleul et al. 2013; Burgreen and Graham
131 2014; McArthur et al. 2019).

132 Their fills mostly comprise Miocene to Recent deep-marine gravity-driven deposits, extensive marine
133 hemipelagic mudstones and carbonate deposits (Figure 4) (Field et al. 1997; Lee and Begg 2002; Bailleul
134 et al. 2007; Bland et al. 2015; McArthur et al. 2019). They conformably or unconformably overlie the
135 Cretaceous to Paleogene pre-subduction basement, which can be divided into two main assemblages:
136 (1) the Lower Cretaceous Torlesse greywackes, witness of an older accretionary prism developed along
137 the south-eastern margin of Gondwana at the time (Spörli 1980; Bradshaw 1989; Mortimer 2004); and
138 (2) the Upper Cretaceous to Oligocene series evolving from detrital to pelagic sediments eastward (Figure
139 4) (Chanier and Ferrière 1991) and indicating a sustained period of tectonic quiescence (Chanier 1991;
140 Chanier and Ferrière 1991; Bailleul et al. 2013).

141 **3.2. Whareama and Te Wharau Basins**

142 The study area is located in the southern Coastal Ranges, and more particularly in the exhumed
143 Whareama and Te Wharau Basins (Figure 3; Figure 5).

144 The Whareama Basin is an elongate, NE-SW trench-parallel slope basin (Figure 3), ~50 kilometres long
145 and two to six kilometres wide, bounded by basement ridges composed of pre-Miocene strata (Chanier
146 1991). It started to form contemporaneously with the onset of subduction on the backlimb of the Glenburn
147 Nappe, a seaward-verging thrust nappe (Chanier 1991; Chanier and Ferrière 1991) that is composed of
148 Lower Cretaceous Torlesse greywackes and Upper Cretaceous to Eocene pelagic to detrital series
149 (Figure 4; Figure 5). Its sedimentary fill unconformably to conformably overlies the Glenburn Nappe and
150 is bounded to the west by the Adams-Tinui Fault complex and Pukeroro Fault (*i.e.*, landward basin
151 margins, Figure 3; Figure 5) and to the east by the Flat Point-Whakataki Fault complex (*i.e.*, seaward
152 basin margin, Figure 3; Figure 5).

153 The Te Wharau Basin is another elongate, thrust-bounded slope basin located in the emerged, inner-
154 portion of the subduction wedge (Figure 3). To the west of the Whareama Basin, the Te Wharau Basin is
155 smaller (~10 kilometres long), narrower (one to five kilometres wide) and oriented North-South (Figure 3;

156 Figure 5) (Chanier 1991; Bailleul et al. 2013). Its fill unconformably overlies the Lower Cretaceous
157 Torlesse greywackes (to the north) as well as the Upper Cretaceous to Eocene detrital series (to the
158 south) (Chanier 1991) (Figure 4; Figure 5). The Adams-Tinui Fault complex represents its seaward basin
159 margin (Figure 3), except in the central portion of the system, where it comprises two synclines and is
160 bounded by both the Adams-Tinui Fault complex and the Pukeroro Fault (Figure 5). Unlike the Whareama
161 Basin, the Te Wharau Basin only records deposits from the Middle to Upper Miocene (Chanier 1991).

162 3.3. Depositional systems

163 Gravity-driven deposits dominate the stratigraphic infill of trench-slope basins (Underwood and Bachman
164 1982; Underwood and Moore 1995; Underwood et al. 2003; Vinnels et al. 2010). Although submarine
165 canyons and channels play an undeniable role in the distribution of sediments, slope destabilisation can
166 act as another, agent of sediment delivery and reorganisation, triggering significant submarine mass-
167 failure and reworking (Underwood and Bachman 1982; Chanier and Ferrière 1991; Bailleul et al. 2007;
168 McArthur et al. 2019; McArthur and McCaffrey 2019).

169 In this study, we specifically focus on the Middle Miocene, Lillburnian (Late Langhian to Serravallian, 15.1
170 – 13.05 Ma) mass-wasting events that reworked shelf-derived material. The related mass-wasting
171 products crop out in the preserved portions of the Whareama and Te Wharau Basins, as well as in the
172 Akitio Basin farther north (Figure 3, sections b, c, n, r, s, tw).

173 Even though deep marine sedimentation dominated at the time, several contemporaneously developing
174 and older (Figure 4) shallow-marine, mixed siliciclastic-carbonate shelves were also reported in the area
175 (Figure 3, sections f, i, m, ms, o, p, t, w) (Crundwell 1987; Chanier 1991; Bailleul et al. 2007; Bailleul et
176 al. 2013; Caron et al. 2019; Bailleul et al. Submitted; Caron et al. Accepted). Bailleul et al. (2013) and
177 Bailleul et al. (Submitted) demonstrated that whether attached to the continent or not, these shelfal
178 systems preferentially formed above trench-slope basin-bounding structures that were affected by active-
179 margin tectonic activity, such as uplift events. The abrupt shallowing provided the suitable depositional
180 settings (*e.g.*, neritic conditions) for carbonates and biogenic sediments.

181 4. DATA AND METHODS

182 We undertook fieldwork in order to characterise the Middle Miocene strata outcropping in the southern
183 emerged portion of the Hikurangi subduction wedge. Over one kilometre of sea cliff outcrop along the
184 Whareama Basin coastline was mapped and studied through acquisition of photogrammetric data

185 (acquired from a drone), traditional fieldwork data (e.g., detailed sedimentary sections) and taphonomic
186 data (Figure 5, Sefton Hills outcrops, sections s-1 and s-2). In parallel, several hinterland localities were
187 also characterised through a series of outcrop observations in the Te Wharau Basin (Figure 5, sections
188 c, n, r, tw-1, tw-2). In the Akitio Basin, the contemporaneous MTD occurrences (Figure 3, section b) were
189 previously described by Bailleul et al. (2007) and Bailleul et al. (2013).

190 **4.1. Drone acquisition and photogrammetry**

191 Ground Control Point (GCP) coordinates and drone pictures of the one-kilometre-long coastal outcrop at
192 Sefton Hills were acquired so that a 3D georeferenced model could be built to observe and describe the
193 lateral and vertical variations of the sediment distribution. Over 500 high-resolution aerial images were
194 captured with a DJI Phantom 4 Pro UAV, and a total of nine GCP coordinates were recorded using a
195 Trimble GeoExplorer 2008 differential global positioning system tool (DGPS) as well as a Trimble
196 Tempest antenna positioned at two metres above the measured point. Standard *Structure from Motion*
197 workflows (Westoby et al, 2012) were then followed for data quality control, processing and rendering. A
198 3D outcrop model was created in the form of a high-resolution triangulated mesh textured with the
199 photographs using the Metashape Professional Edition software by Agisoft (Figure 6).

200 **4.2. Geological mapping and outcrop sedimentology**

201 Field mapping data were recorded with a Trimble ® TDC100 and integrated using ArcGIS software tools.
202 The stratigraphic expressions of the Middle Miocene, Lillburnian aged gravity-driven deposits were
203 examined along the coast at Sefton Hills and captured in three detailed sedimentary sections (total of
204 165 metres at bed scale, Figure 7). Detailed structural measurements (e.g., ductile deformation analysis),
205 as well as bedding and palaeocurrents were also collected. These measurements were corrected using
206 the geomagnetic models from GNS Science New Zealand. A dedicated diagnostic feature template was
207 used to thoroughly describe each MTD occurrence in a standardised manner, both along the coastline
208 and in the hinterland. The age of the sedimentary units and the palaeobathymetries were defined using
209 micro- and macropalaeontological analysis conducted by GNS Science New Zealand. Four samples were
210 collected in the study area to supplement the information already captured in the Fossil Record Electronic
211 Database (<https://fred.org.nz/>) (Appendix 1. Appendix 2).

212

4.3. Taphonomy

213 Due to the significant quantity of macrofossils contained in the MTDs, occurring both as whole skeletons
214 and moderately fragmented remains, a taphonomic analysis was performed in three sectors of the Sefton
215 Hills depositional system on approximately one square metre area of outcrop. It was restricted to the
216 coarsest fraction of death assemblages contained in the MTDs, *i.e.*, on fossil remains larger than five
217 millimetres allowing assignment to a taxonomic group (from, at best, Species to Class level). In this study,
218 three categories of skeleton damage, namely fragmentation, abrasion and bioerosion, were described
219 visually using the graded classification scale presented in Appendix 3, complemented by those proposed
220 by Caron (2011) and Caron et al. (2019). Encrustation of skeletons was also evaluated but was found to
221 be virtually absent. This approach aims at (1) extending the sedimentological knowledge on transport
222 and depositional processes in gravity-driven systems, (2) helping better characterise the source areas
223 and (3) defining diagnostic characteristics to help distinguish between MTDs.

224

4.4. Lithofacies, facies associations and depositional environments

225 The integration of the detailed fieldwork with the digital outcrop model (Figure 6; Figure 7) enabled us to
226 document the lateral and vertical facies variations, recognise the stratigraphic architectures and thus
227 propose facies assemblages and associated depositional environments (Table 1; Figure 8; Figure 9;
228 Figure 10; Figure 11). The facies associations and interpretations follow and complement the initial
229 nomenclature for trench-slope basins that was defined by Bailleul et al. (2007) and Bailleul et al. (2013),
230 whereby **Fa1** refers to turbidite systems and **Fa3** to mass-wasting systems.

231 Because our study focuses on shelf-derived MTDs, we do not provide an extensive description of the
232 turbidite lithofacies, already described in details along the margin (*e.g.*, Bailleul et al. 2007; Bailleul et al.
233 2013; Burgreen and Graham 2014; McArthur and McCaffrey 2019; McArthur et al. 2021), and we used
234 the facies associations **Fa1g** and **Fa1s** defined by Bailleul et al. (2007) and Bailleul et al. (2013) as
235 reference.

236 Alternatively, we scrutinised the different sedimentary expressions of the shelf-derived MTDs (**Fa3p**)
237 recorded on outcrops and recognised four distinct lithofacies (**DF**, **MF-1**, **MF-2**, **SL**) (Table 1). The
238 lithofacies comprise a variety of cohesive gravity flows (**DF**, **MF-1** and **MF-2**) extensively observed and
239 described in the Whareama and Te Wharau Basins (Figure 8, Figure 9, Figure 10; Figure 11) as well as
240 chaotic and contorted facies (**SL**) only witnessed in the Akitio Basin (Bailleul et al. 2007; Bailleul et al.

241 2013). Altogether, the shelf-derived cohesive gravity flows form the facies assemblage **Fa3p-d** whereas
242 the chaotic and contorted expressions form **Fa3p-s** (Table 1).

243 5. MIDDLE MIOCENE SHELF-DERIVED GRAVITY-DRIVEN SYSTEMS

244 5.1. Whareama Basin

245 In this study, we focus on a coastal transect from the eastern part of the Whareama Basin, at the Sefton
246 Hills locality, which is situated four kilometres south of Uruti Point and can be divided into two sections,
247 namely section s-1 and section s-2 (Figure 5). Section s-1 represents the main exposure that extends
248 over one kilometre along the coast. Section s-2 is located 500 metres south of section s-1, on the beach
249 (Figure 5). Both expose Middle Miocene, mid Lillburnian (Langhian, ca., 14 Ma) strata (Appendix 1).

250 Based upon the 3D outcrop model and detailed stratigraphic logging (Figure 6; Figure 7), two main
251 gravity-driven systems and related deposits were identified. The contact between these two systems is
252 stratigraphic, erosive yet can locally appear faulted on part of the outcrop.

253 5.1.1. Turbidite deposits

254 The lower part of the Sefton Hills outcrop (Figure 6) is characterised by a well-developed, several hundred
255 metres thick turbidite system made of laterally continuous, mostly medium-bedded (average 17
256 centimetres thick), fine-grained sandstones. Shell fragments (either diffuse to abundant) and plant debris
257 (either disseminated or organized) are frequent in the structured intervals, typically starting with coarse-
258 grained sands. The overall net-to-gross is of ~65%; mud caps are thus common and on average 10
259 centimetres thick. They often present bioturbations such as *Phycosiphon* sp., *Chondrites* sp., *Zoophycos*
260 sp. and *Thalassinoides* sp. Details on the lithology, stratification and internal bedding characteristics of
261 the different sandstone intervals (**Fa1g** and **Fa1s** as defined by Bailleul et al. (2007) and Bailleul et al.
262 (2013)) are given in Table 1.

263 Observations

264 **Fa1g** mostly comprises normally graded, amalgamated, slightly erosive, medium- to thick-bedded
265 sandstones (Figure 6; Figure 8a, b, g, h). The thicker beds are made of (very) coarse- to fine-grained
266 sands and their base, concave up, truncates the underlying strata with a low angle (centi- to decimetric
267 scale incision). Channel-based drapes (*sensu* Barton et al. 2010) are not uncommon below the erosional

268 cut (Figure 8g, h). These turbidites sometimes evolve into several very fine- to medium-grained
269 sandstone beds overlain by draping muddy layers, before alternating with either (1) fining and thinning
270 upward interbedded sandstones and mudstones (**Fa1g-a**) (Figure 8a, b, g, h), or (2) finer and thinner
271 interbedded mudstones and sandstones displaying local low-displacement features (**Fa1g-f**) (Figure 8b,
272 c, d, e, f). The turbidites tend to be thicker (~20 centimetres), more massive and amalgamated at the top
273 of the turbidite system (Figure 8d; Figure 9f), where they also include a couple episodes of concentrated
274 bioclastic grits (10 to 20 centimetres thick) (Figure 7).

275 Most of the **Fa1g-f** occurrences are recorded in the lower part of the turbidite system, where they are
276 often found interbedded with a series of tabular (sheet-like), continuous thin- to thick-bedded turbidites
277 (**Fa1s**) (Figure 6; Figure 8e, f).

278 Palaeocurrent measurements were collected in the upper part of the system, along the sedimentary
279 section SS-01 (Figure 7); they display a general SW-to-NE direction with a dispersion from the NW to the
280 SE (Figure 6).

281 Interpretations

282 The facies association **Fa1s** was previously described by Bailleul et al. (2007) and Bailleul et al. (2013)
283 and interpreted as sheet-like turbidites. These tabular, highly continuous turbidites commonly result from
284 unconfined, waning turbidity currents (Lowe 1982; Kneller 1995) and either characterise the most distal
285 region of a lobe setting before it evolves into basin plain environment (Galloway 1998) or the basin floor
286 setting. These facies are generally associated with mixed to muddy systems which can disperse sand far
287 into the basin (Galloway 1998). **Fa1s** is generally found interbedded with **Fa1g-f**, inferred to represent
288 the lobe fringe facies from the medial to distal regions (Prélat et al. 2009; Burgreen and Graham 2014;
289 McArthur et al. 2021). This interplay supports the presence of a particularly distal and unconfined setting
290 at the start of the Sefton Hills system (**Fa1s**) that sometimes recorded the distalmost incursions (**Fa1g-f**)
291 of a depositional lobe system.

292 The series then slowly evolve into more confined and proximal settings, recording the emplacement of a
293 depositional lobe system, as was previously described and interpreted as **Fa1g** by Bailleul et al. (2007)
294 and Bailleul et al. (2013) in the Akitio Basin. At Sefton Hills, **Fa1g** can be divided into **Fa1g-c**, **Fa1g-f** and
295 **Fa1g-a** that have contrasting facies and internal architecture outlining the different parts of the lobe
296 system.

297 **Fa1g-c** illustrates the network of small, low-relief distributary channel fills or scours (Galloway, 1998) that
298 likely contributed to the development of the lobe system. **Fa1g-c** differs from lobe axis deposits usually

299 characterised by thick, amalgamated sandstone units and better compares to lobe off-axis deposits
300 (Prélat et al. 2009; Burgreen and Graham 2014; McArthur et al. 2021). Although amalgamation is
301 frequently observed, the strata is mostly medium-bedded and display a lower net-to-gross to the
302 traditional lobe axis deposits (65% instead of 80%) (Prélat et al. 2009).

303 The small channel fills commonly show fining- and thinning- upward sequences (**Fa1g-a**) reflecting both
304 the progressive abandonment of the distributary channel segment and filling of the unfilled relief
305 (Galloway 1998; McHargue et al. 2011). The lobe fringe deposits (**Fa1g-f**) are less frequent towards the
306 top of the sequence.

307 The nature (e.g., shell fragments, plant remains) and abundance of debris in the deposit also highlight
308 that the flow most likely initiated in a shallow marine environment that was continually connected to a
309 hinterland sourcing the land-derived material (Kuenen 1964). Palaeocurrents recorded in the upper
310 turbidite intervals indicate a sourcing from the WSW. Their variations (Figure 6) however outline that the
311 flow of sediments occurred in fairly confined settings. Interactions between gravity currents and
312 topography commonly result in spatial flow variations related to flow deflection (Kneller and McCaffrey
313 1999). We can thus infer the presence of a sublinear topography to the NE of the Sefton Hills locality,
314 responsible for the deflection of the incoming turbidity currents. Yet, the presence of unconfined deposits
315 (**Fa1s**) cropping out at the base of the Sefton Hills turbidite system suggest that such topography did not
316 initially exist. It therefore developed coevally with the overriding **Fa1g** turbidite system.

317 **5.1.2. Locally-derived mass-transport deposits**

318 In the lower part of the Sefton Hills outcrop, the sandstone intervals are interspersed with recurrent, small-
319 scale (one to five metres thick) chaotic, contorted (**Fa3l-s**) to matrix-supported (**Fa3l-d**) deposits (Figure
320 6).

321 Observations

322 **Fa3l-s** is the most commonly occurring and is made of several metre-thick intervals between undeformed
323 turbidites (Figure 6). These intervals mostly comprise contorted turbidite beds (e.g., recumbent folding)
324 and sometimes include dislocated, pebble- to boulder-graded clasts of turbidites, within a silty mudstone
325 background facies (Figure 6; Figure 8a, d, e, f, g, h). Towards the top of the turbidite system, most of the
326 contorted strata indicate a SW apparent direction of movement. Overall, **Fa3l-s** is characterised by a
327 good lateral continuity and thus its occurrences are easily followed across the outcrop. It often seems
328 adjacent to **Fa1g-f** (Figure 6; Figure 8a, b).

329 **Fa3I-d** was only observed once (Figure 8h, lower MTD) and is characterised by a matrix-supported
330 deposit containing at least 50% of intraformational clasts. They are mostly made of pebbles to outsized
331 clasts (deci- to decametric) of turbidites. A couple of skeletons belonging to Molluscan species (*e.g.*,
332 gastropods) were also locally observed, floating in the matrix.

333 Interpretations

334 **Fa3I-s** is interpreted to represent small-scale MTDs resulting from sliding and or slumping of initially
335 coherent turbidite beds under the action of gravity (Nardin et al. 1979; Nemeč 1990). The recurrence of
336 these deposits suggests a generally unstable slope whereas their size, extent and nature imply a rather
337 local source of input. The directions of mass-movements are fairly consistent and would indicate a slope
338 that dipped to the SW (Woodcock 1979; Alsop et al. 2019), thus reinforcing the hypothesis of a ridge that
339 was contemporaneously developing to the NE of Sefton Hills. The high sedimentation rates observed in
340 the turbidite deposits (Table 1) can increase the prospect of depositing water-rich and mechanically weak
341 sediments, more prone to fail along an unstable, rising slope (Lee 2009). We therefore interpret **Fa3I-s**
342 as the result from local failures of the recently deposited turbidites (**Fa1g**) while the topography rose to
343 the NE. **Fa3I-s** sometimes seems to laterally evolve from the lobe fringe deposits, thereby suggesting
344 potential preferential destabilisation of these deposits. Finally, we interpret **Fa3I-d** to represent small-
345 scale MTDs resulting from the transformation of **Fa3I-s** into a cohesive flow as it moved downslope (*e.g.*,
346 Strachan 2008).

347 **5.1.3. Shelf-derived mass-transport deposits**

348 The upper part of the Sefton Hills outcrop is characterised by six distinct matrix-supported deposits,
349 coalescing to over 100 metres of total vertical thickness and 50 to 80 metres of lateral continuity (Figure
350 6). They can be separated into two stacked sets of the same three main lithofacies (Figure 10) deposited
351 in the same order (Figure 6). Despite erosional and sharp bases, one set essentially evolves between
352 matrix-supported deposits containing a high-density (lithofacies **DF**) to a more diluted, dispersed amount
353 of gravel-grade sediments (lithofacies **MF-1** and **MF-2**), thus displaying a general fining upward trend.
354 The matrix of these deposits is made of light grey, silty mudstone and mostly contains extraformational
355 clasts of pre- and syn-subduction material, in varying quantities, sizes and shapes.

356 **Lithofacies Debris Flow (DF)**

357 Observations

358 **DF** is a disorganised, poorly-sorted polymict conglomerate comprising ~50% of matrix. Its basal surface
359 is sharp and slightly (<30 centimetres) to highly erosive into the underlying gravity-driven deposits (Figure
360 6).

361 In **DF**, pre-subduction material largely dominates. It is mostly made of sub-rounded to rounded dark
362 granules to pebbles of Lower Cretaceous Torlesse greywackes. The remaining pre-subduction material
363 (less than 1%) includes sub-rounded pebbles and cobbles of Upper Cretaceous (e.g., calcareous
364 mudstones), Paleocene (e.g., Waipawa black siltstones) and Eocene to Oligocene strata, as well as sub-
365 angular pebbles of Cretaceous to Paleocene strata (Figure 10a, f). Some rare sub-angular cobbles of
366 Lower Cretaceous Torlesse greywackes can also be found.

367 Clasts of syn-subduction material can be divided into lithoclasts and bioclasts.

368 Lithoclasts are characterised by pebbles to boulders (sometimes oversized: deci- to decametric) of
369 coherent to dislocated turbidites of similar nature to the ones from the underlying turbidite system,
370 boulders to oversized mud clasts, sub-angular indurated shell bed clasts and black pieces of organic
371 matter (e.g., wood) (Figure 9b, c, e; Figure 10b, c, d, e). SE-verging recumbent folds were measured
372 throughout the contorted expression of some of the turbidites (Figure 6; Figure 9c; Figure 10c).

373 Bioclasts are abundant and composed of macrofossils mostly belonging to Molluscan species (e.g.,
374 bivalves and gastropods) and rarely to Corals (details in Appendix 2). This bioclastic material can either
375 be found: (1) as shell fragments, finely milled and dispersed in the matrix (Figure 10a); or (2) as skeletons,
376 partly to mostly well-preserved (being one to eight centimetres long) and floating in the matrix (Figure
377 10a, g). *Struthiolaria (Callusaria) callosa*, *Polinices* sp. as well as *Turritella* sp. were identified as the most
378 recurrent macrofossil species of gastropods. Most of the bivalve shells appear to be only partially well-
379 preserved, thereby making it complicated to classify some of the species; *Glycymeris* sp., *Cardium* sp.
380 and *Ostrea* sp. were recognised.

381 Despite their common characteristics, differences exist between the two occurrences of the lithofacies
382 **DF** at the Sefton Hills locality. The diversity encountered in the pre-subduction clasts decreases
383 drastically in **DFb**. Lower Cretaceous Torlesse greywackes still dominate and are also locally particularly
384 abundant (Figure 10a) whereas only a few Cretaceous to Paleocene clasts (e.g., calcareous mudstones)
385 are present. In terms of syn-subduction material, the mud clast content largely increases towards the top
386 of **DFa** (Figure 10d) while this crude sorting does not exist in **DFb**, which records decametric, randomly
387 scattered mud clasts (Figure 9b, e). The transported turbidites evolve from oversized, sometimes
388 overturned rafts (Figure 9f; Figure 10b) to contorted and then dislocated cobbles and or boulders towards

389 the top of **DFa** (Figure 10c), whereas **DFb** is mostly made of dislocated, randomly scattered cobbles to
390 boulders. Both contain several types of shell bed clasts that are typically sub-angular, range from five to
391 20 centimetres in length and constitute a major part of the overall syn-subduction clasts at the base of
392 **DFa**.

393 Finally, the taphonomic analysis of the macrofossil content (Figure 12) shows that bioerosion contrasts
394 markedly between facies **DFa** and **DFb**, being overall low to moderate (combined frequencies of 78.2%
395 to 100%) for both the coarser and the finer skeletal fraction. Fragmentation, for grains larger than three
396 centimetres that include whole skeletons and partly broken ones, is similar within both facies, being
397 predominantly low to moderate (cumulated frequencies of 76.2% and 87%, respectively). Unsurprisingly,
398 fragmentation is high to very high for the finer skeletal fraction dominated by clastic material. The coarser
399 skeletal fractions in facies **DFa** and **DFb** exhibit similar degrees of abrasion (cumulated frequencies for
400 low to moderate abrasion is 71.4% in **DFa** and 60.9% in **DFb**, and for high to very high degrees of
401 abrasion, 28.6% in **DFa** and 39.1% in **DFb**). Interestingly, abrasion for the finer skeletal fraction is higher
402 in **DFa** than in **DFb** (high to very high degrees of abrasion of 33.8% and 16.6% respectively; Figure 12).
403 Macrofaunal assemblages and bioclastic remains are remarkably similar in facies **DFa** and **DFb**. At
404 outcrop scale, concentration of well-preserved skeletons in **DFa** may appear higher than in **DFb**. The
405 square metres of outcrop investigated for the taphonomic analysis show no difference in the
406 concentrations of well-preserved skeletons between both facies. However, the overall bioclastic content
407 is more abundant in **DFa** than in **DFb** (Figure 12).

408 Interpretations

409 **DF** is interpreted to represent a MTD produced by cohesive debris flows (*sensu* Mulder and Cochonat
410 1996; Mulder and Alexander 2001). The disorganised and chaotic arrangement is characteristic and the
411 predominance of matrix in the deposits indicates that matrix strength was the dominant grain-support
412 mechanism for the failed material (Nardin et al. 1979; Lowe 1982). Grain interactions may also be locally
413 important due to the abundance of coarse lithoclastic material.

414 The erosive nature of the deposits and presence of allochthonous, rafted blocks of contemporaneous
415 Miocene turbidites, sometimes completely overturned, at the base (cf. **DFa**) suggest basal interaction
416 between the overriding mass-flow and the substrate. Erosional ploughing and scouring is a common
417 feature of MTDs (Posamentier and Martinsen 2011; Festa et al. 2019) especially when hydroplaning
418 (*sensu* Mohrig et al., 1998) is not seen as the main mechanism responsible for the mobility of the flow.

419 The sedimentary rocks of the substrate are thus incorporated into the overflowing MTD by basal erosion
420 (Posamentier and Martinsen 2011; Sobiesiak et al. 2018). The crude grading observed in their shape and
421 size (outsized clasts to pebbles; raft to contorted or dislocated turbidites) throughout **DF** suggests layer-
422 parallel shearing within the flow. As the flow moved downslope and further substratum material was
423 added, it first remained coherent before partly disaggregating and starting to shear and deform in the
424 direction of the flow (Fonnesu et al. 2016). Alternatively, deformation could result from shearing and
425 compaction after the freezing of the flow (Mulder and Alexander 2001). The SE-verging measurements
426 collected in the contorted turbidites indicate a mass-flow travelling southward, likely parallel to the NW-
427 SE sublinear topography that developed to the NE of Sefton Hills (see 5.1.1 and 5.1.2).

428 Although **DFb** is also characterised by an erosional base, only a small amount of turbidites (of pebble- to
429 cobble-grades) are present. Large-scale mud clasts dominate throughout, thereby suggesting a change
430 in the nature of the underlying substratum being ploughed. **DFa** is the first episode of debris flow recorded
431 at Sefton Hills right above a well-developed turbidite system (Figure 6) whereas **DFb** is the second
432 episode. At least another two MTDs were recorded in between the two debris flows (Figure 6, cf. **MF-1a**
433 and **MF-2a**), thus providing an entirely different substrate (*i.e.*, mud-rich) to be eroded and incorporated
434 into the flow for **DFb**. Mud clasts are also present in the first debris flow although smaller and concentrated
435 towards its top (Figure 9b, e). These could be the result of hydraulic jumps at the time the debris flow
436 reached the base of slope (Henstra et al. 2016) or as it travelled above the uneven basin-floor topography.

437 The variety of lithoclasts and bioclasts encountered in **DF** illustrates the level of internal heterogeneity
438 usually associated with debris flows (*e.g.*, Mulder and Alexander 2001) and also provides insights about
439 the nature of the failed source area (Posamentier and Martinsen 2011). The quantity and diversity of pre-
440 subduction clasts suggest that the event of mass wasting did not only destabilise the sediments that were
441 being deposited in the source area (*i.e.*, Lillburnian sediments), but that the substratum onto which they
442 were depositing was remobilised as well. The nature of the clasts implies that this substratum mostly
443 comprised the pre-subduction series (*e.g.*, Cretaceous up to Oligocene) (Chanier 1991; Chanier and
444 Ferrière 1991). Yet, the few occurrences of Miocene shell bed clasts indicate that it also comprised some
445 syn-subduction sedimentary rocks previously deposited in shallow-marine, mixed siliciclastic-carbonate
446 environments (Chanier 1991; Bailleul et al. 2007; Bailleul et al. 2013; Caron et al. 2019; Bailleul et al.
447 Submitted; Caron et al. Accepted).

448 The macropalaeontological analysis conducted onto the sampled fauna indicates a neritic shelfal
449 environment whereas the micropalaeontological data reveal that the deposition of the debris flow

450 occurred at lower bathyal depths (>1000 metres), with a planktic abundance varying from >80 to >95%,
451 thus indicating deposition in a sub-oceanic to fully oceanic setting.

452 The taphonomic analysis suggests that the first event of mass wasting (**DFa**) remobilised macrofaunal
453 assemblages that were either alive or only recently deceased on the shelf floor, whereas the second
454 event (**DFb**) transported organisms that were, for most part, already dead and bio-eroded. Since the
455 nature of the macrofossils transported in **DFa** and **DFb** remains the same, a repeated destabilisation of
456 the same sourcing region can be inferred, with not enough time between the two events for the molluscan
457 communities to replenish the neritic zone, *i.e.*, shelfal environment.

458 Mass-wasting is therefore interpreted to have initiated in shallow waters, from potential failure of a shelf
459 that developed above a substratum composed of both pre- and syn-subduction material. The coevally
460 developing shallow-marine, mixed siliciclastic-carbonate shelves to the north of Sefton Hills are great
461 candidates for being the source, having formed on a pre- (*e.g.*, Upper Cretaceous to Paleogene series)
462 and syn-subduction (*e.g.*, Miocene sediments) substratum (Figure 3, section f, i, m, p) (Bailleul *et al.*
463 2007; Bailleul *et al.* 2013), and presenting markedly similar faunal assemblages, which include
464 *Struthiolaria* sp., *Polinices* sp., Turritellids, *Glycymeris* sp., Oysters or some Corals (Bailleul *et al.*
465 Submitted). The destabilised material was then transported downslope and resulted in deposition of **DF**
466 at deeper waters, into the Whareama Basin.

467 Finally, the high percentage (>30%) of sub-rounded to rounded, granules and pebbles of Lower
468 Cretaceous Torlesse greywackes unlikely results from the underwater substratum. Instead, it might either
469 come from (1) direct erosion of the hinterland that mostly comprises exhumed Torlesse rocks and or (2)
470 reworking of Upper Cretaceous conglomerates, known to already contain sub-rounded granules and
471 pebbles of Lower Cretaceous Torlesse greywackes, previously reworked through fluvial processes
472 (Chanier 1991; Chanier and Ferrière 1991). Indeed, several shelfal deposits were described as containing
473 sub-rounded pebbles to boulders of Torlesse greywackes (*e.g.*, in the Middle Miocene shelfal series of
474 Oumukura (Chanier 1991) and in the Pliocene limestones of Hawke's Bay (Caron *et al.* 2004)), thereby
475 indicating that Torlesse material, either already reworked or recently eroded, can likely be transported
476 from the hinterland onto a shallow shelf, where it is then exposed to littoral processes. The presence of
477 wood fragments in the deposits also indicates a connection (continuous or not) with an emerged land
478 (Kuenen 1964), which could have also been used to bring and store the reworked sub-rounded Torlesse
479 clasts into the source area.

480 **Lithofacies Mudflow 1 (MF-1)**

481 Observations

482 **MF-1** is another type of disorganised, poorly-sorted polymict conglomerate. It is primarily distinguished
483 by its high matrix content (~95%) and its resemblance to a diluted version of the lithofacies **DF**. It has a
484 sharp, undulating basal surface, that laterally evolves into becoming highly erosive (decametric) towards
485 the south (Figure 6, cf. **MF-1a** and **MF-1b**, Figure 9a, b, c, d, e, h; Figure 10h).

486 Pre-subduction material is largely dominant in **MF-1**, with a very high proportion of sub-rounded to
487 rounded Lower Cretaceous Torlesse greywackes of very coarse sand to granule grades (Figure 10h).
488 Cobbles and boulders of Cretaceous to Paleocene clasts are rarely found scattered in the matrix (Figure
489 10l).

490 The variety of syn-subduction lithoclasts is comparable to that of the **DF** lithofacies, and includes Miocene
491 turbidites, shell bed clasts, organic matter (*e.g.* wood) and some mud clasts. It also punctually includes
492 clasts of the underlying **DF** material. In general, the shell bed clasts and wood fragments (>1% of the
493 total contribution) do not exceed pebble grades and are mostly sub-angular, and rarely sub-rounded
494 (Figure 10k).

495 The bioclastic content remains important, however this material is now mostly found as shell fragments
496 dispersed in the matrix (Figure 10h). A few (well- and partly-) preserved molluscan skeletons were
497 identified (Figure 10m); gastropods tend to be the best preserved (details in Appendix 2).

498 We performed a taphonomic analysis on the finer skeletal fraction of **MF-1a** related deposits, the coarser
499 fraction (*i.e.*, >3 centimetres) being virtually absent (Figure 12). Degrees of fragmentation range from
500 high to very high. Overall, abrasion is low to moderate (45.6% and 50%, respectively; cumulated
501 frequencies of 95.6%). Bioerosion is predominantly low (84.8% of no- or poorly-infested bioclasts) to
502 moderate (10.9%).

503 The two occurrences of the lithofacies **MF-1** display quasi-similar characteristics at the Sefton Hills
504 locality. The main difference affects the incorporated syn-subduction turbidites. In both cases, they are
505 essentially characterised by pebbles to boulders of contorted to dislocated turbidites which can
506 occasionally present bioclastic grits or laminations (Figure 9d, h; Figure 10i). A decametric mass of
507 coherent thin-bedded turbidites (*i.e.*, raft) is however present at the top of **MF-1b** (Figure 9a; Figure 10i).
508 It displays a high number of angles and truncations, and is wrapped by the matrix.

509 Interpretations

510 **MF** is interpreted as a MTD resulting from cohesive mudflow (*sensu* Mulder and Cochonat 1996; Mulder
511 and Alexander 2001). The dominance of matrix suggests that cohesive strength (*i.e.*, matrix strength)
512 was the dominant grain-support mechanism for the incorporated material in this lithofacies (Nardin et al.
513 1979; Lowe 1982). The presence of unusually large clasts (*e.g.*, turbidite decametric raft) floating on top
514 of the flow is not uncommon in MTDs (Posamentier and Martinsen 2011). This occurrence indicates the
515 presence of additional support mechanisms in **MF-1b** such as high local pore pressures, buoyancy and
516 or clast-to-clast interaction (Pierson 1981; Johnson 1984; Nemeč and Steel 1984; Postma et al. 1988;
517 Mulder and Alexander 2001).

518 The nature of the reworked material (lithoclasts and bioclasts) is equivalent to that of **DF**, thereby
519 suggesting destabilisation and remobilisation of a similar, if not identical, sourcing region. The
520 macrofaunal species remain the same as the ones recorded in **DF** and thus indicate that the failure
521 responsible for the deposition of **MF-1** destabilised a neritic shelfal environment as well.

522 The geometry and distribution of the basal incisions recorded in **MF-1** can be used to infer the gross
523 general transport direction. Their characteristics suggest that the flow was moving almost perpendicular
524 to the outcrop orientation along a NW-SE direction, with a migration of incision towards the south (Figure
525 6, cf. **MF-1a** and **MF-1b**). These incisions could either result from basal erosion (Posamentier and
526 Martinsen 2011; Sobiesiak et al. 2018) or could be associated with the build-up of lateral margins (Bull et
527 al. 2009; Posamentier and Martinsen 2011). In both cases, such features provide a primary constraint on
528 the flow direction of the MTD and also indicate the potential position of the lithofacies within the MTD
529 body and across the seafloor. Lateral margins and flow-ploughing commonly develop in the translational
530 domain of the MTD body, which is located between the up and downslope extremes (*i.e.*, the headwall
531 and toe domains) (Bull et al. 2009), outboard of the base of slope. In this domain, the MTD is
532 characterised by intense deformation, dislocation, basal erosion as well as incorporating translated, rafted
533 blocks (Frey-Martínez et al. 2005; Bull et al. 2009; Posamentier and Martinsen 2011), all being features
534 of the **MF-1** lithofacies.

535 Lithofacies Mudflow (MF-2)

536 Observations

537 **MF-2** is mostly made of light grey, silty mudstone (Figure 10n). The matrix represents 99% of the overall
538 flow deposits and the remainder is divided between that with a high bioclast content and that with rare

539 scattered lithoclasts. The basal surface is sharp yet sometimes can appear as slightly gradational from
540 **MF-1**.

541 **MF-2** shows good lateral continuity (Figure 9a, g, h). For example, its second occurrence (**MF-2b**) can
542 be traced over one kilometre from the southern part of the Sefton Hills section 1 locality to the Sefton
543 Hills section 2 (Figure 9g).

544 In **MF-2**, the lithoclasts are rare and do not display much variety. In order of frequency, they are (1) a few
545 syn-subduction decametric mud clasts, (2) rare syn-subduction pebbles to boulders of contorted and
546 dislocated turbidites (Figure 10o) and (3) rare pre-subduction elements of sand sizes, likely of Lower
547 Cretaceous Torlesse greywackes. Where dominated by mud clasts, **MF-2** can easily be mistaken for
548 hemipelagic mudstones; but is differentiated based upon the matrix that surrounds the mud clasts
549 laterally. The bioclasts are essentially shell fragments; only a couple of molluscan skeletons were found
550 floating in the matrix, partly preserved yet highly disarticulated (details in Appendix 2).

551 Interpretations

552 **MF-2** is also interpreted as a MTD resulting from cohesive mudflow (*sensu* Mulder and Cochonat 1996;
553 Mulder and Alexander 2001). Its texture closely resembles that of lithofacies **DF** and **MF-1**, albeit in a
554 very low-density version. Mass-transport processes can either be intergradational or not (*i.e.*, one process
555 can evolve into another with time or remain the same) (Stow 1986; Nemeč 1990). Sediment dilution
556 through water entrainment, particularly at the head (Middleton and Hampton 1973) or at the upper
557 boundary of a flow (Mulder and Alexander 2001) is known as a major mechanism contributing to the
558 transformation of one cohesive flow into another (Lowe 1982; Mulder and Alexander 2001). Therefore,
559 **MF-2** could represent the diluted expression of an initial debris flow (**DF**) or mudflow (**MF-1**). The low
560 density of clasts may also indicate that either the source area was fairly depleted at the time of
561 destabilisation or that the flow did not directly initiated from this location, but further downslope, from a
562 muddier, deeper environment (*e.g.*, the upper- or mid-slope environment (Posamentier and Martinsen
563 2011)).

564 Once again, the clast content suggests the failure of a shelfal environment with a stock of reworked
565 Torlesse clasts whereas the micropalaeontological study (Appendix 1, sample T27/f0643 taken in **MF-**
566 **2b**) reveals that deposition remained at lower bathyal depths (>1000 metres). The mud clast content
567 would have again resulted from the seafloor ploughing effects (Posamentier and Martinsen 2011;
568 Sobiesiak et al. 2018) and thus points towards an erosive character of the flow.

570 Overall, the Sefton Hills outcrop is characterised by deposition of two main syn-subduction gravity-driven
571 systems during the Middle Miocene, mid Lillburnian. The underlying turbidite system evolved from an
572 unconfined, distal sheet-lobe setting (**Fa1s**) to a more confined and proximal depositional lobe setting
573 (**Fa1g**) as a NW-SE sublinear topographic high developed to the north-east and isolated this part of the
574 Whareama Basin from the unconfined basin floor to the east. Most likely controlled by the underlying
575 seaward-verging Flat Point-Whakataki Fault complex, the rise of this topographic high not only resulted
576 in the development of a SW-dipping slope (*i.e.*, backlimb setting) that deflected the incoming turbidity
577 currents but also favoured repeated destabilisation of the syn-kinematic turbidites, thereby generating
578 local gravitational instabilities leading to deposition of small-scale (one to five metres thick) MTDs (**Fa3l**).

579 This turbidite system was then abruptly interrupted by the emplacement of six amalgamated MTDs (**DFa**,
580 **MF-1a**, **MF-2a**, **DFb**, **MF-1b**, **MF-2b**) that reworked a vast quantity of shelf-derived material. Together,
581 they form a large-scale mass-transport complex (MTC) (**Fa3p-d**) of over a hundred metres in thickness,
582 with up to a kilometre of lateral continuity. The nature of these deposits suggests the repeated failures of
583 a shallow marine, shelfal environment developed above a substratum composed of both pre- and syn-
584 subduction material, which also caught and stored land-derived elements (*e.g.*, reworked pebbles of
585 Torlesse greywackes, wood and plant debris). Mass-failures likely initiated at shallow water depths north
586 of the study area. The failed material then travelled southward, parallel to the Whareama Basin seaward
587 margin, and downslope through erosive cohesive flows (*e.g.*, debris flow and mudflow). Deposition
588 eventually occurred onto the Whareama trench-slope basin floor, above the Sefton Hills turbidite system,
589 at greater water depths, *i.e.*, lower bathyal, and within southward migrating depocentres.

590 The two main gravity-driven systems of Sefton Hills are not genetically linked. Yet, they were fed by
591 similar sources of material (shell fragments, wood and plant debris). Shoreline river systems could have
592 directly supplied land- and beach-derived material to the shelfal domain (Posamentier and Walker 2006)
593 making it readily available to be transferred beyond the shelf edge and farther downslope, either caught
594 (1) in canyon heads, generally ending their course downslope into turbidite systems (Posamentier and
595 Allen 1999) or (2) in unconfined shelf edge failures, resulting in large-scale MTDs (Moscardelli and Wood
596 2008; Moscardelli and Wood 2015).

597 The palaeocurrent variations recorded in both systems (north-eastward migrating turbidite system and
598 southward MTDs) indicate that the shallow marine shelfal environment(s) located to the west of the
599 Whareama system at the time was(were) persistent, well-developed and geographically extensive.

600

5.2. Te Wharau Basin

601 In this study, we also examined outcrops located in the main portion of the Te Wharau Basin (Figure 5,
602 sections c and r) and in its easternmost secondary fold portion (Figure 5, sections tw-1, tw-2 and n).
603 These outcrops expose additional occurrences of contemporaneous shelf-derived MTDs from the Middle
604 Miocene, Lillburnian (Late Langhian to Serravallian, 15.1 – 13.05 Ma) (Appendix 1). Intermittent, these
605 inland outcrops did not allow the same detail of descriptions and measurements as the coastal outcrops.
606 Nevertheless, we were able to characterise each outcrop following the same approach and nomenclature
607 defined at the Sefton Hills locality (Table 1; Figure 11).

608 We identified several occurrences of matrix-supported deposits identified in the Te Wharau Basin (Figure
609 5). Their apparent dimensions are of three to 20 metres of vertical thickness and 15 to 30 metres of lateral
610 continuity. However, both the base and top surfaces could not be distinguished, thereby suggesting
611 possibly greater thickness of deposits (Figure 11). They essentially hold similar general characteristics to
612 those of Sefton Hills. Their matrix is made of light grey, silty mudstone and mostly contains gravel-grade
613 extraformational clasts of pre- and syn-subduction origins (Figure 11a). Despite poor outcrop conditions,
614 the deposits seem to hold between 30 to 40% of lithoclasts and bioclasts; which could imply that they are
615 best defined by the lithofacies **DF** (Table 1).

616 Lithofacies Debris Flow (DF)

617 Observations

618 In the Te Wharau Basin, pre-subduction material also largely dominates the disorganised, poorly-sorted,
619 polymict conglomerates of lithofacies **DF**. They mostly include Lower Cretaceous Torlesse greywackes,
620 either as sub-rounded to rounded pebbles or sub-angular cobbles, boulders or outsized clasts (Figure
621 11a, c, d, f). The remaining pre-subduction material comprise sub-angular pebbles to outsized clasts
622 (metric) of other Lower Cretaceous (*e.g.*, red cherts), undifferentiated Cretaceous (*e.g.*, calcareous
623 mudstones) and Paleocene strata. The syn-subduction lithoclasts are essentially characterised by sub-
624 angular pebbles to cobbles of shell beds (Figure 11b, c). Contorted turbidites are rarely found.

625 Bioclasts are abundant and composed of a large variety of Molluscan species (details in Appendix 2;
626 Figure 11b, d, e) either found: (1) as shell fragments, finely milled and dispersed within the matrix or (2)
627 as skeletons, partly to mostly well-preserved (generally two to three centimetres) and floating in the
628 matrix. The gastropods are the best preserved, whereas the bivalves are commonly partly broken and
629 chalky.

630 Despite some characteristics that are similar to those of Sefton Hills, the Te Wharau occurrences present
631 some differences. Overall, the clasts are dominantly sub-angular. The largest clasts (e.g., boulders) are
632 found in the Te Wharau road-2, Ngaumu and Rangiora sections (Figure 5). In particular, pre-subduction
633 material dominates at Ngaumu and Rangiora. It includes Lower Cretaceous Torlesse greywackes,
634 Cretaceous calcareous mudstones and Paleocene glauconitic sandstones. At Ngaumu, Lower
635 Cretaceous red cherts and lavas are also present. At Te Wharau road-1, the syn-subduction lithoclasts
636 are represented by different types of shell beds. At Te Wharau road-2, both shell bed clasts, skeletal and
637 bioclastic fine-grained sandstones (respectively the facies S1 described by Caron et al. (2004) and the
638 facies Fa6b described by Bailleul et al. (2007)) are found (Figure 11e). At Ngaumu, the syn-subduction
639 material comprises shell bed clasts along with rare scattered and contorted turbidites.

640 Interpretations

641 We interpret the different occurrences of DF observed in the Te Wharau Basin to be MTDs produced by
642 cohesive, likely debris flows (*sensu* Mulder and Cochonat 1996; Mulder and Alexander 2001). Despite
643 great internal heterogeneity, the extraformational clast content remains similar across the different
644 occurrences, displaying the same types of pre- and syn-subduction material and thus demonstrating
645 failures of comparable sources.

646 The nature of the lithoclasts, largely dominated by Lower Cretaceous material and Miocene shell bed
647 clasts, suggests slightly different substratum(s) to the one(s) sourcing the contemporaneous MTDs of
648 Sefton Hills. These substrata were made of Lower Cretaceous Torlesse greywackes and cherts, above
649 which Middle Miocene shelfal environments developed, highlighting a substantial sedimentary hiatus.

650 During the Middle Miocene, Clifdenian (Early Langhian, ca. 15.9 – 15.1 Ma) and Lillburnian (Late
651 Langhian to Serravallian, 15.1 – 13.05 Ma), a few episodes of mixed siliciclastic-carbonate shelves
652 unconformably overlying Lower Cretaceous Torlesse basement were documented in the sector of Te
653 Wharau, and more particularly at the Wainuioru and Mapapa stream localities (Figure 5, sections w, o,
654 ms) (Crundwell 1987; Chanier 1991). Their failure could have directly provided the material for the
655 macrofossil content, shell bed and Torlesse clasts recorded in the MTDs of the Te Wharau Basin (Figure
656 5). The rounded clasts of Torlesse greywackes probably resulted from fluvial and or littoral reworking of
657 the material, initially exposed in the hinterland (Chanier 1991; Chanier and Ferrière 1991) and later
658 transferred onto the shelfal environment.

659 Input from the pre-subduction Upper Cretaceous to Paleogene series are scarce and only clearly
660 observed in the MTDs from the Ngaumu and Rangiora sections. Around these areas, owing to the Adams-

661 Tinui Fault complex (Figure 5), the Lower Cretaceous Torlesse basement overrides the Glenburn Nappe
662 and thus locally provides a substratum that also includes the Upper Cretaceous to Paleogene series.

663 Finally, the micropalaeontological studies reveals that the deposition of the debris flows generally
664 occurred at bathyal depths. More particularly, the Te Wharau road occurrence (section tw-1) indicates
665 mid-bathyal water depths (700 metres), which are shallower than in the Whareama Basin, and the
666 planktic abundance of 25% also indicates that an outer neritic water-mass was overlying the site of
667 deposition at the time, thereby suggesting nearby shelfal source(s). Overall, the local source regions
668 (maximum of seven kilometres distance from the known Wainuioru and Mapapa shelves) (Figure 5)
669 support the prospect of the Te Wharau cohesive flow deposits being more proximal to their sources than
670 those at Whareama.

671 **6. DISCUSSION**

672 **6.1. Stratigraphic record of shelf-derived mass-wasting events at outcrop**

673 The shelf-derived mass-wasting products presented in this study are captured across several exhumed
674 trench-slope basins and exhibit a variety of lithofacies and geometries. They always incorporate reworked
675 well-preserved to fragmented shallow marine macrofauna as well as (pre- and syn-subduction)
676 extraformational clasts, suggesting the destabilisation and collapse of similar depositional environments.
677 However, the diversity observed in the shapes, sizes, percentages of reworked material and the
678 interactions with the underlying surface imply that different physical and sedimentary processes
679 interplayed as the failed material moved downslope. Such variety also suggests that the deposits may
680 have been recorded at different locations (*e.g.*, distance) relative to the source regions.

681 **6.1.1. Source regions**

682 The analysis of the macrofossil content (palaeontology and taphonomy) indicates that the staging areas
683 were located at shallow depths in neritic shelfal waters. The analysis of the extraformational content also
684 adds that the events remobilised the fauna and sediments that were depositing in the failed source area
685 (*i.e.*, Middle Miocene, syn-subduction) as well as partially destabilised the substratum upon which they
686 were settling (*i.e.*, syn- and or pre-subduction material). The contemporaneously developing shallow-
687 marine, mixed siliciclastic-carbonate shelves, markedly installed above pre- and or syn-subduction
688 substratum and presenting similar faunal assemblages are thus great candidates for the source regions

689 (Figure 3, sections f, i, m, ms, p, t, w) (Crundwell 1987; Chanier 1991; Bailleul et al. 2007; Bailleul et al.
690 2013; Bailleul et al. Submitted). The failed material was then transported downslope into deeper water
691 settings, being deposited either along the main slope, proximally to the source area (e.g., Te Wharau
692 road MTDs) or onto the trench-slope basin floor, further from the source and at lower bathyal water depths
693 (e.g., Sefton Hills MTDs). The land-derived material (e.g., wood fragments, reworked sub-rounded
694 pebbles) captured in these deposits probably results from the uplift and erosion of hinterland areas, which
695 typically transfer such material to the coastal and shelfal environments, making it readily available to be
696 incorporated into the failed deposits. Isolated islands developed above tectonically controlled topography
697 can also be considered for providing plant material (McArthur et al. 2016).

698 **6.1.2. Taphonomic insights**

699 A key question related to the taphonomic character of the shelfal skeletal sediments contained in the
700 studied MTDs and presented in Figure 12, is as to whether they were inherited or, at least partly, acquired
701 during transport and emplacement of the MTDs. Explanations for limited bioerosion of skeletal material
702 are multifarious, including unfavourable ecological conditions for bioeroders, substrates unsuitable to
703 drilling organisms, high fine-grained siliciclastic inputs, increasing water depths, predominance of
704 organisms buried alive and rapid burial preventing infestation (e.g., Kidwell 1989; Perry 1998; Martin
705 1999; Richet et al. 2011). Notwithstanding the possibility for fragmentation to be related to biotic factors
706 (e.g., Zuschin et al. 2003), the degrees of fragmentation and abrasion may help assess whether flows
707 were either laminar or turbulent, and whether sediments were deposited by traction or suspension (e.g.,
708 Lowe 1982). Due to the abundance of coarse lithoclastic material in the lithofacies **DF**, there is a potential
709 for fragmentation to have originated from *en masse* crushing during transport, and abrasion to reflect *en*
710 *masse* friction as possible mechanisms by which skeletons were altered. Fragmentation during transport
711 of previously broken and abraded material will lower its taphonomic evaluation because this secondary
712 mechanical event generates new angular edges. This process may explain why abrasion values compare
713 well in the various size fractions of lithofacies **DF**. In contrast, the abundance of silty mudstone matrix
714 and the low siliciclastic content in lithofacies **MF**, hence reducing *en masse* friction between grains and
715 making crushing unlikely (e.g., Li et al. 2019), may explain their limited abrasion and could indicate that
716 abrasion and fragmentation were inherited.

717 **6.1.3. Distance to source and facies**

718 In the Te Wharau Basin, we interpret the Te Wharau road cohesive flows to represent the fairly proximal
719 and immature expressions of the failure, captured close to the sourcing area(s), most probably on the

720 slope. The disorganised clast fabric may reflect short travel distance (Nemec and Steel 1984) whereas
721 the high density of angular, boulder-grade clasts could also suggest a rather recent mobilisation (*sensu*
722 Iverson 1997).

723 Further north, in the Akitio Basin, a 175-metre thick series of large-scale slides and slumps (cf. **Fa3p-s**
724 in Table 1) interbedded with a few cohesive flows, similar in nature to the ones of the Te Wharau Basin,
725 were also observed (Branscombe MTDs of Bailleul et al. (2007)). These MTDs deposited in proximal
726 position to the contemporaneously developing mixed siliciclastic-carbonate outer shelf of Pongaroa
727 (Figure 3, sections b and p) (Bailleul et al. 2007; Bailleul et al. 2013) and thus indicate that both sediment
728 mass-failure (*e.g.*, Akitio) and mobilisation (*sensu* Iverson 1997) (*e.g.*, Te Wharau) can occur close to the
729 source areas.

730 In the Whareama Basin however, the cohesive flows captured at Sefton Hills deposited farther from the
731 sourcing shelf area(s), at lower bathyal water depths onto the trench-slope basin floor. More importantly,
732 the Sefton Hills deposits are characterised by amalgamated cohesive flows that can result from several
733 failures that coalesced downslope. In particular, we observed repeated sequences of coalescing, erosive
734 flows that display a rough fining upward trend (**DF**: debris flow, to **MF-1** and **MF-2**: mudflows in Figure 8
735 and Figure 10). Debris flows do not always move downslope as one single flow and commonly break into
736 a series of surges (*e.g.*, Iverson 1997; Mulder and Alexander 2001; Felix et al. 2009; Allen et al. 2020).
737 One flow event can therefore be characterised by a multitude of surges, either arising naturally (*e.g.*,
738 induced by surface wave coalescence (Iverson 1997)) or initiated by external triggers such as sporadic
739 slope failures. Here, each failure would have triggered the development of a cohesive flow, breaking up
740 downslope into at least three separated surges. During multiple-surge events, the first surge is usually
741 the coarsest one, then tailed by surge(s) of medium and finer particles behaving as muddy flow(s)
742 (Zanuttigh and Lamberti 2007). Consistent replications of grading and structure divisions can be expected
743 in such deposits, and we therefore infer that the Sefton Hills deposits recorded two main events of shelf
744 destabilisation (event a and b), each divided into three genetically-linked surging flow deposits (lithofacies
745 **DF**, **MF-1** and **MF-2**).

746 As such, the shelf-derived deposits presented in this study indicate that shelf failures triggered both
747 sediment mass-movement (**Fa3p-s**) and development of debris flows (**Fa3p-d**) close to the source
748 region(s) (*e.g.*, Akitio and Te Wharau MTDs), which may eventually break down into a series of erosive,
749 upward fining surges downslope (*e.g.*, Whareama MTDs) (*e.g.*, Figure 13).

750

6.1.1. Deposit dimension and scale

751 The source regions, regional footprint and internal characteristics of these MTDs all suggest that they
752 belong to *attached* systems sourced from the shelf (Moscardelli and Wood 2008; Moscardelli and Wood
753 2015). In order to better comprehend the full three-dimensionality and extent of these shelf-derived mass-
754 wasting deposits at outcrop scale, we used the set of morphometric relationship equations calculated by
755 Moscardelli and Wood (2015) as a basis for reconstructing their potential dimensions.

756 We used the best outcropping occurrences of Sefton Hills (Whareama Basin) and Branscombe (Akitio
757 Basin) as references, having access to representative thickness estimations from fieldwork
758 measurements. We considered whether or not these MTDs were part of the same event or had a coeval
759 trigger (e.g. a megathrust earthquake); yet, we rapidly discarded this hypothesis since the
760 micropalaeontological analysis showed that they were not contemporaneous; the Branscombe MTDs
761 being slightly older (lower Lillburnian) (Bailleul et al. 2007; Bailleul et al. 2013).

762 The resulting morphometric calculations, whether using the general or specific set of equations, provided
763 volume, area and length values that are generally above the generic thresholds for *attached* systems
764 (Moscardelli and Wood 2015) (i.e., $V > 1$ cubic kilometres; $A > 100$ square kilometres and $L > 11$ kilometres
765 (Figure 14; Appendix 4), thereby reinforcing such an interpretation of these MTDs.

766 In addition, we considered the average deposit length parameter (*sensu* Moscardelli and Wood 2015) to
767 account for the lateral thickness variations that are typical of MTDs and gain additional insights onto the
768 possible source areas, especially those of the Sefton Hills MTDs. Notwithstanding the presence of
769 potentially closer source regions, yet to be discovered in the studied area, we used the shortest distance
770 between the deposits and the already well-known shelfal areas as a proxy (Appendix 4). The results
771 favour a potential source region located 40 to 70 kilometres to the north, nearby the Tinui, Takiritini or
772 Waihoki-Mangatiti shelves (Figure 14; Appendix 4). However, these results should only be considered as
773 general insights since the Sefton Hills deposits have not been proven to be the termination of the MTDs,
774 the input deposit lengths do not account for possible tortuous pathways or closer source regions, the
775 deposit thickness does not take into account potential compaction effects, which can be substantial in
776 muddy sediments (Jones 1944), and the outcrop conditions hindered their full exposure (e.g., upper
777 bounding surface is not visible).

778 Interestingly, the MTDs from the Te Wharau Basin show contrasting results that suggest the coeval
779 presence of smaller (i.e., *detached*) systems (Figure 14; Appendix 4). The limited outcrop exposures may
780 explain such results, preventing the recognition of representative thickness values. Yet, the potential

781 presence of isolated shelves (e.g., Caron et al. Accepted) and or the particular geotectonic settings and
782 triggering mechanisms evidenced for the shelf-derived MTDs we present in this study (i.e.,
783 oversteepened slope due to thrust activity), which contrast with the causal mechanisms traditionally
784 invoked for shelf failure (e.g., sea-level changes, high-sedimentation fluxes) (see 6.2), should also be
785 taken into account. Whilst oversteepened slopes at the thrust fronts (e.g., forelimb settings) appear to
786 generally source reduced MTDs volumes ($\sim V < 5$ cubic kilometres) (e.g., Watson et al. 2020), the complex
787 interactions that exist between sediment supply, slope profile and shelf width along convergent margins
788 can also alternatively promote the development of *attached* or *detached* systems from regional slope
789 settings (e.g., shelf) (e.g., Naranjo-Vesga et al. 2020). Therefore, although further work is required to
790 generalise such observations and interpretations to our study area, the different styles and sizes of shelf-
791 derived MTDs described in this study rather support the prospect of slightly more complicated
792 morphometric relationship and classification along tectonically active margin settings, whereby the shelfal
793 region may contemporaneously source both *attached* and *detached* systems.

794 Overall, the morphometric values suggest seismic-scale shelf-derived MTDs throughout the study area.
795 Traditionally, the seismofacies of mud-dominated cohesive flows is defined by low amplitude, semi-
796 transparent and chaotic reflections (Bull et al. 2009). Here however, we cannot expect for the internal
797 architecture of the Sefton Hills MTC, as described in this high-resolution study (i.e., several coalescing
798 shelf-derived MTDs), to be imaged by the seismic data because of resolution limitations. A mud-
799 dominated deposit containing clasts, whether milli-, deci- or decametric or having contrasting
800 concentrations, would hold similar acoustic impedance characteristics and thus look the same at seismic
801 scale. Therefore, the coalescing shelf-derived MTDs of Sefton Hills will be imaged as one unique MTD
802 (seismofacies) at seismic-scale, thereby missing the potential discrete, multiple-surge events responsible
803 for deposits holding distinct lithological and petrophysical properties at outcrop-scale.

804 **6.2. Causes and controls for continued destabilisation of source regions**

805 We previously demonstrated that the MTDs described in this study were sourced from the destabilisation
806 of the contemporaneously developing shelfal environments. Gravity-driven instabilities can however
807 result from a variety of processes, and fortunately, the MTDs characteristics (e.g., geomorphologic
808 features) provide direct evidence on the former failure processes and basin settings (Mulder and
809 Alexander 2001; Bull et al. 2009; Posamentier and Martinsen 2011; Talling et al. 2012). Accordingly,
810 shelf-derived MTDs are generally inferred to be controlled by extrabasinal, regional-scale processes;
811 notwithstanding gas-hydrate dissociation, storms, longshore currents or tectonic activity (e.g.,

812 earthquakes) as other important causal mechanisms, relative sea-level changes and high sedimentation
813 fluxes remain the most commonly invoked triggers (e.g., Posamentier and Kolla 2003; Moscardelli and
814 Wood 2008; Moscardelli and Wood 2015; Bull et al. 2020).

815 The nature and size of the remobilised material presented here indicates powerful events that
816 destabilised both the shelf substratum and fresh sediments. The resulting products, recorded across
817 several trench-slope basins (along a 70 kilometre-long transect), point towards a margin-wide episode of
818 destabilisation leading to a regional footprint of the associated deposits. The different ages captured in
819 the MTDs (e.g., T27/f632: mid Lillburnian; T27/f638: early Lillburnian) however argue for a period (rather
820 than a single, brief episode) of widespread failure that lasted ca. 1 to 2 Ma. The Sefton Hills MTDs also
821 add that within this period, a series of close, high-frequency collapse events (i.e., multi-surge events)
822 repeatedly occurred.

823 At global scale, the sea-level changes highlighted a couple of drops during the Middle Miocene,
824 Lillburnian (Haq et al. 1987; Miller et al. 2005) that may have punctually influenced the stability of the
825 shelf(ves). However, although shelf edges are commonly steep already (Schlager and Camber 1986)
826 and thus prone to both oversteepening and failure, no statistically significant link or pattern seem to exist
827 between the sea-level changes and occurrences of slope failure (Urlaub et al. 2013). Conversely, sea-
828 level variations will generally have a major impact on seafloor pressures (e.g., hydrostatic pressure) and
829 temperatures (e.g., warm currents) (Urlaub et al. 2013). An increase in temperature of as little as 1°C at
830 water depths <600 metres (e.g., shelf) can shift the gas hydrate stability zone downslope, engender
831 dissociation of the hydrate accumulation, release substantial quantities of free gas and thus promote
832 slope failure (Reagan and Mordis 2008). Widespread evidence of gas-hydrate deposits exists in the
833 Hikurangi Margin; however, it is unclear whether these deposits already existed during the Middle
834 Miocene. Moreover, Moscardelli and Wood (2008) and Moscardelli and Wood (2015) trust that gas-
835 hydrate dissociation preferentially leads to the catastrophic failure of a large sediment volume (rather
836 than a succession of failures), thereby discarding it as a potential cause for the MTDs described in this
837 study. Storm-induced waves and longshore currents are also known to potentially trigger slope failure in
838 shallow waters. In the Akitio Basin, the Middle Miocene Pongaroa shelf displays a shallowing-up trend
839 capped by storm-influenced deposits (Bailleul et al. 2007). However, the related sedimentary features
840 are of too small a magnitude (i.e., two to 10-centimetre-thick shell lineation in 30 to 50-centimetre-thick
841 shell beds) to suggest a powerful event responsible for large-scale destabilisation. The duration of such
842 event, although greater than that of an earthquake, also does not explain the recurrence and surges that
843 were observed in some of the deposits. Also, no indication of contour current deposits has ever been
844 reported on this margin during the Middle Miocene, thereby ruling out this other mechanism.

845 On the Hikurangi Margin, shelves commonly formed in association with margin uplift and are located
846 above tectonically induced stratigraphic surfaces (e.g., angular unconformities) resulting from rapid
847 motion of the basins' margins (Bailleul et al. 2013). For example, the Pongaroa and Waihoki-Mangatiti
848 shelves developed above silty deep-marine deposits (Bailleul et al. Submitted). Interestingly, the angular
849 unconformities not only appear to be coeval with the accumulation of the first shelfal sediments but can
850 also be correlated with the remobilisation and deposition of the associated MTDs along the slope and
851 into deep-water settings. The tectonic activity related to the development of basin-bounding structures
852 (e.g., thrusts) follows timescales of ca. 1 to 2 Ma (Nicol et al. 2002; Bailleul et al. 2013). Therefore, these
853 short tectonic periods have not only recorded discrete, high amplitude structural movements (e.g. uplift)
854 responsible for dramatic changes in depositional environments (e.g., neritic conditions) (Figure 15). They
855 also most likely controlled the continuous (with or without break) propagation of the associated thrust
856 fault(s) and thus favoured the development of abrupt, unstable areas near the shelf edges (e.g., forelimb
857 setting).

858 High sediment fluxes, known to fundamentally modify the dynamic equilibrium of an area and influence
859 the growth of (pre-existing) structures (Storti and McClay 1995; Malavieille 2010; Graveleau et al. 2012;
860 Barrier et al. 2013; Noda 2018) could have also contributed to some of the oversteepening. Hence, we
861 attribute the above-described shelf-derived MTDs to be primarily controlled by tectonic uplift and
862 oversteepening. These findings are in agreement with those of Watson et al. (2020) (although built from
863 the analysis of MTDs sitting on the seafloor), who proposed for these two mechanisms to be mainly
864 responsible for the mass-wasting processes occurring along the Hikurangi Margin thrust ridges. We here
865 bring new insights as to some of the depositional environments being destabilised by these mechanisms
866 in the older stratigraphic record.

867 Finally, vertical movements of the coastline can also result from earthquakes (Pilarczyk et al. 2014) and
868 the Hikurangi Margin has a history of both subduction and upper plate fault earthquakes (Clark et al.
869 2019). The accompanying co-seismic shaking can trigger large-scale subaqueous slope instabilities and
870 the subsequent generation of gravity-driven flows (e.g., MTDs) (Hampton et al. 1996). A series of
871 tsunamigenic waves (i.e., series of surges) can also be induced, resulting in the seaward downslope
872 transport (tsunami backwash) of a wide range of material from terrestrial (e.g., organic matter) to shelfal
873 (e.g., mollusc macrofossils) origins; and despite high-energy transport, the fossils can remain
874 taphonomically unaltered (i.e., pristine) (Einsele et al. 1996; Pilarczyk et al. 2014). However, no seaward
875 to landward current reversals nor violent fluid escape features, characteristics of tsunamites (Dawson
876 and Stewart 2007), were observed in our deposits.

877 [Watson et al. \(2020\)](#) argued against ground shaking as a primary control in thrust-related mass-wasting
878 processes. Although ground shaking is undoubtedly important, we also believe that for the MTDs
879 described in this study, this process may not be the primary (but a secondary) control. We interpret
880 periods of repeated tectonic activity (thrust propagation and uplift) to be the main causal mechanism for
881 shelf destabilisation and collapses (Figure 15). Continued (ca. 1 to 2 Ma) tectonic activity (possibly
882 combined with earthquake(s)) would lead to recurring generation and destruction of oversteepened
883 slopes. The shelf-edge escarpments would thus be repeatedly destabilised, allowing for the development
884 of multiple episodes of mass-wasting along the margin. Like other mechanisms, such as gas-hydrate
885 dissociation or storm-induced waves, sea-level changes and high sedimentation rates, commonly
886 inferred to be the dominant causal mechanisms, most likely contributed to some mass-wasting, punctually
887 influencing the stability of the shelf(ves), however they did not act as the main triggers for the shelf-
888 derived MTDs described here.

889 **6.3. Implications for the Coastal Ranges and active Hikurangi Margin**

890 A number of mixed siliciclastic-carbonate shelfal environments coexisted in the Coastal Ranges during
891 the Middle Miocene, Lillburnian ([Crundwell 1987](#); [Chanier 1991](#); [Bailleul et al. 2007](#); [Bailleul et al. 2013](#);
892 [Bailleul et al. Submitted](#)) and their linear distribution along a 120 kilometre-long, NE-SW transect (Figure
893 3; Figure 5) indicates that they most likely formed a regional continental shelfal domain in the south-
894 western portion of the Hikurangi Margin at the time. The high amount of land-derived material (e.g.,
895 organic matter, reworked sub-rounded pebbles), incorporated in both the shelfal and resulting MTDs, is
896 in favour of a narrow, continent-attached system receiving regular terrigenous input from the hinterland
897 areas. No lateral continuity has yet been established between the different locations, therefore
898 development of partially connected or isolated, continent-detached platform systems upon and about
899 actively fault-growing folds ([Caron et al. 2004](#); [Caron et al. Accepted](#)) may have also locally occurred
900 (e.g., ([Bailleul et al. 2013](#)), Fingerpost shelf).

901 The diversity observed in the nature of the reworked material (e.g., clast content, size) and the regional
902 footprint of the MTDs suggests destabilisation of most, if not all, of these platforms (Figure 16). These
903 shelves developed above substantially different substratum inherited from local tectonics, thereby
904 allowing us through the thorough analyses of the reworked material to retrace the potential sourcing
905 region(s) of the different MTDs recorded in the trench-slope basins (see 5.1.3, 5.2, 6.1). The northern
906 shelves from the Akitio Basin (Figure 3, sections i, p, m, t) most likely sourced the Branscombe and
907 southward-moving Sefton Hills MTDs respectively captured in the Akitio and Whareama Basins (Figure

908 3; Figure 16; sections b, s), whereas the southern shelves of Wainuioru and Mapapa (Figure 3; Figure
909 16; sections ms, w) are great candidates for the MTDs recorded in the Te Wharau Basin (Figure 3; Figure
910 16; sections c, n, r, tw). Therefore, the Middle Miocene, Lillburnian, not only staged the development of
911 regional shelfal domain(s) across the south-western portion of the Hikurangi Margin (Crundwell 1987;
912 Chanier 1991; Bailleul et al. 2007; Bailleul et al. 2013; Bailleul et al. Submitted) but they also recorded
913 their coeval destabilisation and failure(s) (Figure 16).

914 The Akitio and Whareama Basins were connected during the Early Miocene (Bailleul et al. 2013), and
915 this connection most probably persisted, at least partially, during the Middle Miocene to allow for some
916 of the mass-wasting products sourced from the Akitio shelves to travel southwards into the Whareama
917 Basin (e.g., Sefton Hills MTDs) (Figure 16). We therefore propose that the seaward margin of the Akitio
918 Basin, partially emerged at the time (i.e., Cape Turnagain Structural High), formed together with the
919 seaward margin of the Whareama Basin a rather continuous topographic barrier (emerged or submerged)
920 to the east, most probably in the southward continuation of Cape Turnagain (Figure 16). Such ridge was
921 likely controlled by the underlying Whakataki-Turnagain Fault complex to the north, laterally evolving into
922 the Flat Point-Whakataki Fault complex to the south (Figure 3).

923 Finally, from ca. 15 Ma, the Hikurangi Margin is inferred to have undergone a major change in tectonic
924 regime, entering into a period of generalised subsidence, after 10 Ma of active folding and reverse faulting
925 (Chanier and Ferrière 1989; Chanier and Ferrière 1991; Rait et al. 1991; Chanier et al. 1999; Nicol et al.
926 2002; Bailleul et al. 2007; Nicol et al. 2007; Bailleul et al. 2013; Malie et al. 2017; McArthur et al. 2019).
927 However, we just demonstrated (see 6.2) that the southern portion of the Hikurangi Margin was still
928 dominated by shortening and uplift during the Middle Miocene, thereby delaying the age for the onset of
929 subsidence in this region. In the Akitio Basin, the work of Bailleul et al. (2013) supports this result, with a
930 previously established younger subsidence starting at 13.2 Ma. In the Whareama Basin, in the absence
931 of other stratigraphic markers, the age of the MTDs (mid Lillburnian, ca. 14 Ma) can be used as a guide
932 to propose that the subsidence did not start before, at least, 14 Ma. For the Te Wharau Basin, whilst the
933 first recordings of subsidence date from 15 Ma (Chanier et al. 1992; Chanier et al. 1999), periods of active
934 tectonics persisted until the end of the Middle Miocene, particularly affecting the structures to the east
935 (Crundwell 1987). The MTDs spanned the Middle Miocene, Lillburnian and thus cannot be used to
936 precisely refine the age of the generalised subsidence in the Te Wharau Basin. Chanier et al. (1999)
937 observed that this major change in tectonic regime gradually occurred along the margin. We here offer
938 an additional insight as to the subsidence timeframe in the Whareama Basin, shifting the starting age
939 from 15 Ma to 14 Ma at minima.

6.4. Implications for mass-transport deposit nomenclature

941 Mass-wasting *attached* systems can be divided into two types (Moscardelli and Wood 2008; Moscardelli
942 and Wood 2015). The *shelf-attached* systems are essentially sourced by shelf-edge deltas whose stability
943 is mainly controlled by sea-level changes and sedimentation rates whereas the *slope-attached* systems
944 result from isolated, catastrophic sediment collapse(s) typically related to gas-hydrate dissociation and
945 or tectonic activity (e.g., earthquakes) (Moscardelli and Wood 2008; Moscardelli and Wood 2015). The
946 latter will successfully destabilise huge volumes of sediments simultaneously whereas the former will
947 involve multiple, semi-uninterrupted episodes of mass-failure. As highlighted by Moscardelli and Wood
948 (2015), characterising if a system is *shelf-* or *slope-attached* is particularly critical since it does not only
949 inform on the potential sourcing areas but also helps to better predict the impending causal mechanisms
950 and modalities of development.

951 Whether or not the shelf-derived MTDs described in this study correspond to the *shelf-attached* or *slope-*
952 *attached* nomenclature is uncertain. The deposits result from the regional destabilisation of neritic shelfal
953 environments, however there is no evidence of a shelf-edge delta that could have fed such a system in
954 the Hikurangi Margin. In fact, the Hikurangi shelfal environments are often referred to as mixed
955 siliciclastic-carbonate systems formed in association with margin uplift and where the carbonates
956 accumulated on a narrow shelf(ves) receiving recurrent terrigenous input from the hinterland (Caron et
957 al. 2004; Bailleul et al. 2007; Bailleul et al. 2013). As previously discussed, the destabilisation and
958 collapse of these shelfal environments most likely resulted from the generation and destruction of
959 oversteepened slopes controlled by tectonic activity (shortening, uplift and seismicity) rather than
960 changes in eustatic level (see 6.2). The multiple, successive mass-wasting occurrences recorded at
961 outcrop do not point toward an isolated catastrophic event but a series of semi-continuous events with a
962 regional footprint. Similar divergences with such classification have been observed elsewhere in the world
963 in similar tectonically active convergent settings (e.g., in the Sinu fold belt, offshore Colombia (Romero-
964 Otero et al. 2010; Ortiz-Karpf et al. 2018)).

965 We therefore propose that notwithstanding sea-level changes and high sedimentation rates as causal
966 mechanisms (Posamentier and Walker 2006; Moscardelli and Wood 2008; Moscardelli and Wood 2015;
967 and references within), recurrent tectonic activity (shortening, uplift and related seismicity) along active
968 margins also has potential to trigger large-scale shelf(ves) destabilisation and collapses. Therefore,
969 although these systems, sourced from the shelf, seem to preferentially occur at mature stages of
970 convergent margin development (Underwood and Bachman 1982; Bailleul et al. 2007; Vinnels et al. 2010;

971 [Ortiz-Karpf et al. 2018](#)), they will not always post-date the main phases of active tectonics (*i.e.*, can be
972 syn-kinematic) as suggested by [Ortiz-Karpf et al. \(2018\)](#).

973

ACCEPTED MANUSCRIPT

975

976 (1) Sea-level changes and high sedimentation rates are commonly inferred to be the main causal
977 mechanisms for large-scale continental shelf(ves) collapses (*i.e.*, *shelf-attached* systems),
978 thereby underestimating the role of tectonics. This study demonstrates that periods of tectonic
979 activity (shortening, uplift and related seismicity) act as another causal mechanism to consider
980 for large-scale shelf failure. In fact, recurring tectonic motion in compressional settings (*e.g.*,
981 active margins) can not only affect the basin-bounding structures and control the development
982 of the shelfal environments but also drive the recurrent generation and destruction of
983 oversteepened slopes, which can, in turn, favour repeated destabilisation and collapses of the
984 shelves.

985

986 (2) Short-lived periods (ca. 1 to 2 Ma) of tectonic activity can result in the emplacement of recurrent
987 mass-wasting products thereby reinforcing the importance of mass-wasting systems in deep-
988 marine fold-and-thrust belt evolution.

989

990 (3) Shelf-derived mass-wasting products are preferentially recorded and captured during mature
991 stages of trench-slope basin and subduction margin development. Yet, they do not always post-
992 date the main phases of active tectonics. They can result from the destabilisation and collapses
993 of shelves, either directly attached to the continent or potentially locally isolated, developing upon
994 and about actively fault-growing folds.

995

996 (4) The associated shelf-derived products have a regional footprint.

997

998 ○ Both sediment mass-movements (*e.g.*, slides, slumps) and mobilisation (*e.g.*, debris
999 flows) can occur. Yet, cohesive gravity flows dominate, eventually breaking down into a
1000 series of erosive, upward fining surges downslope.

1001

1002 ○ At outcrop scale, the MTDs always incorporate sediments and well-preserved to
1003 fragmented microfossils from neritic shelfal environments and mostly comprise (pre-
1004 and syn-kinematic) extraformational clasts. Their sizes generally oscillate between a ten
to a couple hundreds of metres (minimum thickness). Regionally extensive, they are

1005 deposited across several intra-slope basins, even though smaller, localized MTDs can
1006 also be punctually found.

1007 ○ At seismic scale, both sediment mass-movements and cohesive gravity flows are
1008 commonly observed. However, the seismic resolution does not allow identification of the
1009 multitude of downslope surges observed at outcrop-scale. The coalescing gravity flows
1010 will be commonly imaged as one single seismofacies, thereby missing the lateral and
1011 vertical facies variations. This will, in turn, have a significant impact for both the causal
1012 mechanism and stratigraphic predictions.

1013

1014 (5) Taphonomic analysis of the fossil content of MTDs is a powerful tool to gain additional knowledge
1015 on the transport and depositional processes of mass-wasting events. It also helps identifying and
1016 better characterising the source areas.

1017

1018 (6) Finally, MTDs can be used as a guide to help refining the tectonostratigraphic evolution of
1019 subduction complexes and their related trench-slope basins. Here, the analysis of the MTDs
1020 allowed us to:

1021 ○ Reconstruct the depositional systems and palaeogeography at a particular time: the
1022 Middle Miocene, Lillburnian not only staged the development of a regional mixed
1023 siliciclastic-carbonate shelfal domain across the south-western portion of the Hikurangi
1024 Margin but also recorded its coeval destabilisation, which resulted in the remobilisation
1025 and deposition of shelf-derived MTDs across several trench-slope basins (*i.e.*,
1026 Whareama, Te Wharau and Akitio Basins). The Whareama and Akitio Basins were likely
1027 connected at that time (one single trench-slope basin), sharing the same seaward border
1028 to the east, controlled by the underlying Whakataki-Turnagain Fault complex to the north,
1029 laterally evolving into the Flat Point-Whakataki Fault complex to the south.

1030 ○ Better characterise the Hikurangi Margin tectonic framework: previous studies have
1031 inferred that the margin underwent a major change in tectonic regime at ca. 15 Ma,
1032 entering into a period of generalised subsidence. However, this study demonstrates that
1033 the southern portion of the Hikurangi Margin was still dominated by shortening and uplift
1034 during the Middle Miocene, Lillburnian, and thus, that the subsidence did not start before,
1035 at least, ca. 14 Ma in the Whareama Basin.

1036 **8. ACKNOWLEDGEMENTS**

1037 We thank the Schlumberger HQ teams from London and Oslo, and more particularly Keith Tushingham
1038 and Mark Douglas for their initial support four years ago; without their backing, this work would have not
1039 been possible. Special thanks to Karen and John Barbour for making us feel like home during our stays
1040 at Homewood and for access to the study area. We kindly thank Pierre Malié and Andréa Barrier for their
1041 assistance during the fieldwork mission, as well as Romain Armand, François-Xavier Joanny and Pierre
1042 Saulet from UniLaSalle (France) for their amazing technical support on the GIS and outcrop modelling
1043 workflows. We also thank our colleagues from the Basins-Reservoirs-Resources B2R research unit
1044 (University of UniLaSalle, France) and from GNS Science (Lower Hutt, New Zealand) for thoughtful
1045 insights and discussions. Finally, we thank the guest-editor Lorna Strachan and Suzanne Bull for their
1046 helpful comments and suggestions, this paper also benefiting from feedback from an anonymous
1047 reviewer.

1048 **9. DISCLOSURE STATEMENT**

1049 No potential conflict of interest was reported by the author(s).

1050 **10. FUNDING**

1051 This research was funded by Schlumberger.

1052 **11. DATA AVAILABILITY STATEMENT**

1053 The data that support the findings of this study are openly available in figshare at:

1054 [https://figshare.com/articles/journal_contribution/Claussmann_et_al_NZJGG_Supplementary_material/](https://figshare.com/articles/journal_contribution/Claussmann_et_al_NZJGG_Supplementary_material/13614101)
1055 [13614101](https://figshare.com/articles/journal_contribution/Claussmann_et_al_NZJGG_Supplementary_material/13614101).

1056 **12. REFERENCES**

- 1057 Allen PA, Dorrell RM, Harlen OG, Thomas RE, McCaffrey WD. 2020. Pulse propagation in gravity
1058 currents. *Physics of Fluids*. 32(1):016603. <https://doi.org/10.1063/1.5130576>
- 1059 Alsop GI, Weinberger R, Marco S, Levi T. 2019. Identifying soft-sediment deformation in rocks. *Journal*
1060 *of Structural Geology*. 125:248–255. <https://doi.org/10.1016/j.jsg.2017.09.001>
- 1061 Alves TM. 2015. Submarine slide blocks and associated soft-sediment deformation in deep-water basins:
1062 A review. *Marine and Petroleum Geology*. 67:262–285. <https://doi.org/10.1016/j.marpetgeo.2015.05.010>
- 1063 Bailleul J, Caron V, Chanier F, Mahieux G, Malié P, Gagnaison C, Claussmann B, Potel S. Submitted.
1064 Combined tectonic and eustatic controls on the syn-subduction shelfal sedimentation of the Middle
1065 Miocene lower trench-slope of the Hikurangi thrust wedge (North Island, New Zealand). *New Zealand*
1066 *Journal of Geology and Geophysics*.
- 1067 Bailleul J, Chanier F, Ferrière J, Robin C, Nicol A, Mahieux G, Gorini C, Caron V. 2013. Neogene
1068 evolution of lower trench-slope basins and wedge development in the central Hikurangi subduction
1069 margin, New Zealand. *Tectonophysics*. 591:152–174. <https://doi.org/10.1016/j.tecto.2013.01.003>
- 1070 Bailleul J, Robin C, Chanier F, Guillocheau F, Field B, Ferrière J. 2007. Turbidite Systems in the Inner
1071 Forearc Domain of the Hikurangi Convergent Margin (New Zealand): New Constraints on the
1072 Development of Trench-Slope Basins. *Journal of Sedimentary Research*. 77(4):263–283.
1073 <https://doi.org/10.2110/jsr.2007.028>
- 1074 Ballance PF. 1976. Evolution of the Upper Cenozoic Magmatic Arc and plate boundary in northern New
1075 Zealand. *Earth and Planetary Science Letters*. 28(3):356–370.
1076 [https://doi.org/10.1016/0012-821X\(76\)90197-7](https://doi.org/10.1016/0012-821X(76)90197-7)
- 1077 Barnes PM, Ghisetti FC, Ellis S, Morgan JK. 2018. The role of protothrusts in frontal accretion and
1078 accommodation of plate convergence, Hikurangi subduction margin, New Zealand. *Geosphere*.
1079 14(2):440–468. <https://doi.org/10.1130/GES01552.1>
- 1080 Barnes PM, Lamarche G, Bialas J, Henrys S, Pecher I, Netzeband GL, Greinert J, Mountjoy JJ, Pedley
1081 K, Crutchley G. 2010. Tectonic and geological framework for gas hydrates and cold seeps on the
1082 Hikurangi subduction margin, New Zealand. *Marine Geology*. 272(1–4):26–48.
1083 <https://doi.org/10.1016/j.margeo.2009.03.012>
- 1084 Barnes PM, Nicol A, Harrison T. 2002. Late Cenozoic evolution and earthquake potential of an active
1085 listric thrust complex above the Hikurangi subduction zone, New Zealand. *GSA Bulletin*. 114(11):1379–
1086 1405. [https://doi.org/10.1130/0016-7606\(2002\)114<1379:LCEAEP>2.0.CO;2](https://doi.org/10.1130/0016-7606(2002)114<1379:LCEAEP>2.0.CO;2)
- 1087 Barrier L, Nalpas T, Gapais D, Proust J-N. 2013. Impact of synkinematic sedimentation on the geometry
1088 and dynamics of compressive growth structures: Insights from analogue modelling. *Tectonophysics*.
1089 608:737–752. <https://doi.org/10.1016/j.tecto.2013.08.005>
- 1090 Barton M, O’Byrne C, Pirmez C, Prather BE, van der Vlugt F, Alpak FO, Sylvester Z. 2010. Turbidite
1091 Channel Architecture: Recognizing and Quantifying the Distribution of Channel-base Drapes Using Core
1092 and Dipmetre Data. *AAPG Memoir*. 92:195–210. <https://doi.org/10.1306/13181284M923289>

- 1093 Beavan J, Tregoning P, Bevis M, Kato T, Meertens C. 2002. Motion and rigidity of the Pacific Plate and
1094 implications for plate boundary deformation. *Journal of Geophysical Research: Solid Earth*.
1095 107(B10):ETG 19-1-ETG 19-15. <https://doi.org/10.1029/2001JB000282>
- 1096 Bland KJ, Uruski CI, Isaac MJ. 2015. Pegasus Basin, eastern New Zealand: A stratigraphic record of
1097 subsidence and subduction, ancient and modern. *New Zealand Journal of Geology and Geophysics*.
1098 58(4):319–343. <https://doi.org/10.1080/00288306.2015.1076862>
- 1099 Bradshaw JD. 1989. Cretaceous geotectonic patterns in the New Zealand Region. *Tectonics*. 8(4):803–
1100 820. <https://doi.org/10.1029/TC008i004p00803>
- 1101 Bull S, Browne GH, Arnot MJ, Strachan LJ. 2020. Influence of mass transport deposit (MTD) surface
1102 topography on deep-water deposition: an example from a predominantly fine-grained continental margin,
1103 New Zealand. *Geological Society, London, Special Publications*. 500(1):147–171.
1104 <https://doi.org/10.1144/SP500-2019-192>
- 1105 Bull S, Cartwright J, Huuse M. 2009. A review of kinematic indicators from mass-transport complexes
1106 using 3D seismic data. *Marine and Petroleum Geology*. 26:1132–1151.
- 1107 Burgreen B, Graham S. 2014. Evolution of a deep-water lobe system in the Neogene trench-slope setting
1108 of the East Coast Basin, New Zealand: Lobe stratigraphy and architecture in a weakly confined basin
1109 configuration. *Marine and Petroleum Geology*. 54:1–22. <https://doi.org/10.1016/j.marpetgeo.2014.02.011>
- 1110 Cape CD, Lamb SH, Vella P, Wells PE, Woodward DJ. 1990. Geological structure of Wairarapa Valley,
1111 New Zealand, from seismic reflection profiling. *Journal of the Royal Society of New Zealand*. 20(1):85–
1112 105. <https://doi.org/10.1080/03036758.1990.10426734>
- 1113 Carey JM, Crutchley GJ, Mountjoy JJ, Petley DN, McSaveney MJ, Lyndsell B. 2019. Slow episodic
1114 movement driven by elevated pore-fluid pressures in shallow subaqueous slopes. *Geomorphology*.
1115 329:99–107. <https://doi.org/10.1016/j.geomorph.2018.12.034>
- 1116 Caron V. 2011. Contrasted textural and taphonomic properties of high-energy wave deposits cemented
1117 in beachrocks (St. Bartholomew Island, French West Indies). *Sedimentary Geology*. 237(3):189–208.
1118 <https://doi.org/10.1016/j.sedgeo.2011.03.002>
- 1119 Caron V, Bailleul J, Chanier F, Mahieux G. Accepted. Episodes of seabed rise and rapid drowning as
1120 primary controls for the development of regressive and transgressive heterozoan carbonates and
1121 rhodolitic limestones in a tectonically-active setting (Early Miocene, Wairarapa region, New Zealand).
1122 *New Zealand Journal of Geology and Geophysics*.
- 1123 Caron V, Bailleul J, Chanier F, Mahieux G, Joanny F-X. 2019. A new analytical procedure to graphically
1124 characterise the taphonomic properties of skeletal carbonates. An example from Miocene limestones of
1125 new zealand. *PALAIOS*. 34(8):364–381. <https://doi.org/10.2110/palo.2018.101>
- 1126 Caron V, Nelson CS, Kamp PJJ. 2004. Contrasting carbonate depositional systems for Pliocene cool-
1127 water limestones cropping out in central Hawke's Bay, New Zealand. *New Zealand Journal of Geology
and Geophysics*. 47(4):697–717. <https://doi.org/10.1080/00288306.2004.9515084>
- 1129 Chanier F. 1991. Le prisme d'accrétion Hikurangi : un témoin de l'évolution géodynamique d'une marge
1130 active pacifique (Nouvelle-Zélande) [PhD Thesis]. France: Université de Lille 1.

- 1131 Chanier F, Ferrière J. 1989. On the existence of major tangential movements in the East Coast Range of
 1132 New Zealand: their significance within the framework of Pacific plate subduction. *Comptes Rendus de*
 1133 *l'Académie des Sciences - Séries II - Earth and Planetary Science*. 308(2):1645–1650.
- 1134 Chanier F, Ferrière J. 1991. From a passive to an active margin: Tectonic and sedimentary processes
 1135 linked to the birth of an accretionary prism (Hikurangi Margin, New Zealand). *Société Géologique de*
 1136 *France*. 162(4):649–660. <https://doi.org/10.2113/gssgfbull.162.4.649>
- 1137 Chanier F, Ferrière J, Angelier J. 1992. Extension and tectonic erosion in an accretionary prism: example
 1138 from the Hikurangi Prism, New Zealand. *Comptes Rendus de l'Académie des Sciences - Séries IIA -*
 1139 *Earth and Planetary Science*. 315(2):741–747.
- 1140 Chanier F, Ferrière J, Angelier J. 1999. Extensional deformation across an active margin, relations with
 1141 subsidence, uplift, and rotations: The Hikurangi subduction, New Zealand. *Tectonics*. 18(5):862–876.
 1142 <https://doi.org/10.1029/1999TC900028>
- 1143 Clark K, Howarth J, Litchfield N, Cochran U, Turnbull J, Dowling L, Howell A, Berryman K, Wolfe F. 2019.
 1144 Geological evidence for past large earthquakes and tsunamis along the Hikurangi subduction margin,
 1145 New Zealand. *Marine Geology*. 412:139–172. <https://doi.org/10.1016/j.margeo.2019.03.004>
- 1146 Couvin B, Georgiopoulou A, Mountjoy JJ, Amy L, Crutchley GJ, Brunet M, Cardona S, Gross F, Böttner
 1147 C, Krastel S, Pecher I. 2020. A new depositional model for the Tuaheni Landslide Complex, Hikurangi
 1148 Margin, New Zealand. *Geological Society, London, Special Publications*. 500(1):551–566.
 1149 <https://doi.org/10.1144/SP500-2019-180>
- 1150 Crundwell M. 1987. Neogene stratigraphy and geological history of the Wainuioru Valley, Eastern
 1151 Wairarapa, New Zealand. [BSc Thesis]. Wellington, New Zealand: Victoria University.
- 1152 Dawson AG, Stewart I. 2007. Tsunami deposits in the geological record. *Sedimentary Geology*.
 1153 200(3):166–183. <https://doi.org/10.1016/j.sedgeo.2007.01.002>
- 1154 Einsele G, Chough SK, Shiki T. 1996. Depositional events and their records—an introduction.
 1155 *Sedimentary Geology*. 104(1):1–9. [https://doi.org/10.1016/0037-0738\(95\)00117-4](https://doi.org/10.1016/0037-0738(95)00117-4)
- 1156 Felix M, Leszczyński S, Ślaczka A, Uchman A, Amy L, Peakall J. 2009. Field expressions of the
 1157 transformation of debris flows into turbidity currents, with examples from the Polish Carpathians and the
 1158 French Maritime Alps. *Marine and Petroleum Geology*. 26(10):2011–2020.
 1159 <https://doi.org/10.1016/j.marpetgeo.2009.02.014>
- 1160 Festa A, Ogata K, Pini GA, Dilek Y, Alonso JL. 2016. Origin and significance of olistostromes in the
 1161 evolution of orogenic belts: A global synthesis. *Gondwana Research*. 39:180–203.
 1162 <https://doi.org/10.1016/j.gr.2016.08.002>
- 1163 Festa A, Ogata K, Pini GA, Dilek Y, Codegone G. 2015. Late Oligocene–early Miocene olistostromes
 1164 (sedimentary mélanges) as tectono-stratigraphic constraints to the geodynamic evolution of the exhumed
 1165 Ligurian accretionary complex (Northern Apennines, NW Italy). *International Geology Review*. 57(5–8):1–
 1166 23.
- 1167 Festa A, Pini GA, Ogata K, Dilek Y. 2019. Diagnostic features and field-criteria in recognition of tectonic,
 1168 sedimentary and diapiric mélanges in orogenic belts and exhumed subduction-accretion complexes.
 1169 *Gondwana Research*. 74:7–30. <https://doi.org/10.1016/j.gr.2019.01.003>

- 1170 Field B, Uruski CI, Institute of Geological & Nuclear Sciences. 1997. Cretaceous-Cenozoic geology and
1171 petroleum systems of the East Coast region, New Zealand. New Zealand.
- 1172 Fonnesu M, Patacci M, Haughton PDW, Felletti F, McCaffrey WD. 2016. Hybrid Event Beds Generated
1173 By Local Substrate Delamination On A Confined-Basin Floor. *Journal of Sedimentary Research*.
1174 86(8):929–943. <https://doi.org/10.2110/jsr.2016.58>
- 1175 Frey-Martínez J, Cartwright J, Hall B. 2005. 3D seismic interpretation of slump complexes: examples
1176 from the continental margin of Israel. *Basin Research*. 17(1):83–108.
- 1177 Galloway WE. 1998. Siliciclastic Slope and Base-of-Slope Depositional Systems: Component Facies,
1178 Stratigraphic Architecture, and Classification. *AAPG Bulletin*. 824:569–595.
1179 <https://doi.org/10.1306/1D9BC5BB-172D-11D7-8645000102C1865D>
- 1180 Gamberi F, Rovere M, Marani M. 2011. Mass-transport complex evolution in a tectonically active margin
1181 (Gioia Basin, Southeastern Tyrrhenian Sea). *Marine Geology*. 279(1–4):98–110.
1182 <https://doi.org/10.1016/j.margeo.2010.10.015>
- 1183 Graveleau F, Malavieille J, Dominguez S. 2012. Experimental modelling of orogenic wedges: A review.
1184 *Tectonophysics*. 538–540:1–66. <https://doi.org/10.1016/j.tecto.2012.01.027>
- 1185 Hampton MA, Lee HJ, Locat J. 1996. Submarine landslides. *Reviews of Geophysics*. 34(1):33–59.
1186 <https://doi.org/10.1029/95RG03287>
- 1187 Haq BU, Hardenbol J, Vail PR. 1987. Chronology of Fluctuating Sea Levels Since the Triassic. *Science*.
1188 235(4793):1156–1167. <https://doi.org/10.1126/science.235.4793.1156>
- 1189 Henstra GA, Grundvåg S-A, Johannessen EP, Kristensen TB, Midtkandal I, Nystuen JP, Rotevatn A,
1190 Surlyk F, Sæther T, Windelstad J. 2016. Depositional processes and stratigraphic architecture within a
1191 coarse-grained rift-margin turbidite system: The Wollaston Forland Group, east Greenland. *Marine and*
1192 *Petroleum Geology*. 76:187–209. <https://doi.org/10.1016/j.marpetgeo.2016.05.018>
- 1193 Iverson RM. 1997. The physics of debris flows. *Reviews of Geophysics*. 35(3):245–296.
1194 <https://doi.org/10.1029/97RG00426>
- 1195 Johansen A. 1999. The geology of the upper Tinui Valley, Wairarapa, New Zealand. [BSc Thesis].
1196 Wellington, New Zealand: Victoria University.
- 1197 Johnson AM. 1984. Debris flow. In: Brunsten D, Prior DB, editors. *Slope Instability*. New York, America:
1198 Wiley and Sons; p. 257–361.
- 1199 Jones OT. 1944. The compaction of muddy sediments. *Quarterly Journal of the Geological Society*.
1200 100(1–4):137–160. <https://doi.org/10.1144/GSL.JGS.1944.100.01-04.09>
- 1201 Karig DE, Moore GF, Curray JR, Lawrence MB. 1980. Morphology and shallow structure of the lower
1202 trench slope off Nias Island, Sunda Arc. In: Hayes DE, editor. *The Tectonic and Geologic Evolution of*
1203 *Southeast Asian Seas and Islands*. Washington, America; p. 179–208.
- 1204 Kidwell SM. 1989. Stratigraphic Condensation of Marine Transgressive Records: Origin of Major Shell
1205 Deposits in the Miocene of Maryland. *The Journal of Geology*. 97(1):1–24.

- 1206 Kneller B. 1995. Beyond the turbidite paradigm: physical models for deposition of turbidites and their
 1207 implications for reservoir prediction. Geological Society, London, Special Publications. 94(1):31–49.
 1208 <https://doi.org/10.1144/GSL.SP.1995.094.01.04>
- 1209 Kneller B, McCaffrey W. 1999. Depositional effects of flow nonuniformity and stratification within turbidity
 1210 currents approaching a bounding slope; deflection, reflection, and facies variation. Journal of
 1211 Sedimentary Research. 69(5):980–991. <https://doi.org/10.2110/jsr.69.980>
- 1212 Kuenen PhH. 1964. Deep-Sea Sands and Ancient Turbidites. In: Bouma AH, Brouwer A, editors.
 1213 Developments in Sedimentology. Vol. 3. Netherlands: Elsevier; p. 3–33. [https://doi.org/10.1016/S0070-4571\(08\)70953-1](https://doi.org/10.1016/S0070-4571(08)70953-1)
- 1215 Lamarche G, Joanne C, Collot J-Y. 2008. Successive, large mass-transport deposits in the south
 1216 Kermadec fore-arc basin, New Zealand: The Matakaoa Submarine Instability Complex. Geochemistry,
 1217 Geophysics, Geosystems. 9(4):1–30. <https://doi.org/10.1029/2007GC001843>
- 1218 Lamb SH, Vella P. 1987. The last million years of deformation in part of the New Zealand plateboundary
 1219 zone. Journal of Structural Geology. 9(7):877–891. [https://doi.org/10.1016/0191-8141\(87\)90088-5](https://doi.org/10.1016/0191-8141(87)90088-5)
- 1220 Lee HJ. 2009. Timing of occurrence of large submarine landslides on the Atlantic Ocean margin. Marine
 1221 Geology. 264(1–2):53–64. <https://doi.org/10.1016/j.margeo.2008.09.009>
- 1222 Lee J, Begg J. 2002. Geology of the Wairarapa area. Institute of Geological & Nuclear Sciences 1:250
 1223 000 geological map: Institute of Geological & Nuclear Sciences Limited.
- 1224 Lehu R, Lallemand S, Hsu S-K, Babonneau N, Ratzov G, Lin AT, Dezileau L. 2015. Deep-sea
 1225 sedimentation offshore eastern Taiwan: Facies and processes characterisation. Marine Geology. 369:1–
 1226 18. <https://doi.org/10.1016/j.margeo.2015.05.013>
- 1227 Lewis KB, Barnes PM, Garlick RD. 1999. Central Hikurangi GeodyNZ swath maps: depths, texture and
 1228 geological interpretation.
- 1229 Lewis KB, Lallemand SE, Carter L. 2004. Collapse in a Quaternary shelf basin off East Cape, New
 1230 Zealand: Evidence for passage of a subducted seamount inboard of the Ruatoria giant avalanche. New
 1231 Zealand Journal of Geology and Geophysics. 47(3):415–429.
 1232 <https://doi.org/10.1080/00288306.2004.9515067>
- 1233 Lewis KB, Pettinga JR. 1993. The emerging, imbricate frontal wedge of the Hikurangi margin. In: Ballance
 1234 PF, editor. South Pacific sedimentary basins. Amsterdam, Netherlands: Elsevier Science; p. 225–250.
- 1235 Li KM, Zuo L, Nardelli V, Alves TM, Lourenço SDN. 2019. Morphometric signature of sediment particles
 1236 reveals the source and emplacement mechanisms of submarine landslides. Landslides. 16(4):829–837.
 1237 <https://doi.org/10.1007/s10346-018-01123-1>
- 1238 Lowe DR. 1982. Sediment gravity flows; II, Depositional models with special reference to the deposits of
 1239 high-density turbidity currents. Journal of Sedimentary Research. 52(1):279–297.
 1240 <https://doi.org/10.1306/212F7F31-2B24-11D7-8648000102C1865D>
- 1241 Malavieille J. 2010. Impact of erosion, sedimentation, and structural heritage on the structure and
 1242 kinematics of orogenic wedges: Analog models and case studies. GSAT. 20(1):4–10.
 1243 <https://doi.org/10.1130/GSATG48A.1>

- 1244 Malie P, Bailleul J, Chanier F, Toullec R, Mahieux G, Caron V, Field B, Mählmann RF, Potel S. 2017.
 1245 Spatial distribution and tectonic framework of fossil tubular concretions as onshore analogues of cold
 1246 seep plumbing systems, North Island of New Zealand. *Bulletin de la Société géologique de France*.
 1247 188(4):25. <https://doi.org/10.1051/bsgf/2017192>
- 1248 Martin RE. 1999. *Taphonomy: A Process Approach*. Cambridge, United Kingdom: Cambridge University
 1249 Press. <https://doi.org/10.1017/CBO9780511612381>
- 1250 McArthur AD, Bailleul J, Mahieux G, Clausmann B, Wunderlich A, McCaffrey WD. 2021. Deformation-
 1251 sedimentation feedback and the development of anomalously thick aggradational turbidite lobes:
 1252 subsurface and outcrop examples from the Hikurangi Margin, New Zealand. *Journal of Sedimentary
 1253 Research*. 91(4):362–389. <https://doi.org/10.2110/jsr.2020.013>
- 1254 McArthur AD, Clausmann B, Bailleul J, McCaffrey W, Clare A. 2019. Variation in syn-subduction
 1255 sedimentation patterns from inner to outer portions of deep-water fold and thrust belts: examples from
 1256 the Hikurangi subduction margin of New Zealand. *Geological Society, London, Special Publications*.
 1257 490:285–310. <https://doi.org/10.1144/SP490-2018-95>
- 1258 McArthur AD, Jolley DW, Hartley AJ, Archer SG, Lawrence HM. 2016. Palaeoecology of syn-rift
 1259 topography: A Late Jurassic footwall island on the Josephine Ridge, Central Graben, North Sea.
 1260 *Palaeogeogr Palaeoclimatol Palaeoecol*. 459:63–75. <https://doi.org/10.1016/j.palaeo.2016.06.033>
- 1261 McArthur AD, McCaffrey WD. 2019. Sedimentary architecture of detached deep-marine canyons:
 1262 Examples from the East Coast Basin of New Zealand. *Sedimentology*. 66(3):1067–1101.
 1263 <https://doi.org/10.1111/sed.12536>
- 1264 McHargue T, Pycrz MJ, Sullivan MD, Clark JD, Fildani A, Romans BW, Covault JA, Levy M, Posamentier
 1265 HW, Drinkwater NJ. 2011. Architecture of turbidite channel systems on the continental slope: Patterns
 1266 and predictions. *Marine and Petroleum Geology*. 28(3):728–743.
 1267 <https://doi.org/10.1016/j.marpetgeo.2010.07.008>
- 1268 Middleton GV, Hampton MA. 1973. Sediment Gravity Flows: Mechanics of Flow and Deposition. In:
 1269 Middleton GV, Bouma AH, editors. *Turbidites and Deep-Water Sedimentation*. Society of Economic
 1270 Paleontologists and Mineralogists Pacific Section Short Course; p. 1–38.
- 1271 Miller KG, Kominz MA, Browning JV, Wright JD, Mountain GS, Katz ME, Sugarman PJ, Cramer BS,
 1272 Christie-Blick N, Pekar SF. 2005. The Phanerozoic record of global sea-level change. *Science*.
 1273 310(5752):1293–1298. <https://doi.org/10.1126/science.1116412>
- 1274 Mohrig D, Ellis C, Parker G, Whipple KX, Hondzo M. 1998. Hydroplaning of subaqueous debris flows.
 1275 *GSA Bulletin*. 110(3):387–394. [https://doi.org/10.1130/0016-7606\(1998\)110<0387:HOSDF>2.3.CO;2](https://doi.org/10.1130/0016-7606(1998)110<0387:HOSDF>2.3.CO;2)
- 1276 Moore GF, Aung LT, Fukuchi R, Sample JC, Hellebrand E, Kopf A, Naing W, Than WM, Tun TN. 2019.
 1277 Tectonic, diapiric and sedimentary chaotic rocks of the Rakhine coast, western Myanmar. *Gondwana
 1278 Research*. 74:126–143. <https://doi.org/10.1016/j.gr.2019.04.006>
- 1279 Moore GF, Karig DE. 1976. Development of sedimentary basins on the lower trench slope. *Geology*.
 1280 4(11):693–697. [https://doi.org/10.1130/0091-7613\(1976\)4<693:DOSBOT>2.0.CO;2](https://doi.org/10.1130/0091-7613(1976)4<693:DOSBOT>2.0.CO;2)
- 1281 Mortimer N. 2004. New Zealand's Geological Foundations. *Gondwana Research*. 7(1):261–272.
 1282 [https://doi.org/10.1016/S1342-937X\(05\)70324-5](https://doi.org/10.1016/S1342-937X(05)70324-5)

- 1283 Moscardelli L, Wood L. 2008. New classification system for mass transport complexes in offshore
1284 Trinidad. *Basin Research*. 20(1):73–98. <https://doi.org/10.1111/j.1365-2117.2007.00340.x>
- 1285 Moscardelli L, Wood L. 2015. Morphometry of mass-transport deposits as a predictive tool. *GSA Bulletin*.
1286 128(1–2):47–80.
- 1287 Moscardelli LG, Wood LJ, Mann PC. 2006. Mass-transport complexes and associated processes in the
1288 offshore area of Trinidad and Venezuela. *AAPG Bulletin*. 90(7):1059–1088.
1289 <https://doi.org/10.1306/02210605052>
- 1290 Mulder T, Alexander J. 2001. The physical character of subaqueous sedimentary density flows and their
1291 deposits. *Sedimentology*. 48(2):269–299. <https://doi.org/10.1046/j.1365-3091.2001.00360.x>
- 1292 Mulder T, Cochonat P. 1996. Classification of offshore mass movements. *Journal of Sedimentary*
1293 *Research*. 66(1):43–57. <https://doi.org/10.1306/D42682AC-2B26-11D7-8648000102C1865D>
- 1294 Mulder T, Syvitski JPM, Migeon S, Faugères J-C, Savoye B. 2003. Marine hyperpycnal flows: initiation,
1295 behavior and related deposits. A review. *Marine and Petroleum Geology*. 20(6):861–882.
1296 <https://doi.org/10.1016/j.marpetgeo.2003.01.003>
- 1297 Naranjo-Vesga J, Ortiz-Karpf A, Wood L, Jobe Z, Paniagua-Arroyave JF, Shumaker L, Mateus-Tarazona
1298 D, Galindo P. 2020. Regional controls in the distribution and morphometry of deep-water gravitational
1299 deposits along a convergent tectonic margin. Southern Caribbean of Colombia. *Marine and Petroleum*
1300 *Geology*. 121:104639. <https://doi.org/10.1016/j.marpetgeo.2020.104639>
- 1301 Nardin TR, Hein FJ, Gorsline DS, Edwards BD. 1979. A review of mass movement processes, sediment
1302 and acoustic characteristics, and contrasts in slope and base-of-slope systems versus canyon-fan-basin
1303 floor systems. *SEPM Special Publication*. 27:61–73.
- 1304 Neef G. 1992. Geology of the Akitio area (1:50 000 metric sheet U25BD, east), northeastern Wairarapa,
1305 New Zealand. *New Zealand Journal of Geology and Geophysics*. 35(4):533–548.
1306 <https://doi.org/10.1080/00288306.1992.9514546>
- 1307 Neef G. 1999. Neogene development of the onland part of the forearc in northern Wairarapa, North Island,
1308 New Zealand: A synthesis. *New Zealand Journal of Geology and Geophysics*. 42(1):113–135.
1309 <https://doi.org/10.1080/00288306.1999.9514835>
- 1310 Nelson CH, Escutia C, Damuth JE, Cushman Twichell D. 2011. Interplay of Mass-Transport and
1311 Turbidite-System Deposits in Different Active Tectonic and Passive Continental Margin Settings: External
1312 and Local Controlling Factors. In: Shipp RC, Weimer P, Posamentier HW, editors. *Mass-Transport*
1313 *Deposits in Deepwater Settings*. Oklahoma, America: SEPM; p. 39–68.
- 1314 Nemeč W. 1990. Aspects of Sediment Movement on Steep Delta Slopes. In: Collela A, Prior DB, editors.
1315 *Coarse-Grained Deltas*. Oxford, United Kingdom: John Wiley & Sons, Ltd; p. 29–73.
1316 <https://doi.org/10.1002/9781444303858.ch3>
- 1317 Nemeč W, Steel RJ. 1984. Alluvial and Coastal Conglomerates: Their Significant Features and Some
1318 Comments on Gravelly Mass-Flow Deposits. In: Koster EH, Steel RJ, editors. *Sedimentology of Gravels*
1319 *and Conglomerates, Memoir 10*. Canada: Canadian Society of Petroleum Geologists; p. 1–31.
- 1320 Nicol A, Mazengarb C, Chanier F, Rait G, Uruski C, Wallace L. 2007. Tectonic evolution of the active
1321 Hikurangi subduction margin, New Zealand, since the Oligocene. *Tectonics*. 26(4):1–24.

- 1322 <https://doi.org/10.1029/2006TC002090>
- 1323 Nicol A, VanDissen R, Vella P, Alloway B, Melhuish A. 2002. Growth of contractional structures during
1324 the last 10 m.y. at the southern end of the emergent Hikurangi forearc basin, New Zealand. New Zealand
1325 Journal of Geology and Geophysics. 45(3):365–385. <https://doi.org/10.1080/00288306.2002.9514979>
- 1326 Noda A. 2018. Forearc Basin Stratigraphy and Interactions With Accretionary Wedge Growth According
1327 to the Critical Taper Concept. Tectonics. 37(3):965–988. <https://doi.org/10.1002/2017TC004744>
- 1328 Ogata K, Festa A, Pini GA, Alonso JL. 2019. Submarine Landslide Deposits in Orogenic Belts:
1329 Olistostromes and Sédimentary Mélanges. In: Ogata K, Festa A, Pini GA, editors. Submarine Landslides:
1330 Subaqueous Mass Transport Deposits from Outcrops to Seismic Profiles. America: American
1331 Geophysical Union (AGU); p. 1–26. <https://doi.org/10.1002/9781119500513.ch1>
- 1332 Ogata K, Pogačnik Ž, Pini GA, Tunis G, Festa A, Camerlenghi A, Rebesco M. 2014. The carbonate mass
1333 transport deposits of the Paleogene Friuli Basin (Italy/Slovenia): Internal anatomy and inferred genetic
1334 processes. Marine Geology. 356:88–110. <https://doi.org/10.1016/j.margeo.2014.06.014>
- 1335 Ortiz-Karpf A, Hodgson DM, Jackson CA-L, McCaffrey WD. 2018. Mass-transport complexes as markers
1336 of deep-water fold-and-thrust belt evolution: insights from the southern Magdalena fan, offshore
1337 Colombia. Basin Research. 30(S1):65–88. <https://doi.org/10.1111/bre.12208>
- 1338 Perry CT. 1998. Grain susceptibility to the effects of microboring: implications for the preservation of
1339 skeletal carbonates. Sedimentology. 45(1):39–51. <https://doi.org/10.1046/j.1365-3091.1998.00134.x>
- 1340 Pettinga JR. 1982. Upper Cenozoic structural history, coastal Southern Hawke's Bay, New Zealand. New
1341 Zealand Journal of Geology and Geophysics. 25(2):149–191.
1342 <https://doi.org/10.1080/00288306.1982.10421407>
- 1343 Pickering KT, Corregidor J. 2005. Mass transport complexes and tectonic control on confined basin-floor
1344 submarine fans, Middle Eocene, south Spanish Pyrenees. Geological Society, London, Special
1345 Publications. 244(1):51–74. <https://doi.org/10.1144/GSL.SP.2005.244.01.04>
- 1346 Pierson TC. 1981. Dominant particle support mechanisms in debris flows at Mt Thomas, New Zealand,
1347 and implications for flow mobility. Sedimentology. 28(1):49–60. <https://doi.org/10.1111/j.1365-3091.1981.tb01662.x>
- 1349 Pilarczyk JE, Dura T, Horton BP, Engelhart SE, Kemp AC, Sawai Y. 2014. Microfossils from coastal
1350 environments as indicators of paleo-earthquakes, tsunamis and storms. Palaeogeography,
1351 Palaeoclimatology, Palaeoecology. 413:144–157. <https://doi.org/10.1016/j.palaeo.2014.06.033>
- 1352 Posamentier HW, Allen GP, editors. 1999. Siliciclastic Sequence Stratigraphy - Concepts and
1353 Applications. Oklahoma, America: SEPM Society for Sedimentary Geology.
- 1354 Posamentier HW, Kolla V. 2003. Seismic geomorphology and stratigraphy of depositional elements in
1355 deep-water settings. Journal of Sedimentary Research. 73(3):367–388.
- 1356 Posamentier HW, Martinsen OJ. 2011. The Character and Genesis of Submarine Mass-Transport
1357 Deposits: Insights from Outcrop and 3D Seismic Data. In: Shipp RC, Weimer P, Posamentier HW, editors.
1358 Mass-Transport Deposits in Deepwater Settings. Oklahoma, America: SEPM; p. 7–38.

- 1359 Posamentier HW, Walker RG. 2006. Deep-Water Turbidites and Submarine Fans. In: Posamentier HW,
1360 Walker RG, editors. *Facies Models Revisited*. Oklahoma, America: SEPM Special Publication 84; p. 397–
1361 520. <https://doi.org/10.2110/pec.06.84>
- 1362 Postma G, Nemeč W, Kleinspehn KL. 1988. Large floating clasts in turbidites: a mechanism for their
1363 emplacement. *Sedimentary Geology*. 58(1):47–61. [https://doi.org/10.1016/0037-0738\(88\)90005-X](https://doi.org/10.1016/0037-0738(88)90005-X)
- 1364 Prélat A, Hodgson DM, Flint SS. 2009. Evolution, architecture and hierarchy of distributary deep-water
1365 deposits: a high-resolution outcrop investigation from the Permian Karoo Basin, South Africa.
1366 *Sedimentology*. 56(7):2132–2154. <https://doi.org/10.1111/j.1365-3091.2009.01073.x>
- 1367 Raine JI, Beu A, Boyes A, Campbell H, Cooper R, Crampton J, Crundwell M, Hollis C, Morgans H,
1368 Mortimer N. 2015. New Zealand Geological Timescale NZGT 2015/1. *New Zealand Journal of Geology*
1369 *and Geophysics*. 58(4):398–403. <https://doi.org/10.1080/00288306.2015.1086391>
- 1370 Rait G, Chanier F, Waters DW. 1991. Landward- and seaward-directed thrusting accompanying the onset
1371 of subduction beneath New Zealand. *Geology*. 19(3):230–233. [https://doi.org/10.1130/0091-7613\(1991\)019<0230:LASDTA>2.3.CO;2](https://doi.org/10.1130/0091-7613(1991)019<0230:LASDTA>2.3.CO;2)
- 1373 Raymond LA. 2019. Perspectives on the roles of melanges in subduction accretionary complexes: A
1374 review. *Gondwana Research*. 74:68–89. <https://doi.org/10.1016/j.gr.2019.03.005>
- 1375 Reagan MT, Moridis GJ. 2008. Dynamic response of oceanic hydrate deposits to ocean temperature
1376 change. *Journal of Geophysical Research: Oceans*. 113(C12):1–21.
1377 <https://doi.org/10.1029/2008JC004938>
- 1378 Richet R, Chazottes V, Cabioch G, Frank N, S. Burr G. 2011. Microborer ichnocoenoses in Quaternary
1379 corals from New Caledonia: reconstructions of paleo-water depths and reef growth strategies in relation
1380 to environmental changes. *Quaternary Science Reviews*. 30(19):2827–2838.
1381 <https://doi.org/10.1016/j.quascirev.2011.06.019>
- 1382 Romero-Otero GA, Slatt RM, Pirmez C. 2010. Detached and Shelf-Attached Mass Transport Complexes
1383 on the Magdalena Deepwater Fan. In: Mosher DC, Shipp RC, Moscardelli L, Chaytor JD, Baxter CDP,
1384 Lee HJ, Urgeles R, editors. *Submarine Mass Movements and Their Consequences*. Dordrecht,
1385 Netherlands: Springer Netherlands; p. 593–606. https://doi.org/10.1007/978-90-481-3071-9_48
- 1386 Schlager W, Camber O. 1986. Submarine slope angles, drowning unconformities, and self-erosion of
1387 limestone escarpments. *Geology*. 14(9):762–765.
1388 [https://doi.org/10.1130/0091-7613\(1986\)14<762:SSADUA>2.0.CO;2](https://doi.org/10.1130/0091-7613(1986)14<762:SSADUA>2.0.CO;2)
- 1389 Sobiesiak MS, Kneller B, Alsop GI, Milana JP. 2018. Styles of basal interaction beneath mass transport
1390 deposits. *Marine and Petroleum Geology*. 98:629–639. <https://doi.org/10.1016/j.marpetgeo.2018.08.028>
- 1391 Spörli KB. 1980. New Zealand and Oblique-Slip Margins: Tectonic Development up to and during the
1392 Cainozoic. In: Ballance PF, Reading HG, editors. *Sedimentation in Oblique-Slip Mobile Zones*. United
1393 Kingdom: John Wiley & Sons, Ltd; p. 147–170. <https://doi.org/10.1002/9781444303735.ch9>
- 1394 Storti F, McClay K. 1995. Influence of syntectonic sedimentation on thrust wedges in analogue models.
1395 *Geology*. 23(11):999–1002. [https://doi.org/10.1130/0091-7613\(1995\)023<0999:IOSSOT>2.3.CO;2](https://doi.org/10.1130/0091-7613(1995)023<0999:IOSSOT>2.3.CO;2)
- 1396 Stow DAV. 1986. Deep clastic seas. In: Reading HG, editor. *Sedimentary Environments and Facies*. 2nd
1397 edition. Oxford, United Kingdom: Blackwell Scientific Publications; p. 399–444.

- 1398 Strachan LJ. 2008. Flow transformations in slumps: a case study from the Waitemata Basin, New
1399 Zealand. *Sedimentology*. 55(5):1311–1332. <https://doi.org/10.1111/j.1365-3091.2007.00947.x>
- 1400 Strasser M, Moore GF, Kimura G, Kopf AJ, Underwood MB, Guo J, Screaton EJ. 2011. Slumping and
1401 mass transport deposition in the Nankai fore arc: Evidence from IODP drilling and 3-D reflection seismic
1402 data. *Geochemistry, Geophysics, Geosystems*. 12(5):1–24. <https://doi.org/10.1029/2010GC003431>
- 1403 Talling PJ, Masson DG, Sumner EJ, Malgesini G. 2012. Subaqueous sediment density flows:
1404 Depositional processes and deposit types. *Sedimentology*. 59(7):1937–2003.
1405 <https://doi.org/10.1111/j.1365-3091.2012.01353.x>
- 1406 Underwood M, Moore G, Taira A, Klaus A, Wilson M, Fergusson C, Hirano S, Steurer J. 2003.
1407 Sedimentary and Tectonic Evolution of a Trench-Slope Basin in the Nankai Subduction Zone of
1408 Southwest Japan. *Journal of Sedimentary Research*. 73:589–602.
1409 <https://doi.org/10.1306/092002730589>
- 1410 Underwood MB, Bachman SB. 1982. Sedimentary facies associations within subduction complexes.
1411 Geological Society, London, Special Publications. 10(1):537–550.
1412 <https://doi.org/10.1144/GSL.SP.1982.010.01.35>
- 1413 Underwood MB, Moore GF. 1995. Trenches and trench-slope basins. In: Busby CJ, Ingersoll RV, editors.
1414 *Tectonics of sedimentary basins*. Oxford, United Kingdom: Blackwell Science; p. 179–219.
- 1415 Urgeles R, Camerlenghi A. 2013. Submarine landslides of the Mediterranean Sea: Trigger mechanisms,
1416 dynamics, and frequency-magnitude distribution. *Journal of Geophysical Research: Earth Surface*.
1417 118(4):2600–2618. <https://doi.org/10.1002/2013JF002720>
- 1418 Urlaub M, Talling PJ, Masson DG. 2013. Timing and frequency of large submarine landslides:
1419 implications for understanding triggers and future geohazard. *Quaternary Science Reviews*. 72:63–82.
1420 <https://doi.org/10.1016/j.quascirev.2013.04.020>
- 1421 Vinnels JS, Butler RWH, McCaffrey WD, Paton DA. 2010. Depositional processes across the Sinú
1422 Accretionary Prism, offshore Colombia. *Marine and Petroleum Geology*. 27(4):794–809.
1423 <https://doi.org/10.1016/j.marpetgeo.2009.12.008>
- 1424 Watson SJ, Mountjoy JJ, Crutchley GJ. 2020. Tectonic and geomorphic controls on the distribution of
1425 submarine landslides across active and passive margins, eastern New Zealand. Geological Society,
1426 London, Special Publications. 500:477–494. <https://doi.org/10.1144/SP500-2019-165>
- 1427 Westoby MJ, Brasington J, Glasser NF, Hambrey MJ, Reynolds JM. 2012. ‘Structure-from-Motion’
1428 photogrammetry: A low-cost, effective tool for geoscience applications. *Geomorphology*. 179:300–314.
1429 <https://doi.org/10.1016/j.geomorph.2012.08.021>
- 1430 Woodcock NH. 1979. The use of slump structures as palaeoslope orientation estimators. *Sedimentology*.
1431 26(1):83–99. <https://doi.org/10.1111/j.1365-3091.1979.tb00339.x>
- 1432 Zanuttigh B, Lamberti A. 2007. Instability and surge development in debris flows. *Reviews of Geophysics*.
1433 45(3). <https://doi.org/10.1029/2005RG000175>
- 1434 Zuschin M, Stachowitsch M, Stanton RJ. 2003. Patterns and processes of shell fragmentation in modern
1435 and ancient marine environments. *Earth-Science Reviews*. 63(1):33–82. [https://doi.org/10.1016/S0012-8252\(03\)00014-X](https://doi.org/10.1016/S0012-8252(03)00014-X)

1437 13. FIGURES

1438 Figure 1: Generic model for trench-slope systems. Evolving structural style towards the trench influences the generation of
1439 accommodation space and sediment pathways. (g): Failure of the regional continental shelf and upper-slope regions will
1440 source attached mass-wasting systems (*sensu* Moscardelli and Wood 2008) and thus large-scale mass-transport deposits.
1441 (h): Collapse of the local thrust-related slopes will feed detached systems (*sensu* Moscardelli and Wood 2008), characterised
1442 by smaller, localized mass-transport deposits. Modified from McArthur et al. (2019).

1443 Figure 2: (A): Plate tectonic setting of New Zealand. (B): Major subduction-related morphostructural features of the Hikurangi
1444 Margin. Black arrows show present-day relative plate motion between the Pacific and Australian plates from Beavan et al.
1445 (2002). See (C) for the a – b general cross-section of the Hikurangi subduction complex. (C.R – Coastal Ranges). Modified
1446 after Chanier et al. (1999); Bailleul et al. (2007, 2013).

1447 Figure 3: Bathymetric map (Lewis et al. 1999) and onshore structural map (modified from Chanier et al. (1999), Lee and Begg
1448 (2002) and Bailleul et al. (2013)) of the southern Hikurangi subduction wedge. The offshore area includes the location of the
1449 well Titihaoa-1. Locations of the fault complexes = (I): Adams-Tinui Fault complex, (II): Pukeroro Fault, (III): Flat Point-
1450 Whakataki Fault complex to the south, evolving into the Whakataki-Turnagain Fault complex to the north, (IV): Turnagain
1451 Fault from Malie et al. (2017). Location of the onshore sedimentological vertical sections displaying Middle Miocene [NZ stage:
1452 Lillburnian] shelfal deposits = (f): Fingerpost section, (m): Waihoki-Mangatiti section, (p): Pongaroa section, (t): Takiritini
1453 section from Bailleul et al. (2013) and Caron et al. (2019); (ms) : Mapapa stream section from Chanier (1991); (i): Tinui section
1454 from Johansen (1999) and Bailleul et al. (2013); (w): Wainuioru sections from Crundwell (1987) and Chanier (1991) and late
1455 Middle Miocene [NZ stage: Waiauan] shelfal deposits = (o): Oumukura section from Chanier (1991). Location of the onshore
1456 sedimentological vertical sections displaying Middle Miocene [NZ stage: Lillburnian] MTDs = (b): Branscombe section from
1457 Bailleul et al. (2013); (tw): Te Wharau road sections; (n): Ngaumu section, (r): Rangiora section; (s): Sefton Hills sections; (c):
1458 Craigie Lea section.

1459 Figure 4: Chronostratigraphic chart for the southern emerged portion of the Hikurangi subduction wedge. Lithostratigraphy
1460 details adapted from Chanier (1991), Chanier and Ferrière (1991), Field et al. (1997), Lee and Begg (2002) and Bland et al.
1461 (2015); and detailing the pre- and syn-Hikurangi subduction series. Regional tectonism adapted from Chanier et al. (1999),
1462 Bailleul et al. (2013) and Malie et al. (2017). New Zealand stages after Raine et al. (2015) showing the equivalence with the
1463 international stages.

1464 Figure 5: Satellite map from World Imagery (ESRI), and onshore geological map from Chanier (1991) of the Te Wharau and
1465 Whareama Basin areas. Location of the drone acquisition and related 3D outcrop model = (s-1): Sefton Hills section. Location
1466 of the onshore sedimentological vertical sections displaying Middle Miocene [NZ stage: Lillburnian] shelfal deposits = (ms):
1467 Mapapa stream section from Chanier (1991), (w): Wainuioru sections from Crundwell (1987) and Chanier (1991) and late
1468 Middle Miocene [NZ stage stage: Waiauan] shelfal deposits = (o): Oumukura section from Chanier (1991). Location of the
1469 onshore sedimentological vertical sections displaying Middle Miocene [NZ stage stage: Lillburnian] MTDs = (c): Craigie Lea
1470 section, (n): Ngaumu section, (r): Rangiora section, (s-1, s-2): Sefton Hills sections, (tw-1, tw-2): Te Wharau road sections.

1471

1472 Figure 6: 3D outcrop model (top) and interpretation (bottom) of the Sefton Hills coastal outcrop (section-1). The letters refer
1473 to some of the architectural elements that supported the interpretations and which are detailed in Figure 8 and Figure 9.
1474 Stereoplots (Schmidt, lower hemisphere) highlight the palaeocurrents measured in the turbidites (Fa1g) as well as the fold
1475 axis and planes of the slump-related folds measured in the shelf-derived mass-transport deposits (Fa3p) after back-tilting of
1476 bedding planes to initial horizontal position (assuming cylindrical folding).

1477 Figure 7: Sedimentary section 01 (SS-01) recorded at the Sefton Hills outcrop locality (section s-1). Location is found on
1478 Figure 6. This section covers the upper part of the turbidite system and ends at the top of the first mass-wasting event which
1479 comprises three distinct lithofacies (DF, MF-1, MF-2, see Table 1). Details on the facies assemblages (FA) are provided in
1480 Table 1. All the palaeocurrent and slump measurements were taken along this section, respectively in the turbidites (Fa1g)
1481 and mass-transport deposits (Fa3p).

1482 Figure 8: Detailed views of the turbidite system's main architectural and sedimentary elements supporting the interpretation
1483 of the Sefton Hills 3D outcrop model (Figure 6). (a, b, g, h): thick to thin-bedded turbidites (Fa1g-c to Fa1g-a), comprising
1484 low-angle, concave-up, elongated bodies, sometimes slightly eroding into a basal mud drape and either showing fining and
1485 thinning upward trend or a simple mudstone cap; (a, d, e): contorted and dislocated turbidites between undeformed strata
1486 (Fa3l-s); (c, d): example of very thin- to medium-bedded turbidites from Fa1g-f; (e, f): example of sheet-like turbidites from
1487 Fa1s; (h): intra-turbidite debris flow mostly made of dislocated turbidites and some rare floating bioclasts (Fa3l-d).

1488 Figure 9: Detailed views of the shelf-derived mass-transport deposits (MTDs) main architectural and sedimentary elements
1489 supporting the interpretation of the Sefton Hills 3D outcrop model (Figure 6). (a, b, c, e, h): sharp, slightly erosional bases
1490 between distinct MTDs; (a): pluri-decametric turbidite raft incorporated in lithofacies MF-1 (second occurrence, MF-1b); (b,
1491 e): decametric mud clasts in lithofacies DF (second occurrence, DFb); (c): increasing mud clast content toward the top of
1492 lithofacies DF (first occurrence, DFa); (d): contorted thin-bedded turbidites in MF-2 (second occurrence, MF-2b); (f):
1493 overturned turbidite rafts and stratigraphic, locally structurally-controlled, contact between the MTDs and underlying turbidite
1494 system; (g): lateral continuity of the lithofacies MF-2 which can be traced over one kilometre to the south (Sefton Hills section
1495 s-2).

1496 Figure 10: Detailed description of the three main lithofacies (DF, MF-1 and MF-2) resulting from mass-wasting events that
1497 reworked shelf-derived material. Descriptions mainly summarise the observations made at the Sefton Hills locality (Whareama
1498 Basin) (Figure 6; Figure 7; Figure 9). Insights from the inland outcrops (Te Wharau Basin) were also incorporated. (a, h, n):
1499 matrix; (b, c, d, e, i, j, k, o): syn-subduction lithoclasts, *e.g.*, turbidites, mud clasts, shell bed clasts; (f, l): pre-subduction
1500 lithoclasts; (g, m): syn-subduction bioclasts, *i.e.*, skeletons from neritic faunal assemblages. Details in Table 1.

1501 Figure 11: Detailed views of Te Wharau Basin shelf-derived mass-transport deposits. (a): hinterland outcrop conditions,
1502 gravel-grade extraformational clasts within a silty mudstone matrix; (b): sub-angular cobble of shell bed clast and granules to
1503 pebbles of pre-subduction-dominated lithoclasts; (c): cobbles and boulders of pre- (*e.g.*, Torlesse material) and syn-
1504 subduction (*e.g.*, shell beds) lithoclasts; (d): chalky molluscan skeletons and lithoclasts from (predominantly) pre-subduction
1505 strata floating in a silty mudstone matrix; (e): oversized clast of bioclastic fine-grained sandstones from middle to outer shelf
1506 environments; (f): granules to cobbles of pre-subduction material that includes small, sub-rounded pebbles of already
1507 reworked Torlesse greywackes.

1508 Figure 12: Taphonomic characterisation of fossil remains described from 1x1 m area of outcrop at three different localities,
1509 using frequency histograms of the degree of alteration (e.g., low, moderate, high) for each category of skeleton damage (i.e.,
1510 fragmentation, abrasion, bioerosion) and encrustation. Lithofacies DF and MF-1 are described in details in Figure 10. Note
1511 that data for lithofacies MF-1 are only available for the finest skeletal fraction, coarser material being rare (n=3). Photographs
1512 of fossil remains illustrate the qualitative grading evaluation of taphonomic features in the field. Arrows in photographs 3 and
1513 4 point to bio-erosional features. Arrows in photographs 5 and 6 point to the analysed bioclasts. Scales in cm.

1514 Figure 13: Depositional processes and stratigraphic record of shelf-derived mass-wasting event at outcrop scale. Shelf failure
1515 will trigger both: (1) sediment mass-failure and mobilisation close to the source region(s), on the slope and (2) cohesive
1516 gravity flow deposition onto the basin floor: either as a single cohesive flow or eventually breaking down into a series of
1517 erosive, upward fining surges downslope. The wide range of lithofacies always incorporates reworked well-preserved to
1518 fragmented macrofaunal assemblages from neritic shelfal environments. They will also include extraformational clasts either
1519 (1) originating from the failed source area, (2) incorporated during the transport downslope and or (3) resulting from the
1520 partial destabilisation of the substratum upon which the shelfal environment was settling.

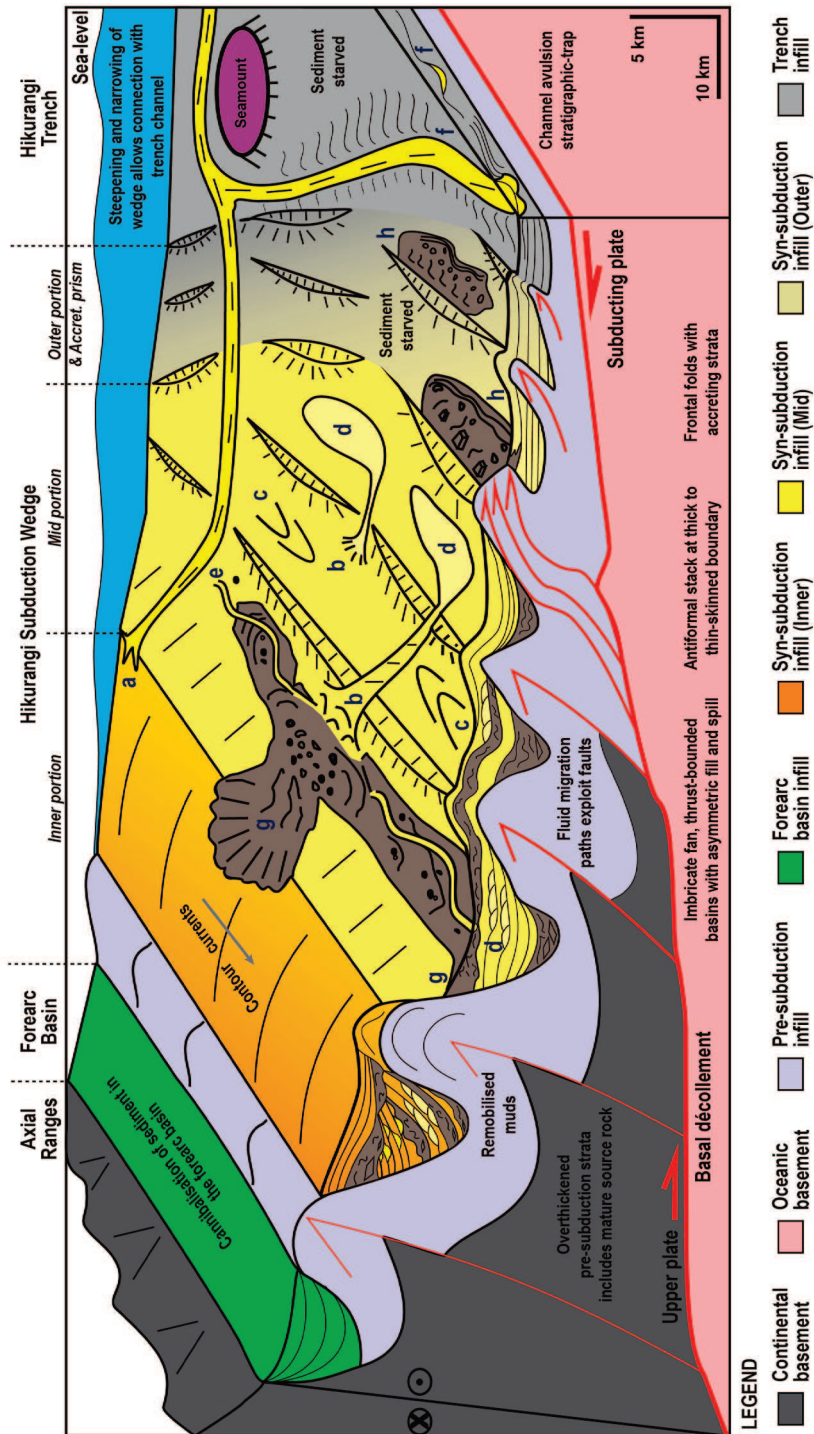
1521 Figure 14: Area vs length log-log plot showcasing the morphometric parameter values calculated for the mass-transport
1522 deposits (MTDs) described in this study using the sets of equations from [Moscardelli and Wood \(2015\)](#). See Appendix 4 for
1523 details on the equations, calculations and associated results for each of the occurrences. Whether using the general or specific
1524 set of equations, two main families of MTDs were identified using the nomenclature from [Moscardelli and Wood \(2015\)](#): (1)
1525 the Te Wharau Basin shelf-derived MTDs are best regrouped under the detached systems whereas (2) the Akitio and
1526 Whareama Basin shelf-derived MTDs under the attached systems.

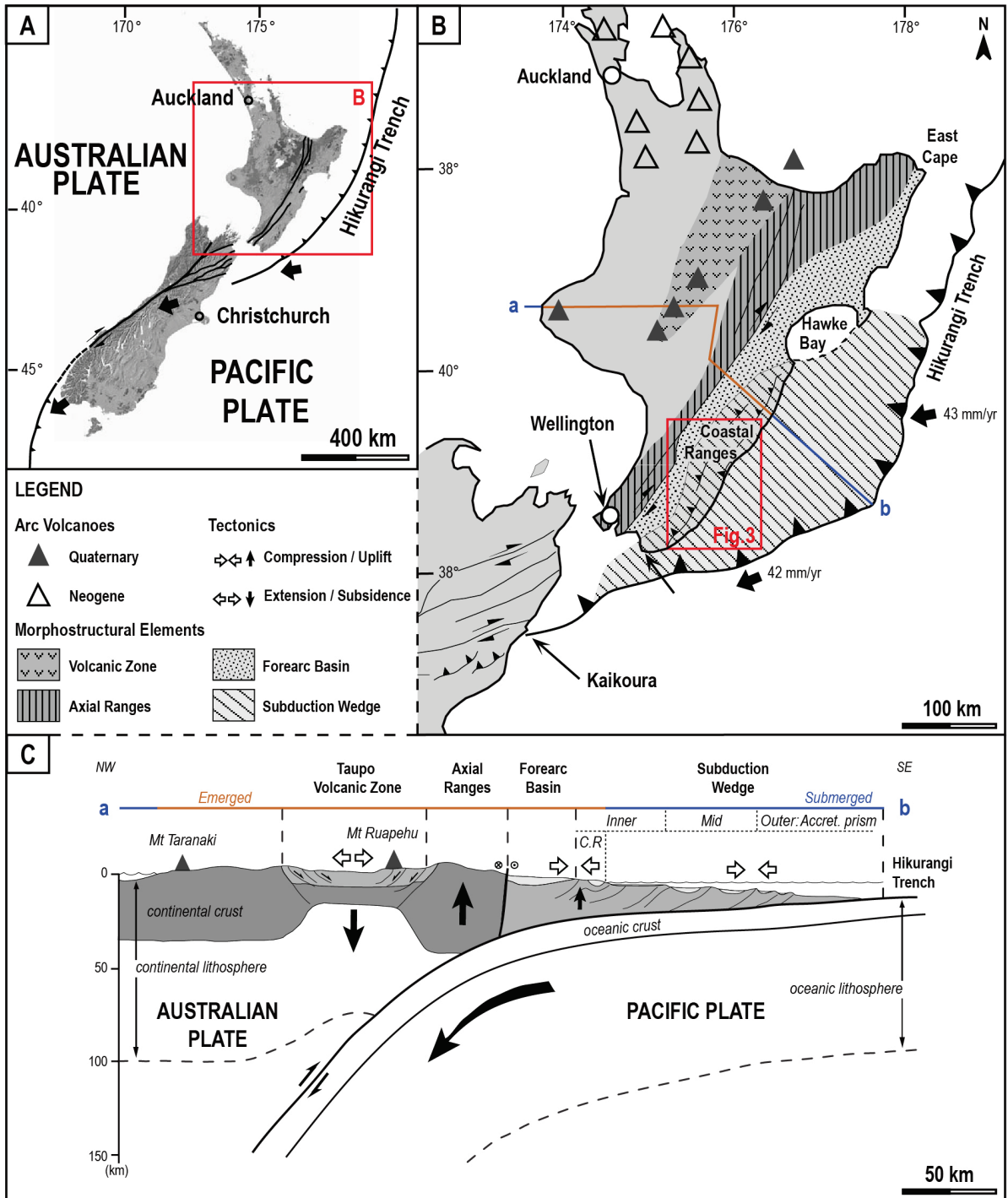
1527 Figure 15: Periods of repeated tectonic activity at basin-bounding structures will not only result in the development of neritic
1528 conditions and settlement of related faunal assemblages at shallow waters, but also favour the expansion of abrupt, unstable
1529 areas close to the shelf-margins installed above the thrust forelimb. The recurring generation and destruction of
1530 oversteepened slopes will in turn favour the repeated destabilisation and collapses of the shelves.

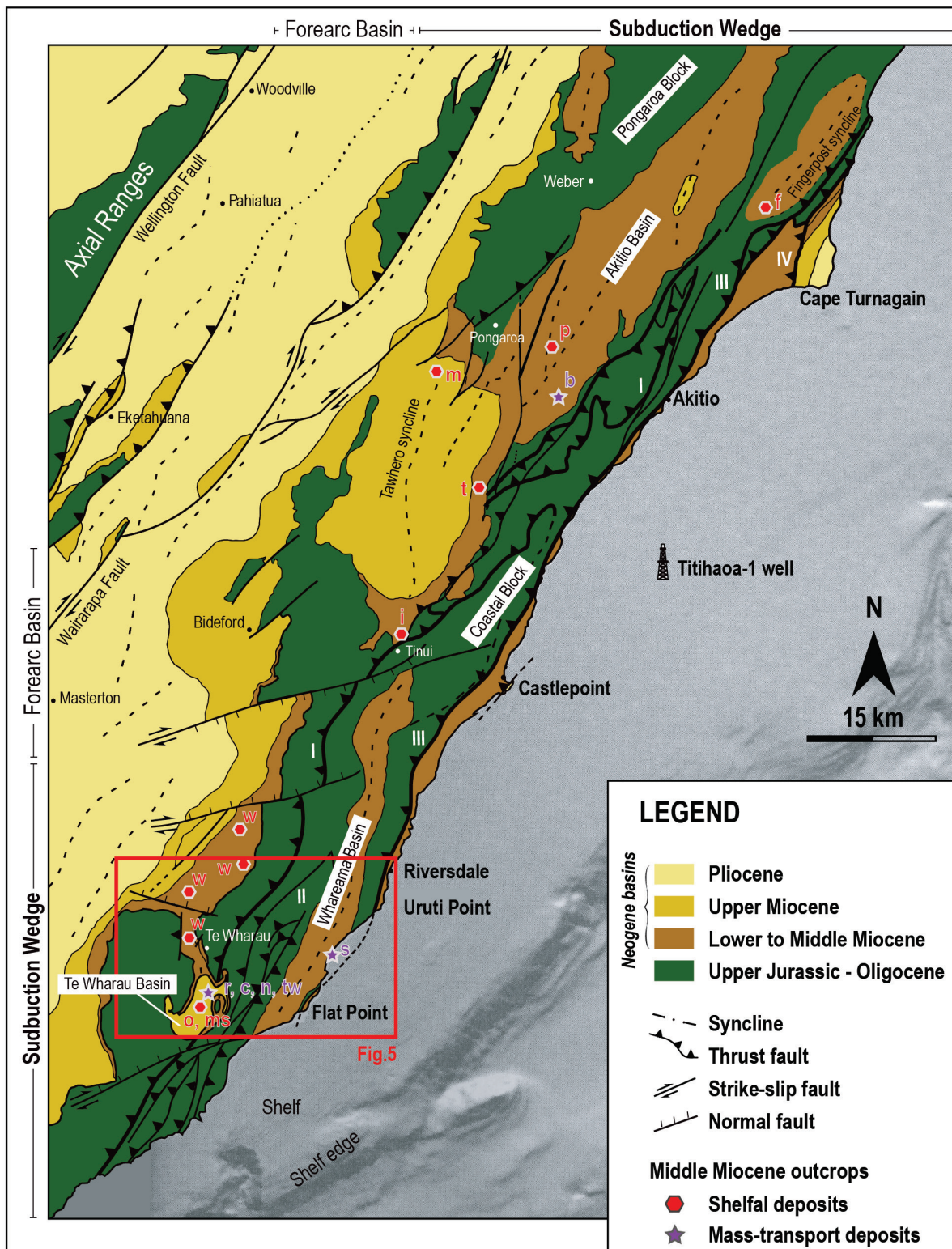
1531 Figure 16: Schematic palaeogeographic map of the south-western portion of the Hikurangi Margin (Coastal Ranges) during
1532 the Lillburnian. This period not only staged the development of regional shelfal domain(s) ([Crundwell 1987](#); [Chanier 1991](#);
1533 [Bailleul et al. 2007](#); [Bailleul et al. 2013](#)) but also recorded their concomitant destabilisation and failure(s). This(these) resulted
1534 in the emplacement of a multitude of MTDs, occluding the previously developing systems, such as the Sefton Hills turbidite
1535 systems in the Whareama Basin or the Kings canyon system (see [McArthur and McCaffrey \(2019\)](#) in the Akitio Basin. The
1536 development of the shelves occurred above substantially different substratum inherited from local tectonics, thereby allowing
1537 through the analysis of the reworked material to retrace the potential sourcing region(s) of the different MTDs (e.g., southern
1538 and northern shelfal domains). See Figure 3 for the name of the shelfal and MTD outcrops.

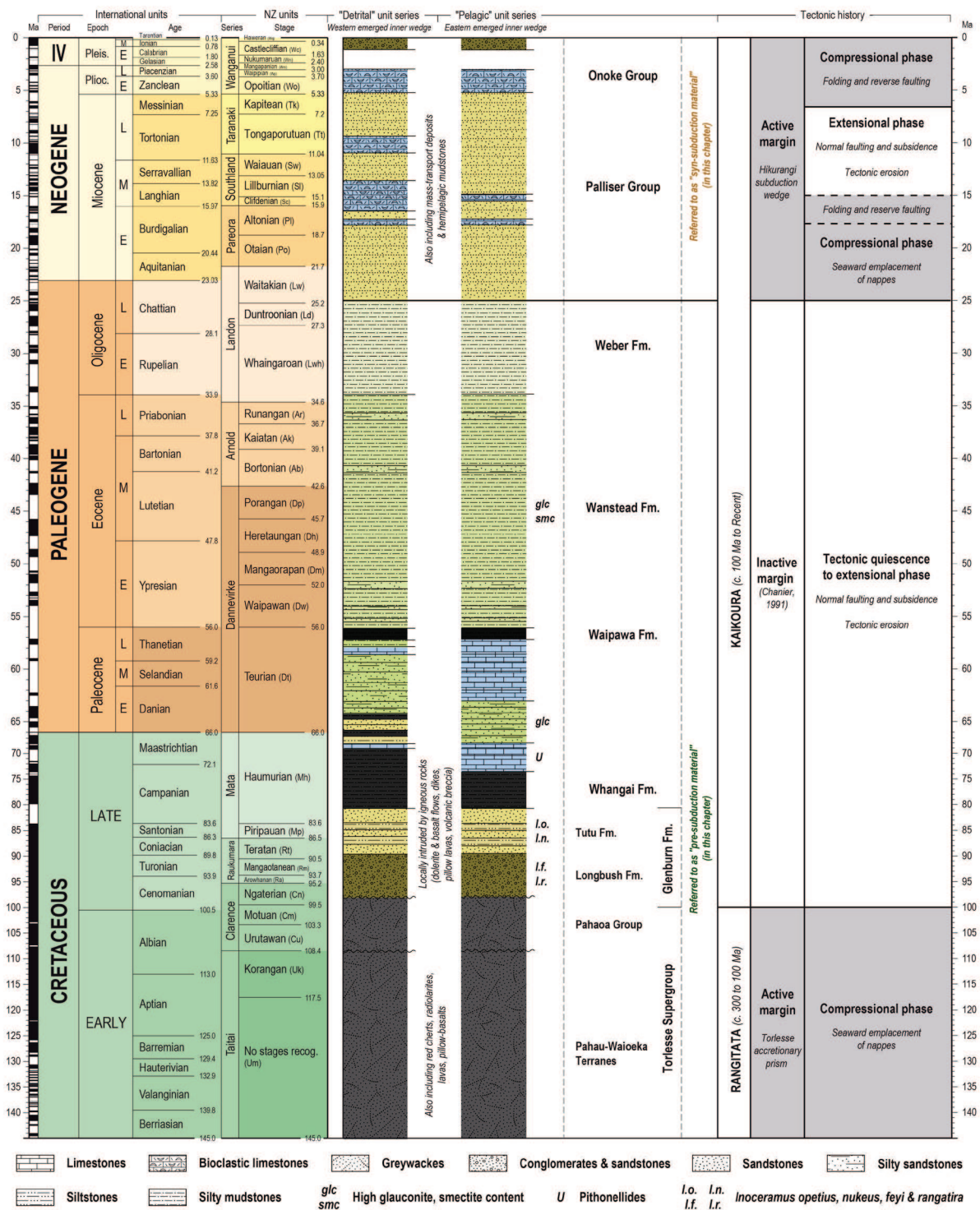
1539

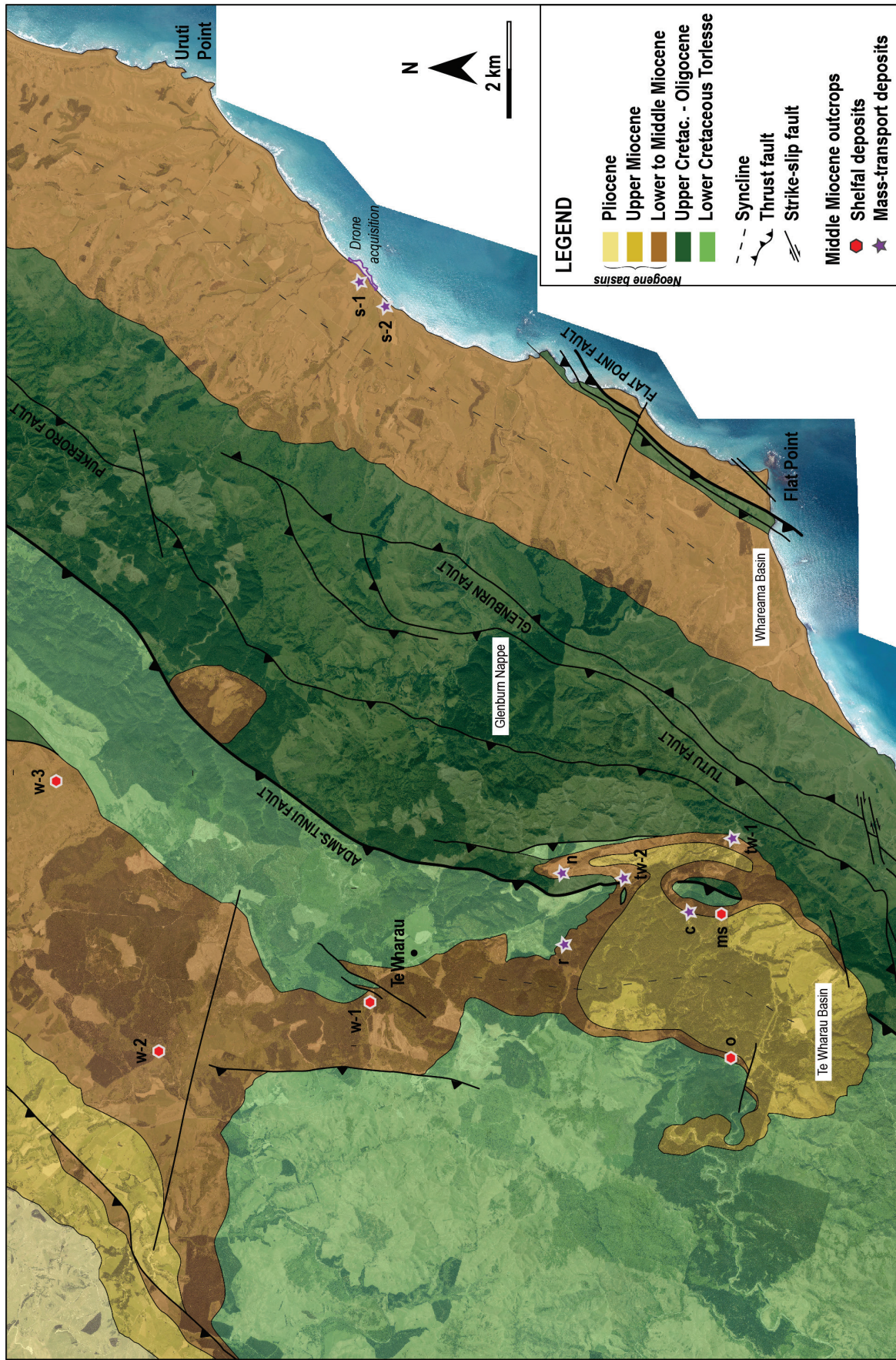
1540 Table 1: Characteristics and interpretation of the sedimentary facies for the turbidite systems (Fa1) and mass-wasting systems
1541 (Fa3) observed in the study area, mostly from the Sefton Hills outcrop (Whareama basin). The nomenclature is based upon
1542 the initial classification defined by [Bailleul et al. \(2007\)](#) and [Bailleul et al. \(2013\)](#). Pictures of the facies associations can be
1543 found in Figure 8, Figure 9, Figure 10; Figure 11.

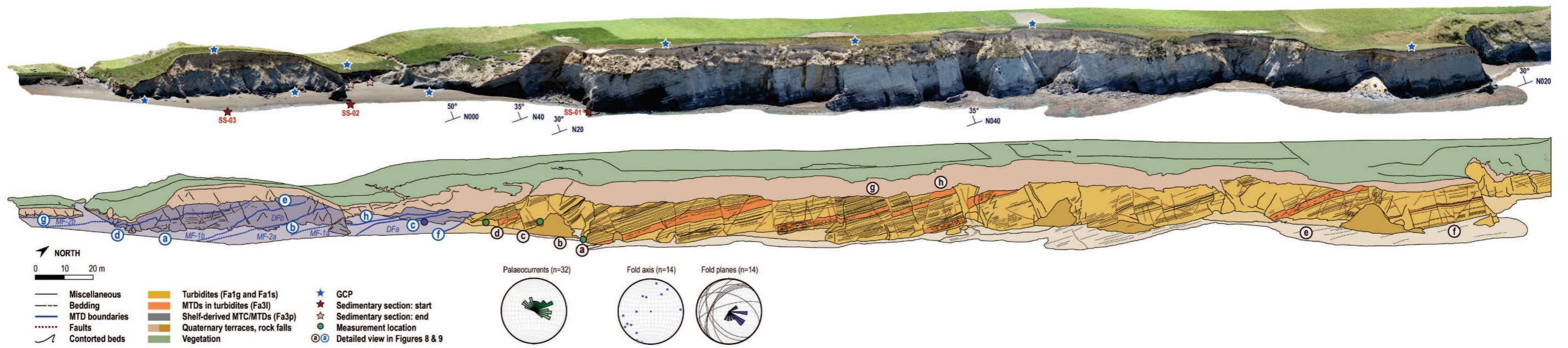


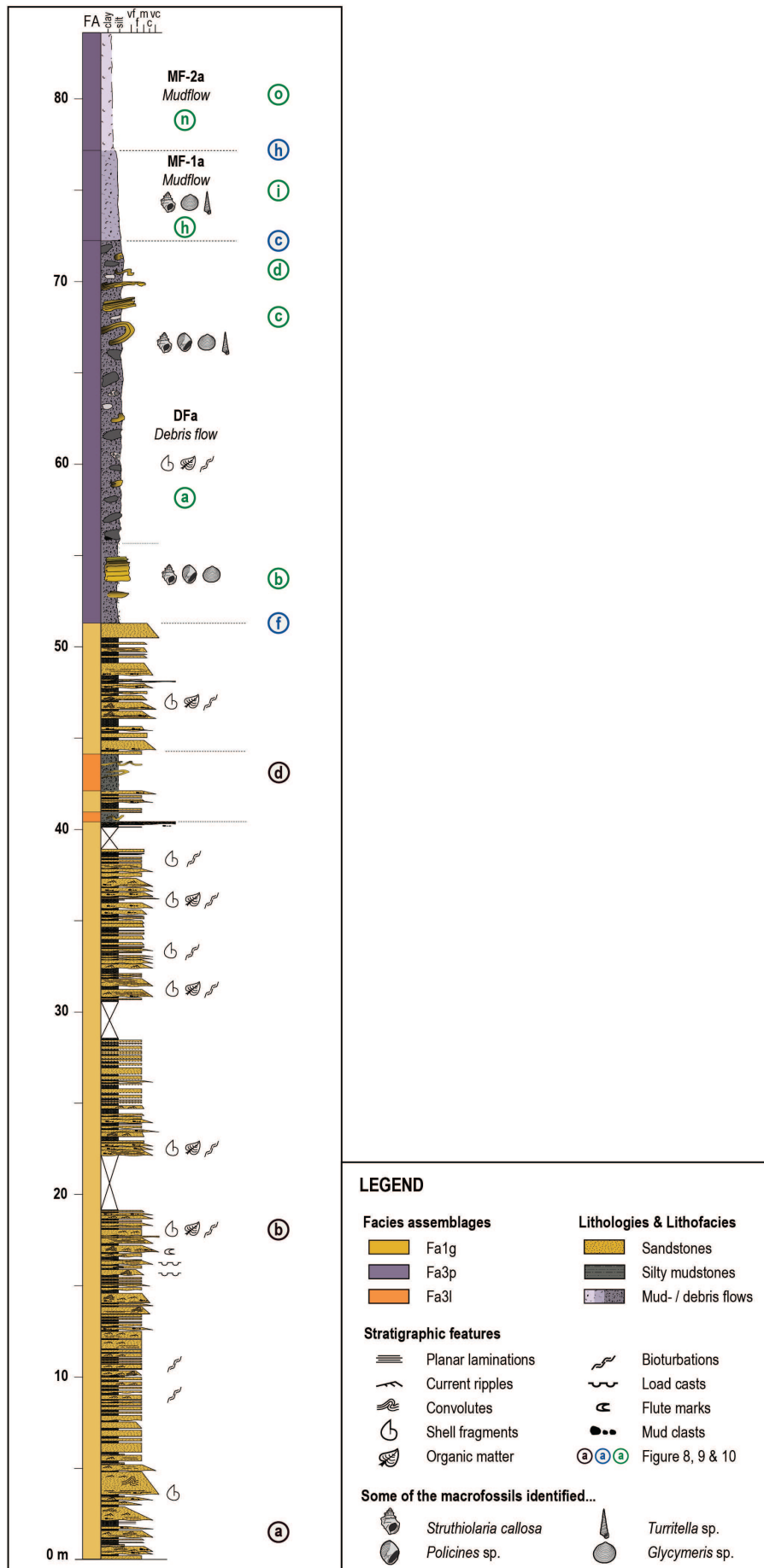


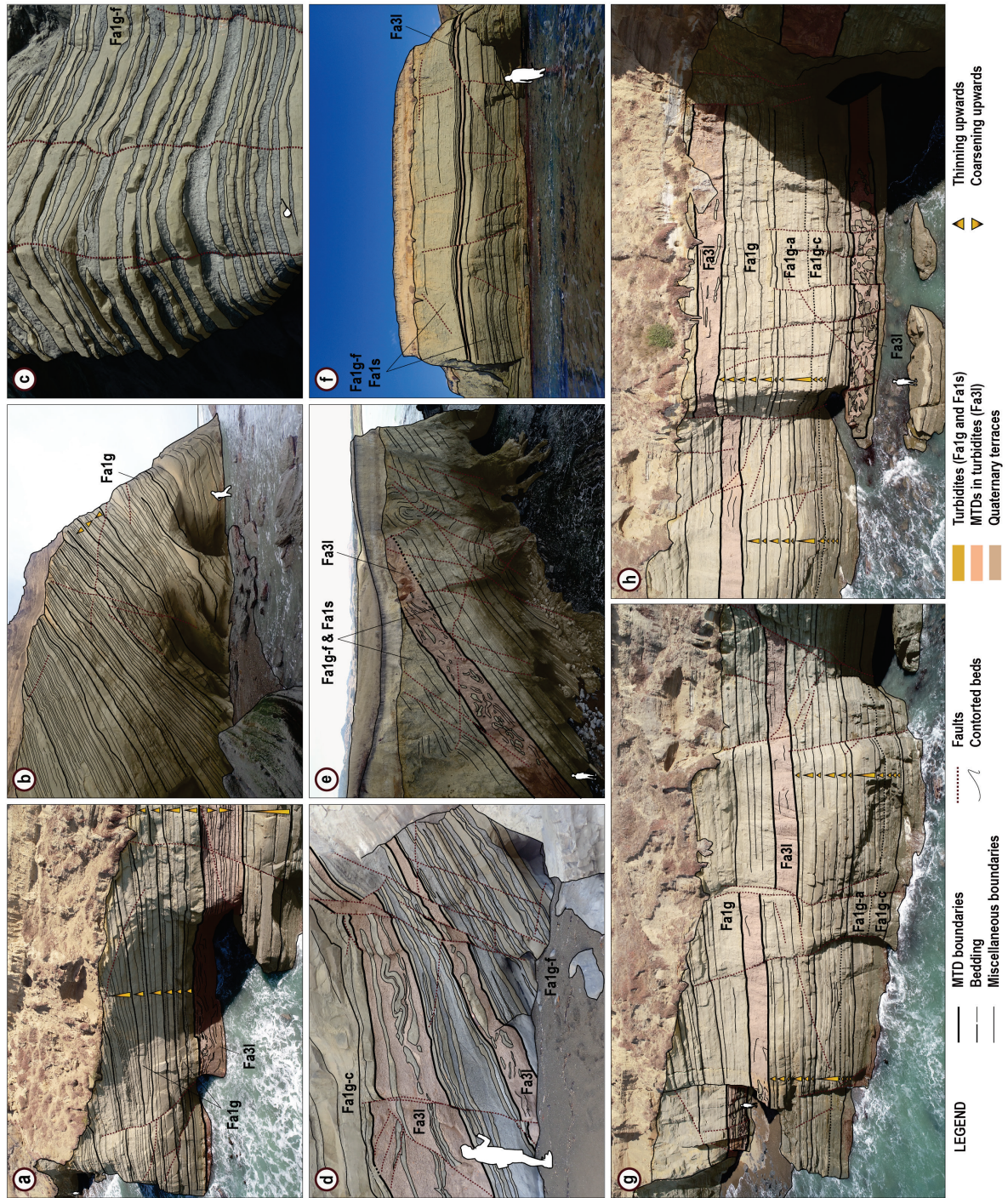


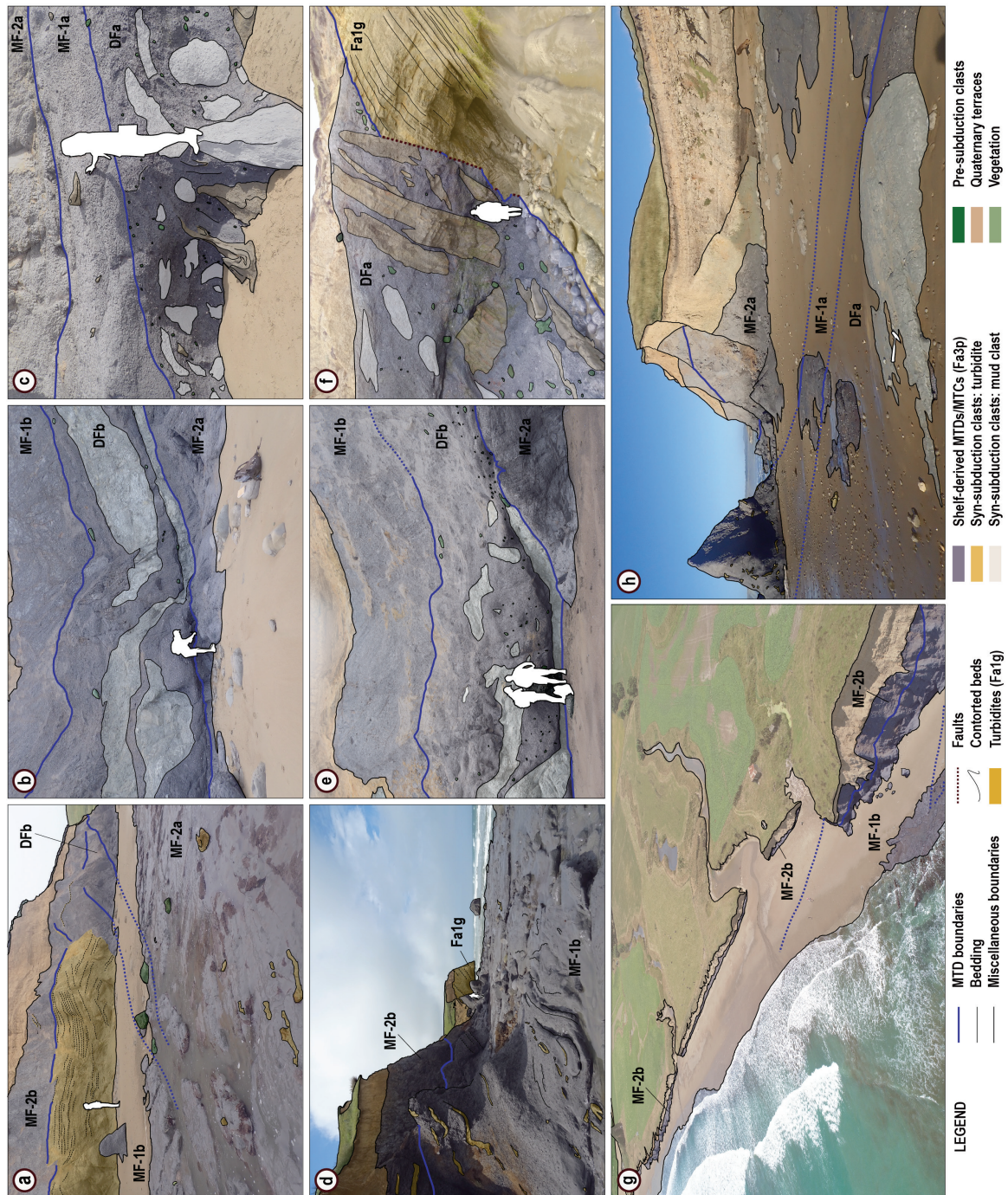


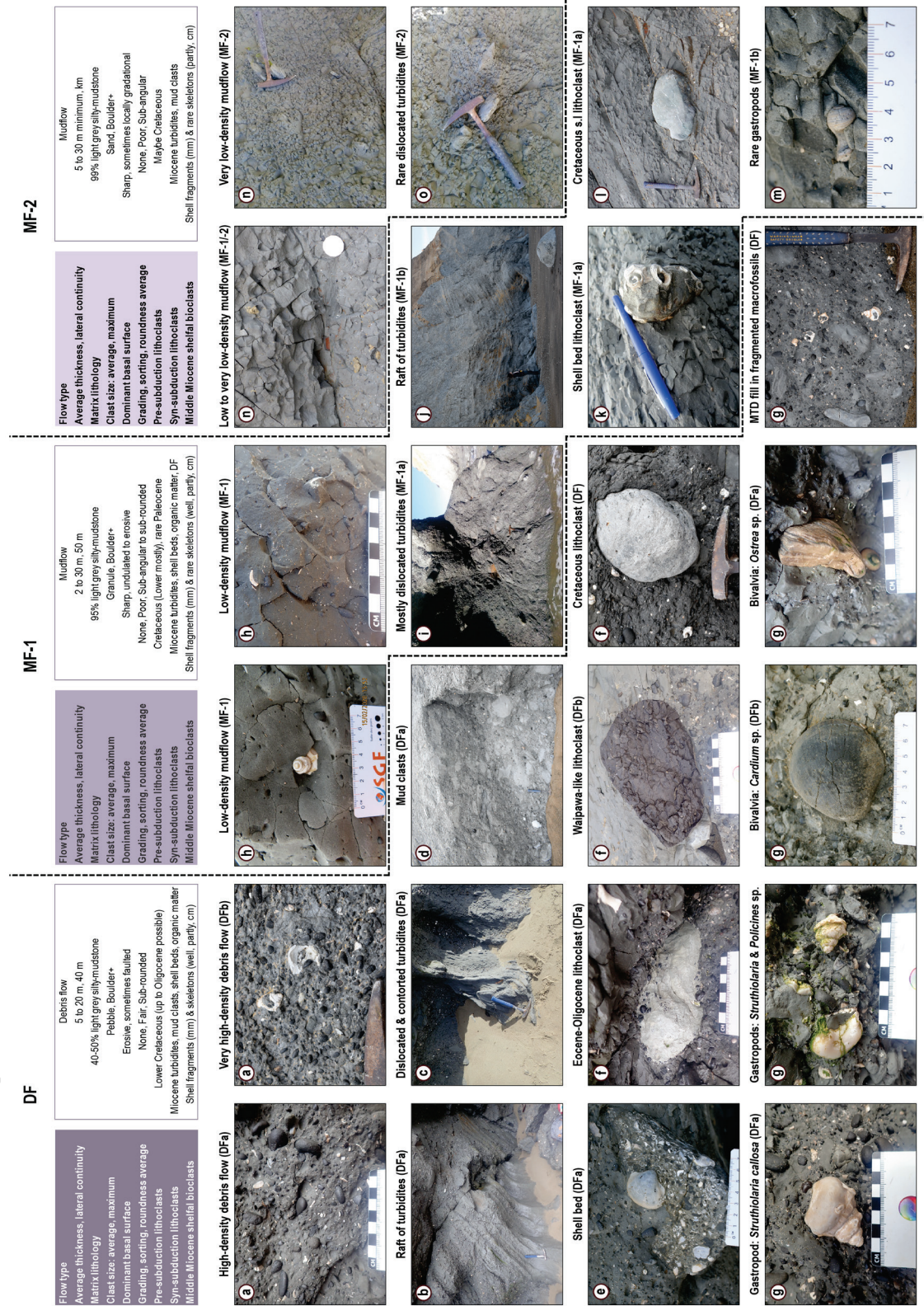


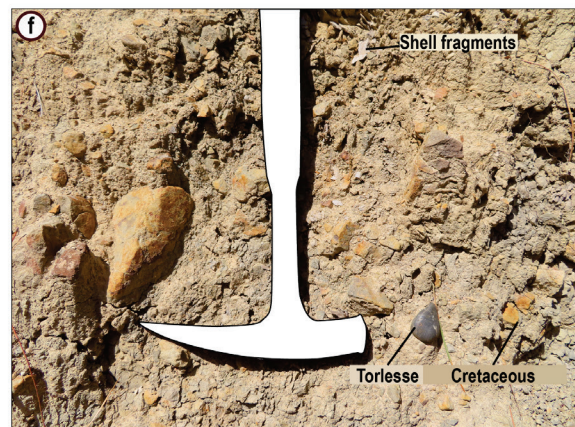
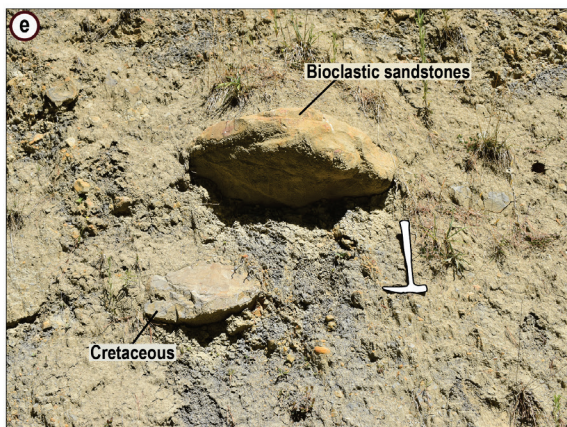
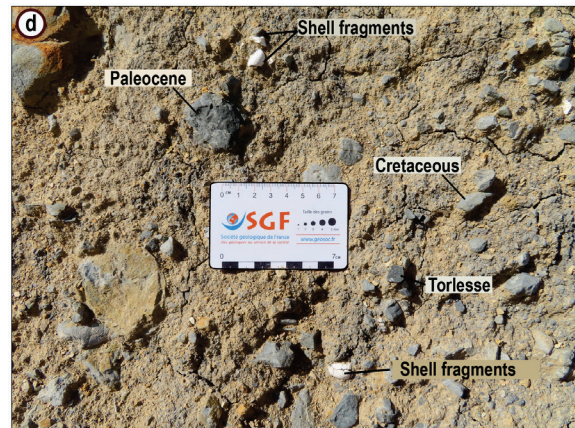
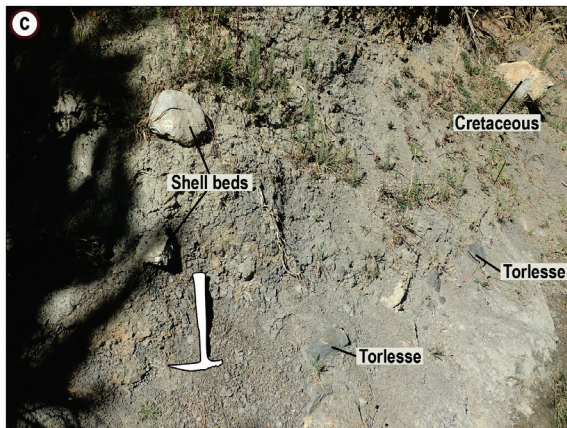
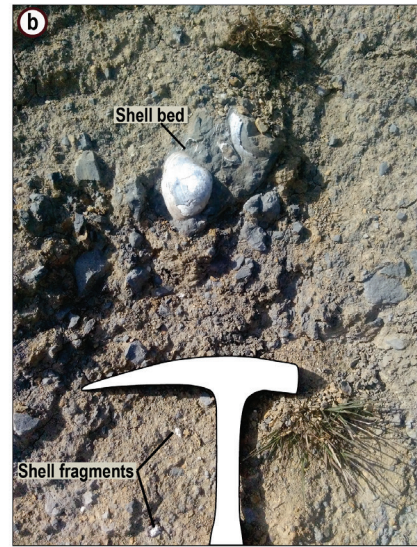






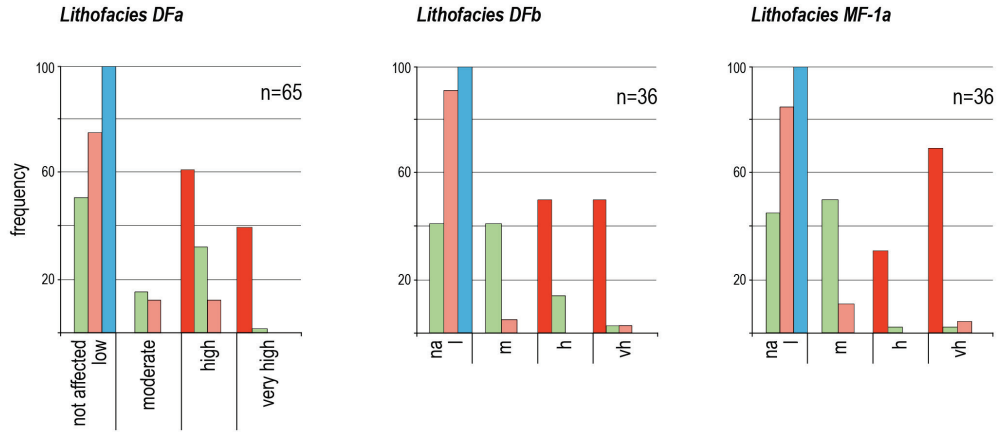




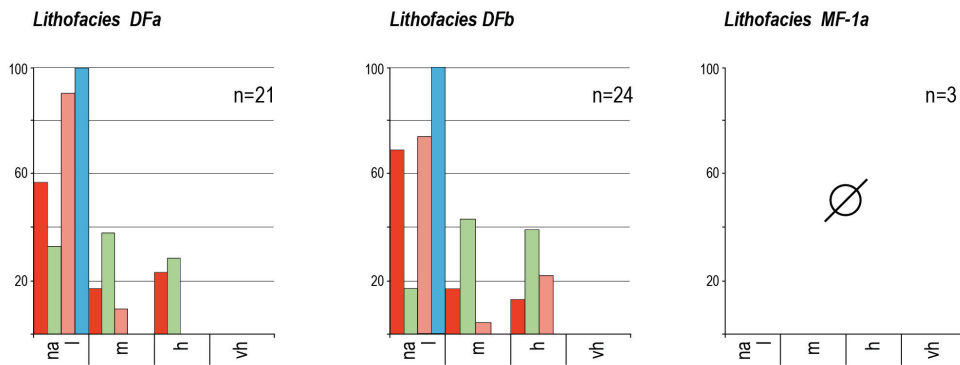


SEFTON HILLS OUTCROP - SECTION S-1

Bioclastic fraction (0.5 cm-3 cm)

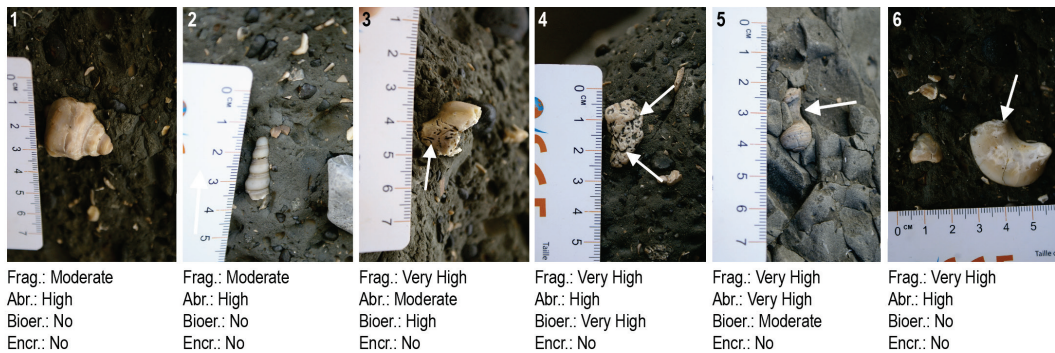


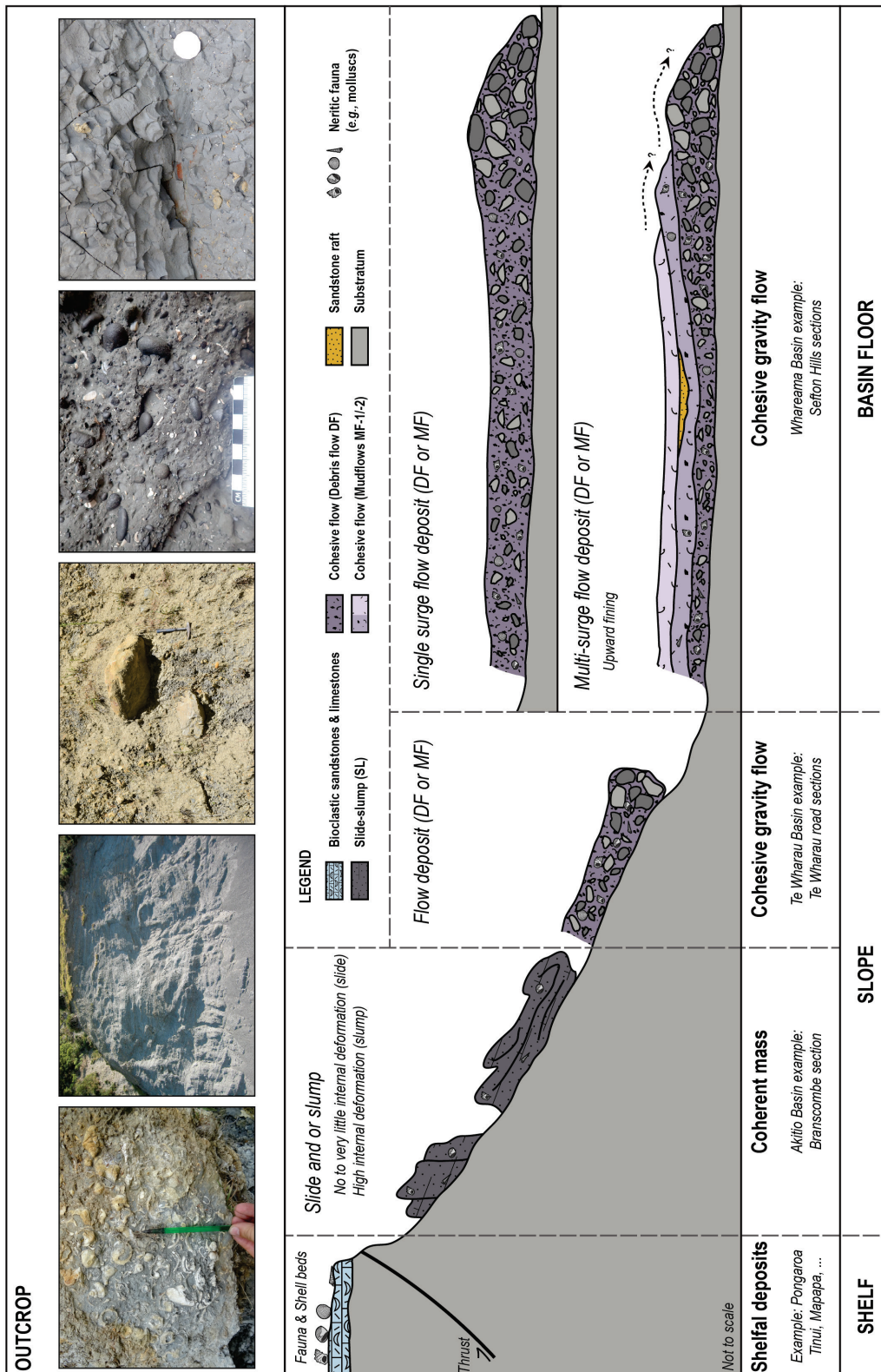
Bioclastic fraction (>3 cm)



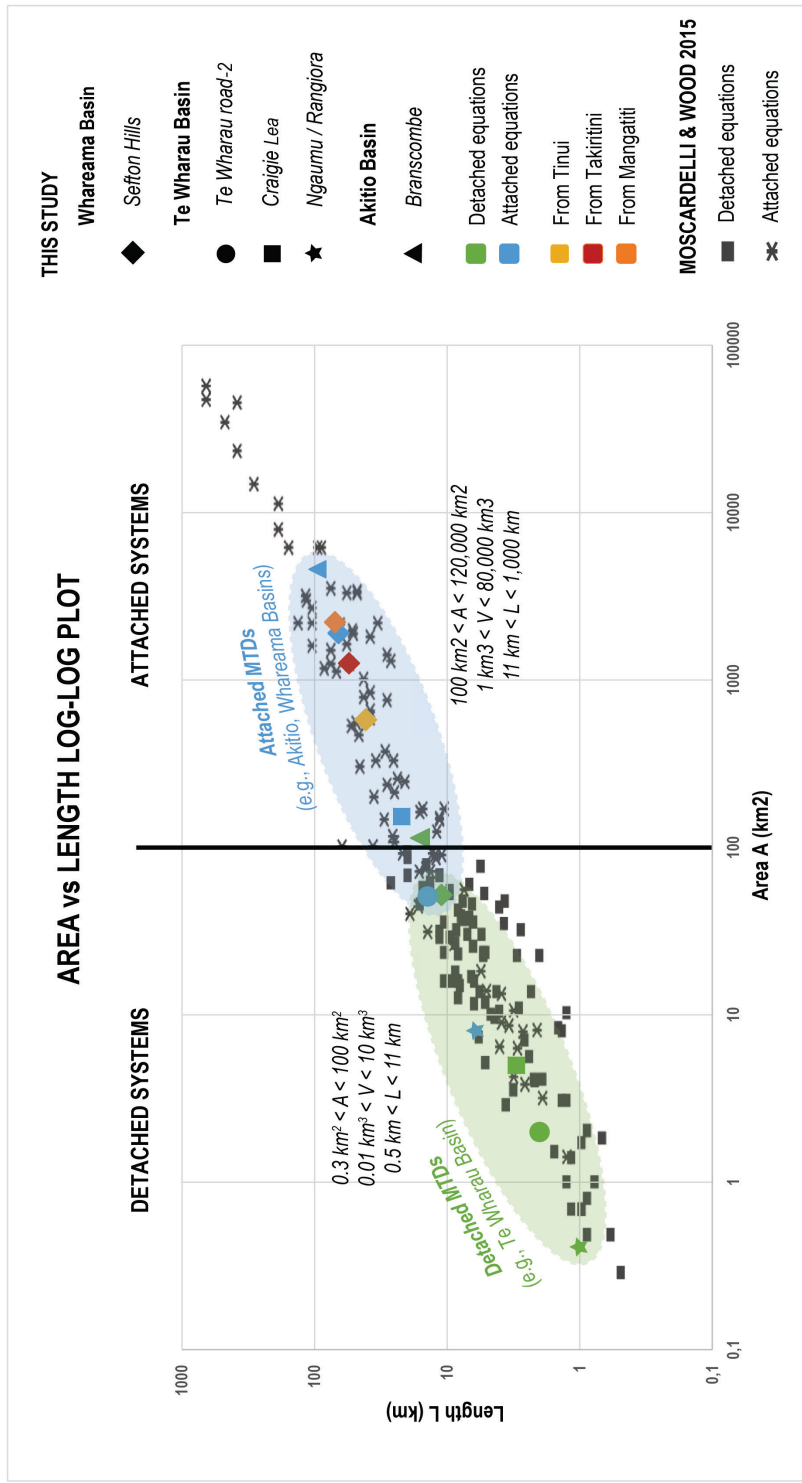
LEGEND ■ Fragmentation ■ Abrasion ■ Bioerosion ■ Encrustation

Field photographs showing examples of shell damages

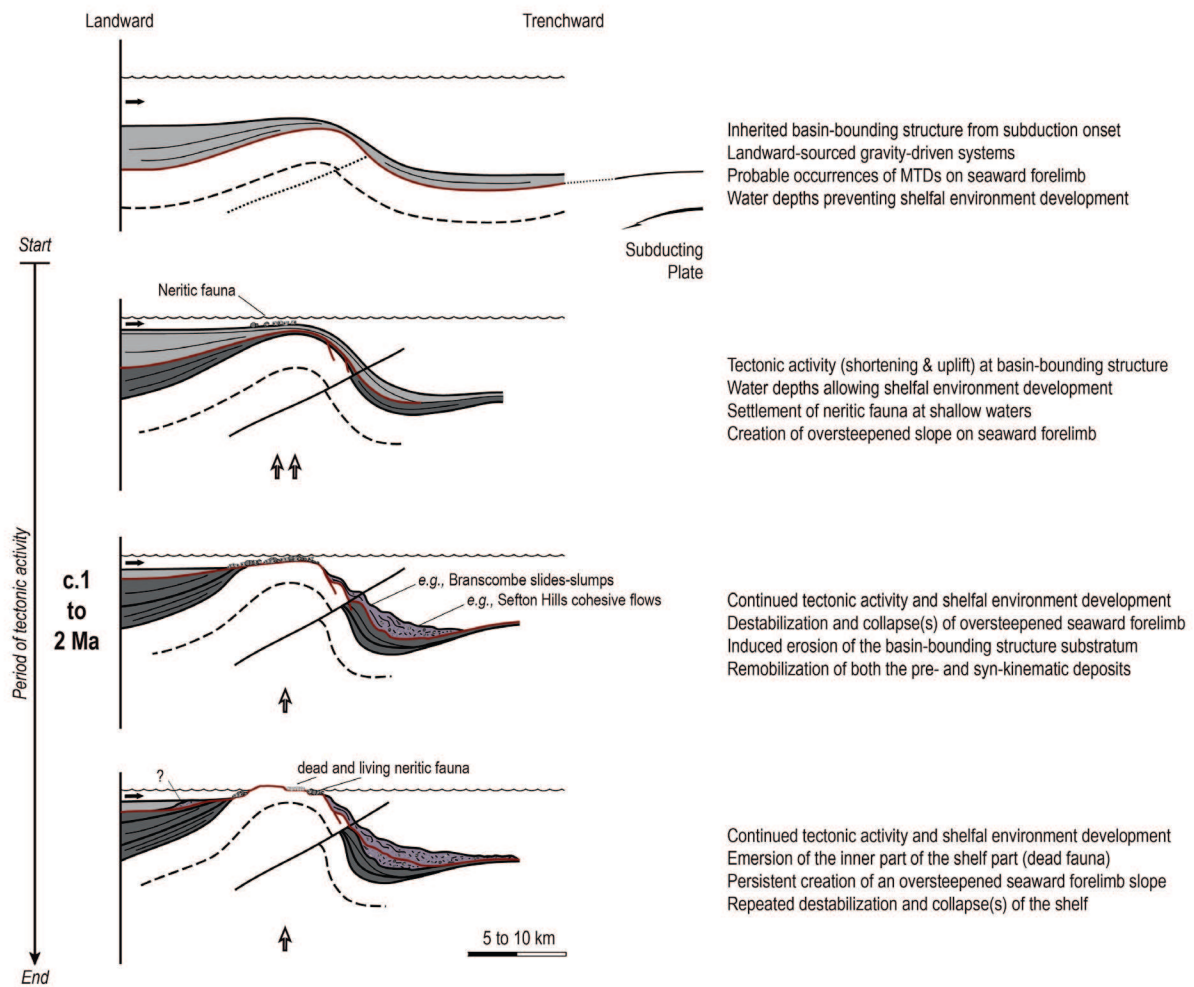












ACS

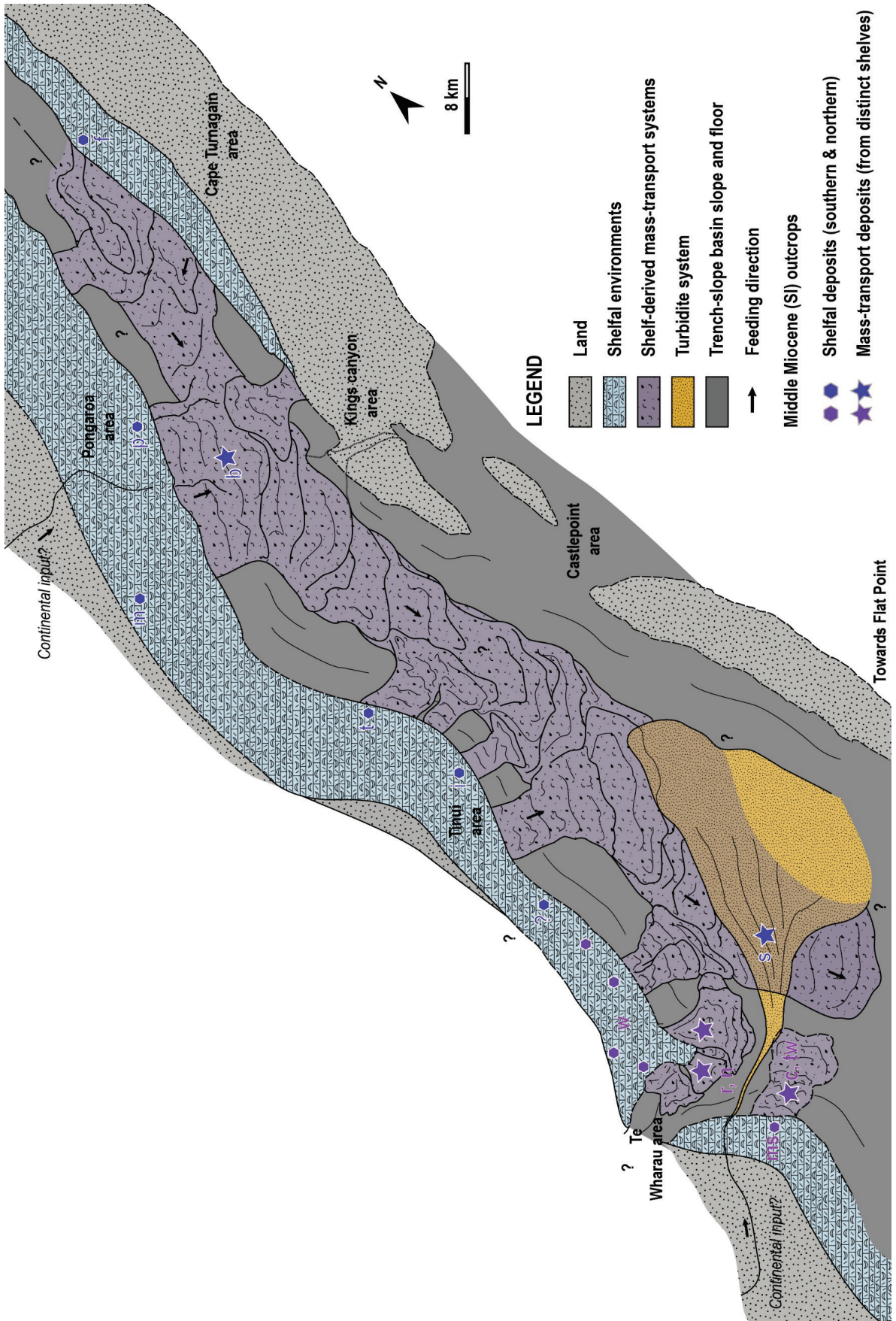


ACCEPTED MANUSCRIPT



LEGEND

- | | | | |
|---|---|---|--|
|  | Syn-subduction, syn-kinematic mass-transport deposits |  | Feeding direction, possible direct continental input |
|  | Syn-subduction, syn-kinematic undiff. gravity-driven deposits |  | Uplift |
|  | Syn-subduction, pre-kinematic undiff. gravity-driven deposits |  | Neritic fauna (e.g., molluscs) |
|  | Pre-subduction basement |  | Shell fragments |



System code	Fa code	LF code	Lithology	Stratification	Internal bedding	Interpretations	Depositional environment
Fa1 Turbidite systems Alternation of sandstones, siltstones and mudstones	Fa1g-c	LF2 (Burgreen and Graham, 2014); Fa1g (McArthur et al., 2020); Fa1g (Bailleul et al., 2007)	Fine- to coarse-grained sandstones and siltstones, well-sorted, with mudstone cap.	Thin- to thick-bedded sandstones, thickness varies laterally, but remains relatively continuous, irregular incisional base with cm to dm scale incisions truncating underlying strata sometimes with channel-based drapes (CBDs), gradational to sharp tops.	Medium to coarse-grained Ta in thicker beds, commonly massive / structureless, with mud clasts, shell and plant fragments, sometimes displaying sole marks such as flute casts. Planar laminations (Tb), often dewatering or soft sedimentation deformation structures above well-developed climbing ripples (Tc). Lamination often highlighted by organic rich, carbonaceous and shell fragments. Common amalgamation and some aggradational successions. Rare bioturbation in mudstone cap. Possible stack of several set-scale cycles with intrachannel mudstones.	High sedimentation rate with rapid suspension fall-out from high density, mostly erosive turbidity currents (Lowe, 1982; Kneller, 1995). Small-scale incisional features suggesting small erosional channels and discontinuous scours developing on the surface of a lobe (Burgreen and Graham, 2014). CBDs resulting from abandonment after initial incision or developing progressively as the channel fills (Barton et al., 2010). Fragment content suggests that flow initiated in shallow marine environment.	Distributary channels and scours. Lobe off-axis, proximal to medial region.
	Fa1g-a	LF2 (Burgreen and Graham, 2014); Fa1g (Bailleul et al., 2007)	Very fine- to medium-grained sandstones and siltstones, well-sorted, with mudstone cap.	Thin- to medium-bedded sandstones, fining and thinning upwards, lateral continuity good lateral continuity yet pinches out, sharp or slightly irregular bases and gradational to sharp tops.	Rare basal coarse Ta intervals, occasional planar laminations (Tb) passing into climbing ripples (Tc), mostly climbing ripples passing into massive (due to bioturbation?) / structureless facies. Lamination often highlighted by organic rich, carbonaceous and shell fragments. Rare amalgamation. Very common bioturbation in mudstone cap. (2011).	Slow deposition from a mostly non-erosive, waning, high- to low-density turbidity currents (Lowe, 1982; Kneller, 1995). Fragment content suggests that flow initiated in shallow marine environment. Upward fining and thinning suggest abandonment of the channel and filling of the unfilled relief (McHargue et al., 2011).	Abandonment / Spill of distributary channels. Lobe off-axis, proximal to medial region.
	Fa1g-f	LF1 (Burgreen and Graham, 2014); LF4, LF5, LF6 or LA2 (McArthur et al., 2020); Fa1g (Bailleul et al., 2007)	Very fine- to fine-grained sandstones and siltstones, well-sorted, with bioturbated mudstone cap.	Very thin- to medium-bedded sandstones, thinning or thickening upwards, lateral continuity good lateral continuity, sharp erosional bases and gradational to sharp tops, local low-displacement slumps and slump scours (Fa3l-s).	Mostly weathered or bioturbated, occasional planar laminations (Tb) passing into climbing ripples (starved) and rare convolutes (Tc). Sometimes alternation of parallel-ripple-laminated sandstone to siltstone. Rare incisional features with coarser material and occasional bioclastic grits. Lamination often highlighted by organic rich, carbonaceous and shell fragments. Variable degree of bioturbation, tends to be highly bioturbated.	High sedimentation rate with deposition from a mostly non-erosive, waning, low-density turbidity currents (Lowe, 1982; Kneller, 1995). Alternation of waxing then waning flow possibly indicating hyperpycnal flows (Mulder et al., 2003). Fragment content suggests that flow initiated in shallow marine environment.	Lobe fringe, medial to distal region.
Fa3 Mass-wasting systems Disorganized gravels, sandstones, siltstones and mudstones	Fa3l	Fa3l (Bailleul et al., 2007)	Mostly fine-grained sandstones and siltstones, well-sorted, with bioturbated mudstone cap.	Thin- to very thick-bedded, tabular (sheets), good lateral continuity, sharp erosional bases and gradational to sharp tops, local low-displacement slumps and slump scours (Fa3l-s).	Commonly massive, sometimes planar laminations (Tb), rare ripples and convolutions (Tc), intra-beds erosional to non-erosional amalgamation surfaces. Lamination can be highlighted by organic rich, carbonaceous and shell fragments. Mostly a sandy, succession.	Unconfined turbidity currents. Deposition from waning, low density turbidity currents (Lowe, 1982; Kneller, 1995).	Sheet-lobe, distal region. Sheet-like turbidites.
	Fa3l-d	LF6 (Burgreen and Graham, 2014)	Matrix-supported, siltstones to silty mudstones with varying quantity of granule- to boulder-grade syn-subduction extraformational clasts.	Sharp and planar base and sharp sometimes undulated top, laterally continuous with sometimes the undeformed interval laterally available and visible, usually between 1 to 5 m thick interval.	Ungraded, disorganized. Syn-subduction siltstones (sandstone to siltstone). Rare syn-subduction bioclasts. Possible recumbent folds, shear and load structures.	Cohesive flow: debris flow or mudflow (Nardin et al., 1979; Mulder & Alexander, 2001). Possible flow transformation of Fa3l-s. Located within a deep-marine turbidite system thereby suggesting a local destabilization. Punctual bioclastic material could result from storms.	Locally-sourced mass-transport deposits.
	Fa3l-l	LF6 (Burgreen and Graham, 2014)	Disorganized interbedded sandstones, siltstones and mudstones. Silty mudstone background facies with occasional granule- to boulder-grade intraformational clasts.	Sharp and planar base and sharp sometimes undulated top, laterally continuous with sometimes the undeformed interval laterally available and visible, usually between 1 to 5 m thick interval.	Contorted (recumbent folds) remobilized. Possible scattered, syn-subduction siltstones (dislocated turbidites). Syn-sedimentary deformation.	Cohesive mass of sediment that moves along a glide plane internal deformation. Slide or slump (function of basal shearing surface). Located within turbidite system thereby suggesting local destabilization.	Locally-sourced mass-transport deposits.
Fa3p Shell-derived	Fa3p-d	DF, MF-1, MF-2	Matrix-supported, siltstones to silty mudstones with varying quantity of granule- to boulder-grade pre- and syn-subduction extraformational clasts.	Slightly to highly erosive base and sharp to undulated top, sometimes gradational top, laterally discontinuous, variable thickness (m to dm).	Ungraded, disorganized. Pre- and syn-subduction siltstones (sandstone to siltstone). Rare syn-subduction bioclasts (gastropods, bivalvia, corals) and or shell fragments. Common recumbent folds, shear and load structures.	Cohesive flow: debris flow or mudflow (Nardin et al., 1979; Mulder & Alexander, 2001). Macrofaunal assemblages suggest that mass-wasting initiated in shallow marine environment.	Shell-derived mass-transport deposits.
	Fa3p-s	SL	(Dis)organized interbedded sandstones, siltstones and mudstones. Silty mudstone background facies with granule- to boulder-grade pre- and syn-subduction extraformational clasts (litho- & bioclasts).	Sharp and planar base and sharp sometimes undulated top, laterally continuous with sometimes the undeformed interval laterally available and visible, usually 10s of m thick intervals.	Cohesive to contorted (recumbent folds), remobilized. Pre- and syn-subduction siltstones. Syn-subduction bioclasts, either as skeletons (gastropods, bivalvia, corals) and or shell fragments. Syn-sedimentary deformation.	Cohesive mass of sediments that moves along a glide plane internal deformation. Slide or slump (function of basal shearing surface). Macrofaunal assemblages suggest that mass-wasting initiated in shallow marine environment.	Shell-derived mass-transport deposits.